NASA Contractor Report 198487

Multiple Scale k-ε Turbulence Modeling of the Transitional Boundary Layer for Elevated Freestream Turbulence Levels

Sheng-Yi Wu and Eli Reshotko
Case Western Reserve University
Cleveland, Ohio

May 1996

Prepared for
Lewis Research Center
Under Cooperative Agreement NCC3–124

National Aeronautics and
Space Administration

MULTIPLE SCALE k-ε TURBULENCE MODELING OF THE TRANSITIONAL BOUNDARY LAYER FOR ELEVATED FREESTREAM TURBULENCE LEVELS

by

Sheng-Yi Wu and Eli Reshotko

Department of Mechanical and Aerospace Engineering
Case Western Reserve University

Abstract

A multiple-scale k-ε turbulence model is developed to calculate the development of the transitional flat-plate boundary layer under elevated freestream turbulent conditions. The model uses the split-spectrum concept which divides the energy spectrum into low and high wavenumber regions, each of which have their own modeling equations. Damping functions are used to accommodate the near-wall and transitional behaviors. The model constants are determined from the exact solutions of the simplified model equations for the cases of grid turbulence flow, homogeneous shear flow, and the near-wall equilibrium turbulent flow. By this calibration, the model constants are automatically tuned to the characteristics of the freestream energy spectrum.

The results show that the partition of the energy spectrum in the freestream also affects the transition location. A spectrum partitioning parameter S_g is identified whose optimal value correlates with freestream turbulence level. Comparison with five different sets of experimental data shows that the multiple-scale model with the optimal values of S_g emulates many features of the transitional boundary layer. The start of transition can be predicted reasonably well, however the length of the transition zone is consistently shorter than in the experiments. The present model is insensitive to the shape of the initial turbulence energy and dissipation profiles.

ACKNOWLEDGMENT

This project is supported by NASA Lewis Research Center and NASA Grant NCC3-124. The authors wish to thank the program manager, Dr. Frederick F. Simon, for his continued interest and support. The authors also wish to acknowledge many fruitful discussions with Professor Michael E. Crawford of the University of Texas at Austin during the early phases of this work.

TABLE OF CONTENTS

LIST OF TABLES

LIST OF FIGURES

NOMENCLATURE

Roman

a_1	Structure coefficient in dissipation profile
a_i, b_i, c_i	Coefficients of Taylor series expansion
A, B	Coefficients in the damping function of turbulent model
C_f	Friction coefficient
C_p	Specific heat
C_{p1}, C_{p2}	Model constants in ε_p equation
C_{t1}, C_{t2}	Model constants in ε_t equation
$e^{(m)}$	Turbulent kinetic energy of the m-th slice of the energy spectrum
$E^{(m)}$	Three-dimensional energy spectrum function
$E_{i,j}$	Fourier transform of $Q_{i,j}$
f_{p1}, f_{p2}	Damping functions of the k_p equation
f_{t1}, f_{t2}	Damping functions of the k_t equation
f_μ	Damping function of eddy viscosity
$F_{i,kj}$	Fourier transform of $S_{i,kj}$
$F^{(m)}$	The energy transfer function at κ_m
h	Enthalpy
H	Total enthalpy
$H_{i,p}$	Fourier transform of $K_{i,p}$
k	Turbulent kinetic energy $\equiv k_p + k_t$
$K_{i,p}$ or $K_{p,i}$	Two-point velocity-pressure correlation
l_m	Mixing length

l_t	Turbulence characteristic length scale
L	Turbulent length scale
E	Turbulent energy spectrum
$P^{(m)}$	Turbulent energy production within the m-th slice of energy spectrum
P_k	Production term in turbulent kinetic energy equation
Pr	Molecular Prandtl number
Pr_t	Turbulent Prandtl number
$\dot{q}_w$	Wall heat flux
$Q_{i,j}$	Second-order two-point velocity correlation tensor
$R_{i,j}^{(m)}$	Partial Reynolds stress for the m-th slice of energy spectrum
Re_x	Reynolds number, based on stream wise distance
Re_θ	Reynolds number, based on Momentum thickness
R_t	Turbulent Reynolds number, $\equiv k^2/\nu\varepsilon$
r_g	Turbulent energy ratio k_t/k_p of the grid turbulence
r_s	Turbulent energy ratio k_t/k_p of the homogeneous shear flow
S	Mean shear rate of the homogeneous shear flow
S_g	Freestream energy spectrum parameter
$S_{i,kj}$ or $S_{ik,j}$	Third-order two-point velocity correlation tensor
St	Stanton number
T	Temperature
S_ϕ	Source term in transport equation
Tu	Freestream turbulent intensity
T_τ	Friction temperature
U	Mean stream wise velocity

U_τ	Friction velocity $\equiv \sqrt{\tau_w/\rho}$
U^+	Mean stream wise velocity in wall units $\equiv U/U_\tau$
$<u'>$	Turbulent intensity $\equiv \sqrt{2k/3}$
$-\overline{u'v'}$	Reynolds stress
V	Mean normal velocity
x	Stream wise coordinate
$(x_k)_{AB}$	Eulerian coordinates of two-point correlation
y	Cross stream coordinate
y^+	Vertical distance in wall units $\equiv U_\tau y/\nu$

Greek

Γ_ϕ	Generalized diffusion coefficient
γ	Turbulent energy production over dissipation rate at equilibrium point in homogenous shear flow
δ	Boundary layer thickness
δ^*	Boundary layer displacement thickness
ε	Turbulent energy dissipation rate
$\varepsilon^{(m)}$	Dissipation within the m-th slice of energy spectrum
$\tilde{\varepsilon}$	Energy transfer function in spectrum
ε_p	Net turbulent energy transfer function in production zone
ε_t	Net turbulent energy transfer function in transfer region
η	Similarity variable
$\imath$	Complex number $\sqrt{-1}$
κ	Three-dimensional wave number

κ_m	Three-dimensional wave number at the m-th partitioning
μ_t	Dynamic eddy viscosity
ν_t	Kinematic eddy viscosity
ξ_i	Eulerian distance coordinates of two-point correlation
ρ	Density
σ_{kp}, σ_{kt}, $\sigma_{\varepsilon p}$ and $\sigma_{\varepsilon t}$	Model constants
τ	Non-dimensional convection time of the homogeneous shear flow
ϕ	General turbulent quantity; or the time scale ratio of the homogeneous shear flow
ψ	Stream function
ω	Dimensionless stream function

Superscript

(m)	The m-th slice (from κ_{m-1} to κ_m) of the energy spectrum
$+$	Wall unit
$\bar{}$	Time mean average
$'$	Fluctuating component

Subscript

e	Freestream value
eff	Effective quantity
E	External boundary
I	Internal boundary

p	Quantity in production region of energy spectrum
t	Quantity in transfer region of energy spectrum
μ	Quantity in eddy viscosity formulation
0	Initial condition
∞	At equilibrium condition; long-time solution

CHAPTER ONE

INTRODUCTION

1.1 Overview of Transitional Boundary Layer

The transition process from laminar to turbulent flow within the boundary layer has been of interest for a long time. The understanding of the transitional boundary layer is important in many fields, including that of gas turbine engines (see Mayle, 1991, and Walker, 1993). For example, the accurate prediction of laminar-turbulent transition can prevent the overprediction of losses in turbomachinery blade rows. Since the flow is transitional on a turbine blade and since the fully turbulent heat transfer rate is many times larger than the laminar one, transition always plays an important role in turbine blade heat transfer.

The transitional boundary layer is a very complicated phenomenon. Since the classical experiment of Reynolds in 1883, a lot of questions still remain unanswered. Even after more than a century there is no general theory which can completely describe the transition process.

For boundary layer flow over a smooth surface with very low freestream turbulence intensity ($Tu<0.03\%$ referenced to the mean freestream velocity), an imposed disturbance (such as freestream vorticity or sound) through a receptivity process excites the normal modes of the flow and causes disturbed motion inside the

boundary layer. The normal mode behavior can be described by linear stability theory which predicts the growth rates of the amplified disturbance and the critical Reynolds number, below which the flow is stable. The initial instability often occurs as two-dimensional Tollmien-Schlichting (T-S) waves traveling in the mean flow direction. However, spanwise variations soon appear showing three-dimensional effects. These result from secondary instabilities giving rise to Λ-vortices and begin a cascading breakdown of T-S waves into smaller units. The breakdown is accompanied first by the appearance of three-dimensionality and frequency spikes, then by decreasing spanwise non-uniformity and spectral broadening until the frequency spectrum approaches the full randomness. This may be accompanied by turbulence bursts at random times and locations near the wall, as the flow is becoming fully turbulent. In many natural circumstances, or when disturbances are artificially introduced, turbulent spots could appear in this final stage. The spot grows in both streamwise and lateral directions, eventually merging with neighboring spots and coalescing into a fully turbulent flow. This final stage of the transition scenario is represented by sharp increases in skin friction coefficient and Stanton number if heat transfer is involved. Although the onset of transition can be defined in different ways, in this work, the onset of transition is defined as the departure of the friction coefficient from its laminar value. Thus, the onset of transition from the leading edge of the flat plate is far downstream of the first appearance of T-S waves.

For elevated freestream turbulence, the initial disturbance can be sufficiently large so that transition evolves without T-S waves and the transition process is essentially non-linear. The terminology "bypass transition" was first introduced by Morkovin (1979) to describe this phenomenon. A classical experiment of bypass

transition is the fully developed Poiseuille pipe flow by Wygnanski and Champagne (1973) and Wygnanski, Sokolov and Friedman (1975). In their experiments, transition was initiated at low Reynolds number ($2000 < Re < 2700$) when a large disturbance was introduced in the inlet section of the pipe. The effects of elevated freestream turbulence for flat plate boundary layers were studied by many researchers. The experiments of Blair and Werle (1980) and Blair (1981a and 1983a,b) show the significant effect of freestream turbulence intensity (Tu) by large increases (up to approximately 20% for Tu=6%) of both the skin friction coefficient and Stanton number for fully turbulent boundary layers. These effects can be correlated by freestream turbulence intensity, the turbulent length scale and the boundary layer momentum thickness Reynolds number. The location of transition moves progressively upstream with increasing Tu until it is ahead of the first row of measured data. Suder, O'Brien and Reshotko (1988) studied bypass transition for unheated flat plate boundary layers with Tu from 0.3% to 5%. For Tu greater than 0.65% the bypass transition mechanism prevailed. Recently, Sohn and Reshotko (1991) documented in detail the behavior in the transitional boundary layer over a heated flat plate for Tu from 0.4% to 6%. From spectral measurements, T-S waves were significant for Tu=0.4%. They were present but not significant for Tu=0.8% and 1.1%. For higher Tu cases, there was no evidence of occurrence of T-S waves. These results are consistent with those reported by Kosorygin and Polyakov (1985).

The influence of freestream turbulence and pressure gradient on transition were studied and correlation-type prediction methods were formulated by Van Driest and Blumer (1963), Hall and Gibbings (1972) and Abu-Ghannam and Shaw (1980). All of these correlations predict the start and end of transition as a function of local Reynolds

number or momentum thickness Reynolds number for freestream turbulence levels up to 9%. Among these experiments, Abu-Ghannam and Shaw considered many experimental data sets and developed a correlation without bias to any particular set of data they used, but the correlation is biased against the quiescent environment condition. For very high freestream turbulence levels, transition is moved even further upstream. Thole (1992, Tu=10 to 20%), and Maciejewski and Moffatt (1992a and 1992b, Tu=20 to 60%) show only fully turbulent flow. The transition is not captured in their data.

The effects of favorable pressure gradient (accelerating flow) on transitional boundary layer with elevated freestream turbulence has been widely studied by Blair (1981b, 1983a,b and 1992a,b), Rued and Witting (1985), Volino and Simon (1991), and Keller (1993). The pressure side of a turbine blade or vane experiences a strong acceleration along the blade length. Favorable pressure gradient causes stretching of the turbulent eddies, delaying the onset of transition, extending the length of the transition zone and diminishing the surface heat transfer rate. On the suction side of a turbine blade, the first half chord length is in strong acceleration. After reaching the minimum pressure, the flow experiences a mild adverse pressure gradient (decelerated flow). The experiment of Gostelow and Blunden (1989) shows that transition lengths are greatly reduced even in weak adverse pressure gradient which they attribute to a strong increase in turbulent spot rate.

It is known that surface curvature has an effect on transition. A convex surface can destroy the large scale eddies and delay the transition process. On a concave surface, the turbulent eddies penetrate and augment transport across the

boundary layer more effectively than for the flat plate boundary layer. It is a destabilizing effect that promotes transition. Wang and Simon (1984 and 1987) investigated two levels of turbulence (Tu=0.68 and 2%) on a convex surface. They found that the curvature on a convex surface (radius=180 cm) has less influence on transition than freestream turbulence intensity. When a smaller radius of curvature (radius=90 cm) was used, there was no further delay in transition. Kim, Simon and Russ (1991 and 1992) studied the transitional boundary layer on a concave surface. Gortler vortices were observed in both laminar and turbulent flow for low level freestream turbulence. This confirmed the earlier experiment of Barlow and Johnston (1988a and 1988b). But there is no evidence of coherent vortices for high turbulence intensity (Tu=8.6%).

It is widely accepted that transitional and turbulent boundary layers are intermittent. The outer intermittent region of fully turbulent boundary layers have been studied extensively by Corrsin and Kistler (1955), Fiedler and Head (1966), Kovasznay et al. (1970), Blackwelder and Kovasznay (1972), and Hedley and Keffer (1974). After the turbulent spot was discovered by Emmons (1951), the transitional boundary layer was considered as a coexistence of laminar and turbulent flows. Emmons provided a parameter called "intermittency" for the fraction of time the flow is turbulent. The time-averaged quantities were calculated by superposition of local turbulent and non-turbulent quantities. Schubauer and Klebanoff (1955) measured turbulent spot propagation and recorded the streamwise intermittency distribution. Dhawan and Narasimha (1958) revised Emmons' model and provided a so called "universal intermittency distribution" for a transitional boundary layer. Although the intermittency is a function of both the streamwise distance and the normal distance,

Dhawan and Narasimha claim the latter has only a secondary effect. An excellent review of intermittency as a feature of laminar-turbulent transition can be found in Narasimha (1985).

Recently, Kuan (1987), Sohn and Reshotko (1991) and Young et al. (1993) have recognized that the turbulent and non-turbulent parts in a boundary layer are not fully-turbulent flow and Blasius flow respectively, but turbulent-like and laminar-like behavior. Sharma et al. (1982) and Walker and Gostelow (1990) measured the intermittency distribution in adverse pressure gradient, and indicated that the intermittency in the transitional flow was independent of the pressure gradient. The use of intermittency in estimating transitional behavior in gas turbine engines is discussed by Mayle (1991) and Walker (1993).

1.2. Overview of Turbulence Models

Transition prediction methods based on the classical linear/non-linear stability analysis, although widely used, cannot describe the evolution of transition for elevated freestream turbulence levels. From the measurements of Suder et al. (1988) and by Sohn et al. (1991) for Tu > 1%, one should note that the disturbance spectra are of turbulent character even while the mean flow is still laminar. It is therefore thought appropriate to use turbulent flow methods to simulate the transitional boundary layer. These methods use the Reynolds-averaged equations with closure approximations to calculate the turbulent quantities from the pre-transition flow to fully turbulent flow.

These methods are considered here in attempting to mimic the transitional boundary layer.

The first and simplest model used in turbulent calculations is that based on the Prandtl mixing length hypothesis. Considering shear layers with only one significant turbulent stress $\overline{u'v'}$ and velocity gradient $(\partial U/\partial y)$, the shear stress can be formulated through an eddy viscosity based on a mixing length l_m:

$$-\rho\overline{u'v'} = \mu_t\left(\frac{\partial U}{\partial y}\right) \tag{1-1}$$

$$\mu_t = \rho V_t l_m = \rho l_m^2\left|\frac{\partial U}{\partial y}\right| \tag{1-2}$$

The eddy viscosity is determined by the velocity scale V_t and length scale l_m, and this relationship is known as the Kolmogorov-Prandtl expression. The only unknown parameter is the mixing length l_m whose distribution over the flowfield has to be prescribed by empirical data. From numerical testing of the model, a lot of experience has been gathered for various flow conditions, in particular for wall boundary layers (see Cebeci and Smith, 1974, Crawford and Kays, 1976).

Although the model has some success in fully turbulent flow, there are a few shortcomings in this model when it is applied to transitional flow. First, because the transition location and its process must be specified with the aid of correlations, the model cannot by itself predict the onset of transition. Second, the model is based on the assumption that the flow is in local equilibrium, that is, the turbulent energy is

dissipated at the same rate at any point of the flow. This means the turbulent energy at one point cannot influence any other parts of the flow. Therefore, the model cannot take the freestream turbulence into account. Third, the turbulent transport will be zero wherever the mean velocity gradient is zero. This contradicts many experimental results.

More general models require considering the transfer of turbulence within the flow. To do so, we must introduce the transport equation of turbulence quantities. The transport equation for a turbulent quantity ϕ can usually be written as

$$\frac{D\phi}{Dt} = \nabla \cdot \left(\Gamma_\phi \nabla \phi \right) + S_\phi \tag{1-3}$$

Here, D/Dt is the substantial derivative, Γ_ϕ is the generalized diffusion coefficient and S_ϕ is the net source. The equation describes the convection, diffusion and net production of the quantity ϕ. The more turbulent transport quantities involved, the more transport equations are used. The number of turbulence differential equations used identifies the category of the n-equation model.

If velocity fluctuations are characterized by the square root of turbulent kinetic energy k, we may overcome some of the limitations of the mixing length model. The turbulent kinetic energy is a direct measure of normal stresses in three directions. Thus most one-equation turbulence models employ a transport equation of turbulent kinetic energy k,

$$\frac{Dk}{Dt} = \frac{\partial}{\partial x_i}\left[\left(\nu + \frac{\nu_t}{\sigma_k}\right)\frac{\partial k}{\partial x_i}\right] + P_k - \varepsilon \tag{1-4}$$

In this equation, the left-hand-side is convection; the first term on right-hand-side is diffusion; and P_k and ε are the production and dissipation rate of turbulent kinetic energy respectively. The coefficient σ_k is the effective ratio of the diffusion of turbulent momentum to the diffusion of turbulent kinetic energy, and is assumed to be constant. The dissipation rate ε and turbulent viscosity are defined as

$$\varepsilon = C_D \frac{k^{3/2}}{L_\varepsilon} \tag{1-5}$$

$$\nu_t = C_\mu \sqrt{k} L_\mu \tag{1-6}$$

where C_D and C_μ are constants for high Reynolds number flow; L_ε and L_μ are the length scales that characterize the flow. These length scales are usually specified empirically and are the same in the log-law regions. In the vicinity of a wall, they have different roles: L_μ as the length scale for viscosity and L_ε as for dissipation. Both are formulated as functions of the normal distance from wall and are diminished by viscous action. As for boundary conditions, wall functions cannot be used in transitional boundary layer calculations because they are generated by log-region of the turbulent boundary layer, which does not exist before transition. The major advantage of the one-equation model is that the shear stress does not depend on mean velocity gradient. An important shortcoming of the model is the inability to account for the transport effect on the turbulence length scales. This is a direct consequence of the model's assumption that length scale distributions are prescribed empirically.

McDonald and Fish (1973) used the integral k equation to study freestream turbulence and surface roughness effects in transitional boundary layers. Empirically based formulae were used to input values of the dissipation length scale, the mixing length and a number of the structure coefficients that were required in the formulation. A damping factor was used to control the length scale within the viscous sublayer, which in turn controlled the transition. They obtained very good agreement between experiment and prediction. However, Daniels and Browne (1981) applied the model on a gas turbine blade and found that the method did not show improvement over the mixing length model.

The two-equation turbulence model usually uses the equation of turbulent kinetic energy and a transport equation of some other turbulent quantity to relate to the length scale. The choice of variable in the length-scale-determining equation is very wide. It could be the turbulent dissipation rate ε, pseudovorticity ω, turbulent time scale τ, length scale l, or their combination, such as kl and ω^2. These variables are related to each other, thus the equation can be transformed from one to another with the modification of source terms. Among these two-equation models, the k-ε model is currently the most popular one for turbulence closure. The dissipation rate ε and its equation are usually defined as

$$\varepsilon = \frac{\nu}{2}\overline{\left(\frac{\partial u_i'}{\partial x_j'} + \frac{\partial u_j'}{\partial x_j'}\right)^2} \tag{1-7}$$

$$\frac{D\varepsilon}{Dt} = \frac{\partial}{\partial x_i}\left[\left(\nu + \frac{\nu_t}{\sigma_\varepsilon}\right)\frac{\partial \varepsilon}{\partial x_i}\right] + (c_{\varepsilon 1}P_k - c_{\varepsilon 2}\varepsilon)\frac{\varepsilon}{k} \tag{1-8}$$

At high Reynolds number, the dissipation rate is related to the turbulent vorticity and is called "isotropic dissipation". The transport equation represents physical effects analogous to those in the k equation, that is, the convection of ε is balanced by diffusion and by production and destruction processes.

Equations (1-4) and (1-8) constitute the k-ε model which employs the Boussinesq eddy viscosity concept and relates the eddy viscosity to k and ε via the Kolmogorov-Prandtl formula:

$$-\overline{u_i u_j} = \nu_t \left(\frac{\partial U_i}{\partial x_j} + \frac{\partial U_j}{\partial x_i} \right) - \frac{2}{3} \delta_{ij} k \tag{1-9}$$

$$\nu_t = C_\mu V_t L = C_\mu \frac{k^2}{\varepsilon} \tag{1-10}$$

where the velocity scale V_t is defined as $\sqrt{k}$ and length scale L is $k^{3/2}/\varepsilon$. The original k-ε model is devised for high Reynolds number flow in which effects of molecular viscosity are unimportant. In regions close to walls, the character of the motion is significantly changed. Jones and Launder (1972, 1973) introduced the low-Reynolds-number (LRN) form of the k-ε model which accounts for the near-wall effect and allows continuous computation from the freestream to the wall. The modification basically damps the production/destruction terms of the ε equation and the eddy viscosity. After Jones and Launder's modification, a lot of LRN k-ε models were proposed. Patel et al. (1985) systematically evaluated eight LRN k-ε models and showed that each model may have flaws in certain flows. They concluded that the k-ε

models of Launder and Sharma (1974), Chien (1982), Lam and Bremhorst (1981), and the k-ω^2 model of Wilcox and Rubesin (1980) yield comparable results and perform considerably better than the others for fully turbulent boundary layers.

The standard k-ε model is based on the assumption that the eddy viscosity is the same for all components of Reynolds stress. For simple shear flow, this assumption does not influence the calculation since the dominant Reynolds stress is $\overline{u'v'}$ alone. For recirculation flows, the normal stress and shear stress are of the same order in the momentum equations, but they are usually much smaller than the convection and pressure terms. Therefore the nonisotropic nature of Reynolds stress is unimportant in this case. However, in some flow situations, an anisotropic eddy viscosity is necessary. The k-ε model must be modified by introducing nonlinear terms in the linear Boussinesq approximation. Anisotropic k-ε models, also called nonlinear k-ε models, have been proposed by Nisizima and Yoshizawa (1987), Speziale (1987) and Myong and Kasagi (1990). To the best of the author's knowledge, these models have not yet been used for transitioning boundary layers.

Jones and Launder (1973) explored the capability of the LRN k-ε model in predicting transition in pipe flow and channel flow. Although showing excellent agreement between experiment and predictions for laminar and fully turbulent regimes, the calculated transition occurs at a too low a Reynolds number and is too abrupt.

Wilcox (1975, 1977) used Saffman and Wilcox's k-ω^2 model for prediction of the transitional boundary layer. The results show that the calculated start of transition is in good agreement with the experimental data for cases with very low freestream

turbulence intensity. Daniels and Browne (1981) applied Wilcox's model to calculate the heat transfer rate to a gas turbine blade. The transition region on the suction surface is not well predicted. On the pressure surface, the agreement between prediction and experiment is generally poor. They conclude that the model has no obvious advantages over the mixing length models.

Wang, Jen and Hartel (1985) predicted the transitional flow on a flat plate with high freestream intensity (up to 10%) by the Jones and Launder LRN k-ε model. No experimental data within the transition regime were compared. They also applied the model on turbine airfoils. Their predicted heat transfer coefficients on the pressure side of the airfoil agree well with experimental data. On the suction side of airfoil, the heat transfer is overpredicted for transitional and turbulent regions.

Rodi and Scheuerer (1985) studied the flow over a turbine blade using the Lam and Bremhorst (1981) LRN k-ε model. The initial profiles of k and ε were proposed from empirical correlations. They are the first to calculate the freestream values of k and ε from the simplified k and ε equations. The model gives general agreement with experiment at a relatively high level of freestream turbulence and with pressure gradient. The results also show that the onset of transition is well predicted, but the length of transition is consistently under-predicted.

Schmidt and Patankar (1988) modified the production term of the turbulent kinetic energy equation in the Lam and Bremhorst LRN k-ε model. The limited production of turbulent kinetic energy controlled the onset and progress of transition. The model was referred to as the Production Term Modification (PTM) model. The

PTM model parameters were calibrated with freestream turbulent intensity to match the correlation of Abu-Ghannam and Shaw (1980). The comparison of PTM model prediction with the experimental flat plate data and turbine blade data is excellent even in the transition region. They also demonstrated that the sensitivity to starting location and initial profiles of k and ε is largely reduced. Sullivan (1988) coupled the Chien k-ε model with an intermittency model and the PTM model to investigate transitional flow of flat plate and circular cylinder flows. He obtained good prediction of transition for the flat plate but generally poor agreement for the start of transition on the cylinder. Although the PTM model has given reasonable results in transitional boundary layers, it is basically an ad hoc model. For the elevated turbulence environment, the turbulent kinetic energy is gradually diffused from the freestream to the boundary layer. The PTM model does not provide for this process but correlates the turbulent production to freestream turbulent intensity. In other words, the PTM does not actually reflect the *transport* features of the transitional boundary layer in an elevated freestream turbulence environment.

Recently, Fujisawa (1990) evaluated five different LRN k-ε models, namely Launder and Sharma (1974), Chien (1982), Lam and Bremhorst (1981), Nagano and Hishida (1987), and Myong and Kasagi (1988) in the calculation of transitional boundary layers with freestream turbulence. He found that the Launder and Sharma model gives better performance than the other models, but fails to reproduce the pressure gradient effect. Savill (1990) compiled 16 turbulence models to simulate two benchmark tests, T3A and T3B, issued by the European ERCOFTAC science committee. He concluded that the skin friction C_f and shape factor H are best described by the Launder and Sharma k-ε model within the two-equation turbulence

model category. The common discrepancies of the predictions by two equation models are that the peak C_f (overshoot) is not captured; the prediction of transition length is rather too short; and the fully turbulent level of C_f is only approached asymptotically from below.

The work of Yang and Shih (1992) suggests that a new time scale based k-ε formulation with an intermittency factor can improve the prediction of the transitional boundary layer. The intermittency factor used by Yang is defined by a correlation with the boundary layer shape factor through the transition region. They also point out that the Launder-Sharma model does not predict fully turbulent boundary layers very well, although it has better capability in transition zone prediction.

To describe the intermittent character in turbulent flow, the conditioned continuity, momentum, energy and intermittency factor equations were developed by Byggstoyl and Kollmann (1981, 1986), Vancoillie and Dick (1988), and Cho and Chung (1992). The model contains the equations for intermittency factor, the turbulent zone and non-turbulent zone mean velocities, and turbulent kinetic energy and dissipation rate for the turbulent zone. Simon and Stephens (1991), followed the development of Vancoillie and Dick, using the intermittency factor in conditioned transport equations and a LRN k-ε model. The intermittency factor is prescribed algebraically and based on the knowledge of the transition length. Simon and Stephens adopted the approach of Narasimha (1985) which expressed the transition length in terms of the transition Reynolds number and a turbulent spot formation rate from experiments. The results in general are in good agreement with experimental

data. But, so far the predictions are only for zero pressure gradient boundary layers with elevated turbulence environment.

In the conditioned turbulence modeling, if the intermittency factor of transition is not known beforehand, we must instead solve the differential equation of intermittency factor. Since the equation is based on the dynamics of the interface between turbulent and non-turbulent zones for free boundary shear flow, the distinction of turbulent/non-turbulent zones is not clear if the turbulence is of small amplitude in the low and high frequency ranges simultaneously. Thus all the low amplitude fluctuations (which are usually at high frequency) are eliminated by the modeling itself. Furthermore, the evolution equation of the intermittency factor itself is questionable because there is no physical basis for a conservation equation for intermittency factor.

One of the turbulent characteristics that is not clearly represented by conventional k-ε models is the turbulent kinetic energy cascade. The large eddies, which are associated with the low frequency fluctuations, are determined by the boundary conditions of the flow and contribute most of the kinetic energy. On the other hand, the small eddies are responsible for the energy dissipation. The kinetic energy cascade means that the large eddies extract energy from the mean flow and transfer it to the small eddies by vortex stretching.

Schiestel (1974) introduced a multiple-time-scale model while Hanjalic, Launder and Schiestel (1980) developed a scheme in which the turbulent energy spectrum is split into low, intermediate and high wave number regions, as illustrated in

figure 1-1. The low wave number region or "production" region transfers spectral energy to the high wave number region or "dissipation region". Between these two regions, the energy is just transferred through it, thus it is called the "transfer region". The kinetic energy within the production and transfer regions are k_p and k_t respectively while the dissipation zone contains a negligible amount of turbulent kinetic energy. The total turbulent kinetic energy k will be the sum of k_p and k_t. The kinetic energy transfer rates $\tilde{\varepsilon}_p$ and $\tilde{\varepsilon}_t$ are associated with the energy out of the production and transfer regions; the latter is equal to the energy dissipation rate ε. In single-point closure turbulence models, the energy transfer rates are simply $\tilde{\varepsilon}_p = \varepsilon$, that is the energy spectrum has no effect in the turbulence modeling. This is usually not true however, particularly in boundary layer flow.

Under this split-spectrum concept, there will be four transport equations in two-scale modeling to describe the turbulence, that is, two turbulent kinetic energy equations and two energy transfer rate equations. The eddy viscosity stress-strain formulation is still used in the model. As might be expected, the transport equations of the lowest wave number region will have the same formulation as those in single-scale k-ε models. If the spectrum is split into more slices, the number of transport equations are increased. Therefore, the two-scale approach is an extension of single-scale k-ε model that could involve more physics and bring some benefits within reasonable computational costs.

Hanjalic et al. (1980) applied the multiple-scale concept to the decay of grid turbulence passed through a sudden contraction; plane and axisymmetric jets; and fully turbulent boundary layer. All the computational results show that the model gives

striking improvement over those employing the single-scale concept. Fabris, Harsha and Edelman (1981) tested the multiple-scale modeling of boundary layer flow for scramjet application. An appreciable overall improvement of prediction was observed. Kim and Chen (1987) calibrated the model coefficients by grid turbulence, homogeneous shear flow and the equilibrium turbulent boundary layer. Kim applied the model to many different problems (see Kim, 1988, 1991, 1992) and generally compared favorably with the experimental data. Recently, Duncan, Liou and Shih (1993) also calibrated the model by grid turbulence and homogeneous shear flow and tested it for boundary-free turbulent shear flow. The results show that the model gives good predictions.

In the calibration of model coefficients, Kim and Chen (1987) and Duncan et al. (1993) assumed that the grid turbulence obeys a decaying power law. The ratio of the turbulent kinetic energy of production and transfer regions is kept constant. It follows that one model coefficient can be obtained directly from the exact solution of simplified turbulence model for grid turbulence. In homogeneous shear flow, both of them assumed that the ratios of turbulent production to dissipation rate $P_k/\tilde{\varepsilon}_t$ and the energy transfer rate to dissipation rate $\tilde{\varepsilon}_p/\tilde{\varepsilon}_t$ are constants, so that

$$\frac{\tilde{\varepsilon}_p}{k_p}\frac{dk_p}{d\tilde{\varepsilon}_p}=\frac{\tilde{\varepsilon}_t}{k_t}\frac{dk_t}{d\tilde{\varepsilon}_t}=\frac{\tilde{\varepsilon}_t}{k}\frac{dk}{d\tilde{\varepsilon}_t}=\text{constant} \tag{1-11}$$

With the help of experimental data, all model coefficients can be determined in Duncan's model. Since Kim developed the model with two more coefficients, he used the equilibrium boundary layer (where the production equals to the dissipation rate) in

providing two constraint conditions to determine these coefficients. In all models mentioned above, the wall function was used when calculating the flow close to a wall.

In summary, review of literature reveals that the zero- and one-equation models cannot predict the bypass transitional boundary layers very well. The LRN two-equation model must have some modifications to mimic the behavior of transitional boundary layers. The modification could be the PTM, the intermittency factor to eddy viscosity, the intermittency model embedded in the conditioned transport equations etc. On the other hand, the multiple-scale model gives promise not only of a better description of the turbulence but also can represent the freestream spectrum effects in prediction of the transitional boundary layer. However, all the aforementioned multiple-time-scale k-ε modeling are closely derived from the Schiestel's formulation without detailed evaluation. In this work, the model equations will be derived from the two-point velocity correlation. With some different assumptions, the final formulations are different from the other multiple-scale models. The model coefficients are also calibrated from grid turbulence and homogeneous shear flow but by exact solution of a simplified version of the model. As a result, some of the model coefficients are not constants but depends on the spectrum shape of the freestream turbulence. All of these will be developed in the next chapter.

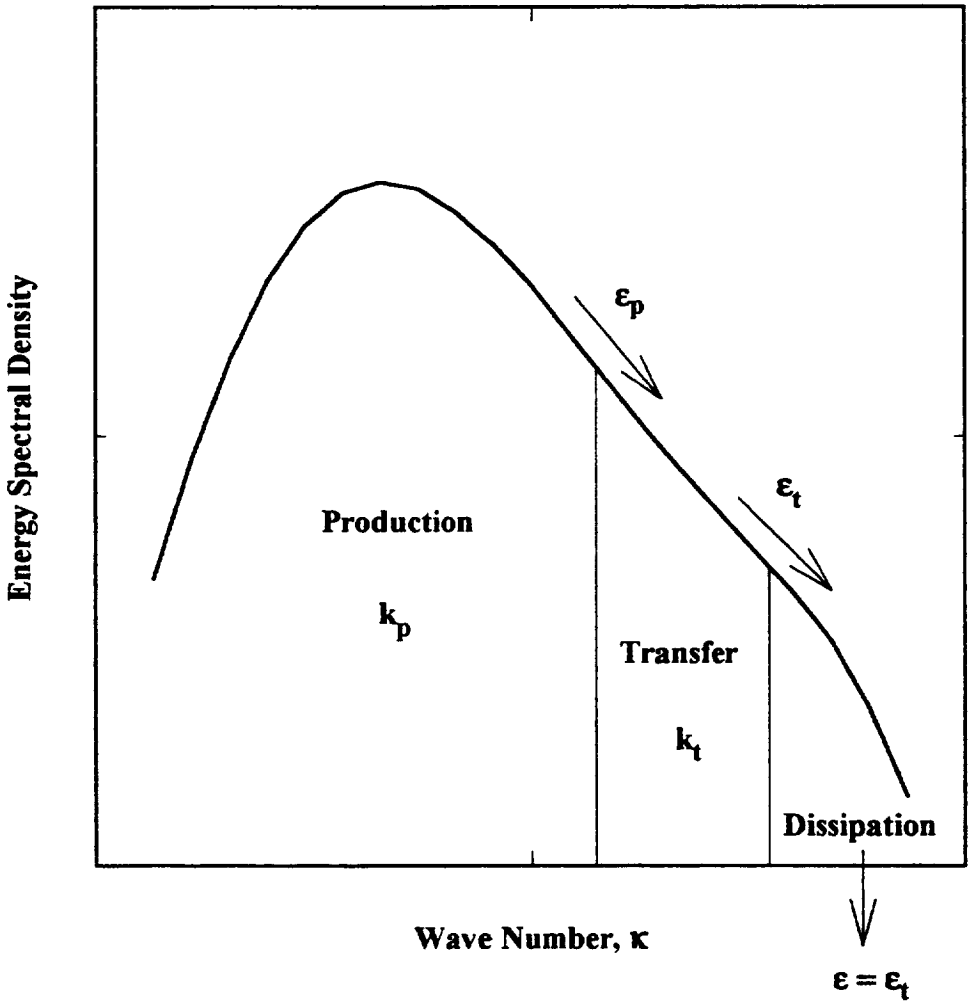

Figure 1-1 Description of the multiple-scale turbulence model.

CHAPTER TWO

MATHEMATICAL MODEL AND NUMERICAL METHOD

2.1 The Boundary Layer Equations

The problem considered is the region close to a solid wall where viscous effects are as important as inertia effects. The viscous layer can be described by the boundary layer equations in which viscous diffusion in the streamwise direction is negligible compared to that in the transverse direction. The boundary layer equations are derived from the Navier-Stokes equation by the order-of-magnitude technique. The derivation of these equations can be found in many text books, and is not repeated here.

For a two-dimensional incompressible turbulent boundary-layer flow, x is the streamwise direction and y is the direction normal to the wall, the conservation of mass and momentum can be written as follows:

$$\frac{\partial U}{\partial x}+\frac{\partial V}{\partial y}=0 \tag{2-1}$$

$$\rho U\frac{\partial U}{\partial x}+\rho V\frac{\partial U}{\partial y}=-\frac{dP}{dx}+\frac{\partial}{\partial y}\left(\mu\frac{\partial U}{\partial y}-\rho\overline{u'v'}\right) \tag{2-2}$$

$$\rho U\frac{\partial H}{\partial x}+\rho V\frac{\partial H}{\partial y}=\frac{\partial}{\partial y}\left[\frac{\mu}{\mathrm{Pr}}\frac{\partial H}{\partial y}-\rho\overline{h'v'}+\mu\left(1-\frac{1}{\mathrm{Pr}}\right)U\frac{\partial U}{\partial y}\right] \tag{2-3}$$

where U and V are the time averaged mean velocities, ρ is the density, u' and v' are the instantaneous velocity fluctuations, and the overbar implies the time average of the fluctuation quantities. In the energy equation, h is the enthalpy, H is the total enthalpy and is defined as

$$H = h + \frac{1}{2}U^2 \tag{2-4}$$

Assuming that the gas is ideal and the specific heat of the gas is constant, the equation of state and the static enthalpy can be written

$$P = \rho RT \tag{2-5}$$

$$h = C_p T \tag{2-6}$$

Here, $-\rho\overline{u'v'}$ is the Reynolds stress and $-\rho\overline{h'v'}$ is the turbulent heat transfer rate. To solve equations (2-1) to (2-3), we must use some empirical formulation for Reynolds stress and turbulent heat transfer rate. By the Boussinesq assumption, we define the turbulent eddy viscosity to relate the Reynolds stress to the mean flow field.

$$-\rho\overline{u'v'} = \mu_t\left(\frac{\partial U}{\partial y}\right) \tag{2-7}$$

An analogous quantity, the eddy diffusivity of heat, can be defined for the turbulent heat transfer rate. The eddy diffusivity of heat is assumed proportional to the Reynolds stress

$$-\rho\overline{h'v'} = \frac{\mu_t}{\mathrm{Pr}_t}\left(\frac{\partial U}{\partial y}\right) \tag{2-8}$$

where Pr_t is the turbulent Prandtl number. We cannot expect an exact analogy between heat transfer and momentum transfer in turbulent flow. However, Pr_t is usually of the order of unity and in the absence of better information, can be considered nearly constant. In this work, the turbulent Prandtl number is assumed constant at *0.9*. Substituting equations (2-7) and (2-8) into equations (2-2) and (2-3), we have

$$\rho U\frac{\partial U}{\partial x} + \rho V\frac{\partial U}{\partial y} = -\frac{dP}{dx} + \frac{\partial}{\partial y}\left(\mu_{eff}\frac{\partial U}{\partial y}\right) \tag{2-9}$$

$$\rho U\frac{\partial H}{\partial x} + \rho V\frac{\partial H}{\partial y} = \frac{\partial}{\partial y}\left(\frac{\mu_{eff}}{\mathrm{Pr}_{eff}}\frac{\partial H}{\partial y}\right) + \frac{\partial}{\partial y}\left[\left(1-\frac{1}{\mathrm{Pr}_{eff}}\right)\mu_{eff}\frac{\partial}{\partial y}\left(\frac{U^2}{2}\right)\right] \tag{2-10}$$

where $\mu_{eff} = \mu + \mu_t$ (2-11)

$$\mathrm{P_{r}}_{eff} = \frac{\mu_{eff}}{\frac{\mu}{\mathrm{P_r}} + \frac{\mu_t}{\mathrm{P_{r}}_t}} \tag{2-12}$$

are the effective viscosity and effective Prandtl number respectively. Equations (2-9) and (2-10) are the governing equations for both laminar and turbulent flows in the absence of body forces and heat sources. When the flow is laminar and the Reynolds stress is zero, the equations become the steady laminar boundary layer equations. The correct prediction of eddy viscosity is determined by the appropriate turbulence model.

2.2 Two-Scale Turbulence Model

The turbulence model proposed herein employs two independently calculated scales with which to characterize different turbulent interactions. The concept is based on the split-spectrum methodology, introduced by Schiestel in his Ph.D. work and further developed by Hanjalic et al. (1980, 1983) and Schiestel (1983a, 1983b, 1987). In the derivation of the model, first, the dynamic equation of the two-point velocity correlation equation is Fourier transformed. Then partial turbulent stresses are derived by the partial integration over each slice (or shell) of the three-dimensional energy spectrum. By tensor contraction, we obtain the partial turbulent kinetic energy equation. The transport equation of energy flux through the energy spectrum can be obtained from straightforward algebra. The derivation of these equations can be found in detail in Appendix A. The resulting equations of the model are

$$U\frac{\partial k_p}{\partial x}+V\frac{\partial k_p}{\partial y}=\frac{\partial}{\partial y}\left[\left(\nu+\frac{\nu_t}{\sigma_{kp}}\right)\frac{\partial k_p}{\partial y}\right]+P_k-\varepsilon_p \tag{2-13}$$

$$U\frac{\partial k_t}{\partial x}+V\frac{\partial k_t}{\partial y}=\frac{\partial}{\partial y}\left[\left(\nu+\frac{\nu_t}{\sigma_{kt}}\right)\frac{\partial k_t}{\partial y}\right]-\varepsilon_t \tag{2-14}$$

$$U\frac{\partial \varepsilon_p}{\partial x}+V\frac{\partial \varepsilon_p}{\partial y}=\frac{\partial}{\partial y}\left[\left(\nu+\frac{\nu_t}{\sigma_{\varepsilon p}}\right)\frac{\partial \varepsilon_p}{\partial y}\right] +\left(C_{p1}f_{p1}P_k-C_{p2}f_{p2}\varepsilon_p\right)\frac{\varepsilon_p}{k_p} \tag{2-15}$$

$$U\frac{\partial \varepsilon_t}{\partial x}+V\frac{\partial \varepsilon_t}{\partial y}=\frac{\partial}{\partial y}\left[\left(\nu+\frac{\nu_t}{\sigma_{\varepsilon t}}\right)\frac{\partial \varepsilon_t}{\partial y}\right] +C_{t1}f_{t1}\left(\frac{k_t}{k_p}\right)^{3/2}\frac{\varepsilon_p^2}{k_p}-C_{t2}f_{t2}\frac{\varepsilon_t^2}{k_t} \tag{2-16}$$

In these equations, k_p and k_t are the partial turbulent kinetic energy in the *production* zone and *transfer* zone respectively; ε_p and ε_t are the *net* energy fluxes transferred out of each zone. In each equation, there are convection, diffusion, production and destruction terms. Damping functions f are added as appropriate to accommodate near-wall viscous behavior. The first term on the right-hand-side in each equation is diffusion and is approximated by the effective viscosity. The contribution of turbulent diffusion for each quantity is related to the eddy viscosity through the coefficient σ. This is not true in general, but in this work, the coefficient σ's are assumed to be constants. The production of the turbulent kinetic energy P_k is given by

$$P_k = \nu_t\left(\frac{\partial U}{\partial y}\right)^2 \tag{2-17}$$

The eddy viscosity model is generally written as $\nu_t = C_\mu \upsilon \ell$, where υ and ℓ are the turbulent characteristic velocity and length scales, respectively. In the proposed

model, $(k_p + k_t)^{1/2}$ is used as the characteristic velocity, and the length scale is characterized by that in the production region, i.e. $\ell = k_p^{3/2} / \varepsilon_p$. In other words, the turbulent energy is produced by the large eddies only. Hence, the eddy viscosity is written as

$$\nu_t = C_\mu f_\mu (k_p + k_t)^{1/2} \frac{k_p^{3/2}}{\varepsilon_p}. \tag{2-18}$$

Here, C_μ is a constant and set to be *0.09* and f_μ is the damping function incorporating the near wall behavior. In this formulation, the single-scale model will be recovered if the transfer zone turbulent kinetic energy is set to zero.

There are eight model constants, C_{p1}, C_{p2}, C_{t1}, C_{t2}, σ_{kp}, σ_{kt}, $\sigma_{\varepsilon p}$ and $\sigma_{\varepsilon t}$, and five damping functions, f_μ, f_{p1}, f_{p2}, f_{t1} and f_{t2}, in the transport equations. These eight constants, compared to four in the single-scale k-ε model, are determined from the analysis of grid-generated isotropic turbulence, homogeneous shear flow, near wall equilibrium flow, and adjusted by numerical optimization. The calibration of model constants is detailed in Appendix B and the results are as follows:

C_{p1}	C_{p2}	σ_{kp}	σ_{kt}	$\sigma_{\varepsilon p}$	$\sigma_{\varepsilon t}$
1.55	*1.90*	*1.0*	*1.0*	*1.3*	*1.3*

with $C_{t1} = \dfrac{(\gamma - 1)^2 (C_{p2} - 1)}{\sqrt{r_s} - \sqrt{r_g}(\gamma - 1)^2}$ and $C_{t2} = C_{t1}\sqrt{r_g} + C_{p2}$ (2-19a,b)

where $r_s = 0.3$ and $\gamma = 1.625$. It should be noted that the coefficients C_{t1} and C_{t2} are not constants for all cases but depend on the turbulent kinetic energy ratio r_g $(= k_t/k_p)$ in the external flow of the boundary layer. In this way, the turbulence model is automatically tuned to the free-stream energy spectrum. The damping functions are used to provide the proper influence of the wall especially in the viscous sublayer. These functions will be unity if there is no wall in the flow or far away from the wall. They are characterized by the turbulent Reynolds number and will be discussed in the next section.

2.3 The Damping Functions

Momentum transfer in the boundary layer is basically controlled by turbulent diffusion in the presence of a wall. The wall suppresses the mixing effect of turbulent flow and generates the kinematic blocking effect especially in the normal turbulent fluctuation velocity. The turbulence model must be modified, by damping the eddy viscosity, to include this near-wall behavior especially in the viscous sublayer. It follows that the damping functions in each equation must have the proper variation with y to have an asymptotically consistent solution.

The variation of the instantaneous velocity components (u', v' and w') near a wall can be expressed by the Taylor series

$$u' = a_1 y + a_2 y^2 + \ldots \qquad \text{(2-20a)}$$

$$v' = \qquad b_2 y^2 + \ldots \qquad \text{(2-20b)}$$

$$w' = c_1 y + c_2 y^2 + \ldots \tag{2-20c}$$

where the coefficients a_i, b_i and c_i are functions of time, but their time averages are zero. This formulation leads to

$$k = k_p + k_t = Ay^2 + By^3 + \ldots \tag{2-21}$$

$$\varepsilon = \varepsilon_p + \varepsilon_t = 2(A + 2By + \ldots) \tag{2-22}$$

$$-\overline{u'v'} = \nu_t \frac{\partial U}{\partial y} = -\overline{a_1 b_2} y^3 - \left(\overline{a_1 b_3} + \overline{a_2 b_2}\right) y^4 - \ldots \tag{2-23}$$

where $A = \frac{1}{2}\left(\overline{a_1^2} + \overline{c_1^2}\right)$ and $B = \overline{a_1 a_2} + \overline{c_1 c_2}$ (2-24a,b)

Although in the log-law region where the energy production is approximately equal to the net dissipation and the major contribution of turbulent kinetic energy is from large eddies (i.e. production region), there is no reason to assume that in the near-wall region the asymptotic behavior of k_t has a different order of that of k_p. Similarly, equations (2-16) and (2-17) suggest that ε_p and ε_t are of the same order.

$$k_p = A_p y^2 + B_p y^3 + \ldots \qquad k_t = A_t y^2 + B_t y^3 + \ldots \tag{2-25a,b}$$

$$\varepsilon_p = 2(A_p + 2B_p y + \ldots) \qquad \varepsilon_t = 2(A_t + 2B_t y + \ldots) \tag{2-25c,d}$$

where $A = A_p + A_t$ and $B = B_p + B_t$. Since $\partial U / \partial y = O(1)$, and the near-wall asymptotic behavior of eddy viscosity ν_t is $O(y^3)$, equation (2-21) tells us that the

damping function f_μ has to be $O(y^{-1})$. In the present study of the modeling of f_μ, we first consider two different length scales, one is the length scale of energy containing eddies L_p, the other is the Kolmogorov microscale η. These length scales are defined as

$$L_p = C_L \frac{k_p^{3/2}}{\varepsilon_p} \propto \frac{k^{3/2}}{\varepsilon} \quad \text{and} \quad \eta = \left(\frac{\nu^3}{\varepsilon}\right)^{1/4} \tag{2-26a,b}$$

These length scales L_p and η can be related as

$$\frac{L_p}{\eta} \propto R_t^{3/4} \quad \text{where} \quad R_t = \frac{k^2}{\nu\varepsilon} \tag{2-27a,b}$$

Here, $R_t^{3/4}$ serves as a link between two length scales and behaves as $O(y^3)$ in the near-wall region. Thus, the proposed damping function f_μ is as

$$f_\mu = \left[\frac{1-\exp\left(-R_t^{1/4}\right)}{1-\exp\left(-A_\mu R_t\right)}\right]\left[1-\exp\left(-y^+/B_\mu\right)\right]^2 \tag{2-28}$$

where A_μ and B_μ are constants (*0.25* and *26* respectively) and y^+ is the wall coordinate defined as yU_τ/ν. When away from the wall, the eddy viscosity is determined by the large eddies; but very close to the wall, the eddy viscosity is dominant by small eddies. It can also be seen that $L_p = O(y^3)$ and $\eta = O(1)$ in the near-wall region, thus the damping function f_μ has the proper asymptotic behavior near a wall $f_\mu \propto y^{-1}$.

The function f_{p2} is introduced primarily to incorporate the different decay laws of the grid-generated turbulence in the ε_p-equation (see Appendix B). It is written as

$$f_{p2} = 1 - A_p \exp\left(-R_t^2 / B_p^2\right) \tag{2-29}$$

where $A_p = 0.3$ and $B_p = 6$. In the near-wall region where $\nu >> \nu_t$ and the convection terms are negligibly small, the ε_p-equation becomes

$$\nu \frac{\partial^2 \varepsilon_p}{\partial y^2} + C_{p1} f_{p1} \frac{P_k \varepsilon_p}{k_p} - C_{p2} f_{p2} \frac{\varepsilon_p^2}{k_p} = 0 \tag{2-30}$$

In considering the behavior of near-wall turbulence where the production is much less than the destruction, the equation (2-30) tells that the damping function f_{p2} must vary as in $O(y^2)$ and f_{p1} can be in order lower than $O(y^2)$. Thus the following function is proposed

$$f_{p2} = \left[1 - A_p \exp\left(-R_t^2 / B_p^2\right)\right]\left[1 - \exp\left(-R_y / \lambda_p\right)\right] \tag{2-31}$$

where the constant $\lambda_p = 8$ is decided by numerical experiment and R_y defined as $\sqrt{k}y/\nu$. Near the wall, $R_y = O(y^2)$, the equation (2-31) varies $f_{p2} = O(y^2)$ and satisfy the limiting behavior. In order to simplify the model, the damping function f_{p1} is defined as unity. Similarly, approaching the wall, the ε_t-equation becomes

$$\frac{\partial^2 \varepsilon_t}{\partial y^2} + C_{t1} f_{t1} \left(\frac{k_t}{k_p} \right)^{3/2} \frac{\varepsilon_p^2}{k_p} - C_{t2} f_{t2} \frac{\varepsilon_t^2}{k_t} = 0 \tag{2-32}$$

which indicates that both damping functions f_{t1} and f_{t2} are $O(y^2)$. In the present model, in order to have the proper balance between production and destruction in transfer region, the damping functions f_{t1} and f_{t2} are defined as

$$f_{t1} = f_{t2} = \left[1 - A_p \exp\left(-R_t^2 / B_p^2 \right) \right] \left[1 - \exp\left(-R_y / \lambda_t \right) \right] \tag{2-33}$$

The numerical value $\lambda_t = 10$ is decided on the basis of numerical experiment, but this number is not sensitive to the calculation.

2.4 Numerical Solution Procedure

Because the purpose of this research is primarily to developing the turbulence model and test its application to the transitional boundary layer, any numerical method is suitable as long as it can solve the parabolic type equations. The Patankar-Spalding method is used throughout this work simply because the author is familiar with this method. A detailed description of this algorithm can be found in Spalding (1977) and Patankar (1980, 1988); only a summary will be given here.

The algorithm of Patankar-Spalding is based on solving the governing equation in x-ω coordinates, instead of x-y coordinate. Here, ω is the normalized stream function coordinate ψ after a von Mises transformation. The transformation eliminates

the V velocity from the continuity and momentum equations and reduces the number of governing equations by one. The coordinate ω is defined by

$$\omega = \frac{\psi - \psi_I}{\Delta\psi}, \quad \text{with} \quad \Delta\psi = \psi_E - \psi_I \tag{2-34}$$

where the subscripts I and E denote the internal and external surfaces of the computational domain. The use of the ω coordinate, always between zero and unity, allows the grid system to follow the growth of the boundary layer, and therefore retains the same grid system irrespective of the actual boundary-layer thickness (see Figure 2-1). As Long as ψ_I and ψ_E are varied appropriately with x, the x-ω coordinate could provide the same accuracy along the space-marching computation. With the help of equation (2-34), all the transport equations can be written in a general form, such as

$$\frac{\partial\phi}{\partial x} + (a + b\omega)\frac{\partial\phi}{\partial\omega} = \frac{\partial}{\partial\omega}\left(c\frac{\partial\phi}{\partial\omega}\right) + d \tag{2-35}$$

where $a = -\frac{1}{\Delta\psi}\frac{d\psi_I}{dx}$, $\qquad b = -\frac{1}{\Delta\psi}\frac{d}{dx}(\Delta\psi)$ (2-36a,b)

$$c = \frac{\rho U}{(\Delta\psi)^2}\Gamma_\phi, \qquad d = \frac{S_\phi}{\rho U} \tag{2-36c,d}$$

and $\quad \psi = \left(\int_0^y \rho U dy\right)_{x=\text{constant}}$ (2-36e)

where S_ϕ and Γ_ϕ are the net source and diffusion coefficient in each equation. The general variable ϕ can stand for the mean velocity U, turbulent kinetic energy k_p, k_t, net turbulent energy transfer rate ε_p, ε_t, or total enthalpy H. The source terms in each equation are linearized, such as

$$S_\phi = S_c - S_p \phi \tag{2-37}$$

The negative sign before S_p is necessary to ensure no negative value of ϕ. Once the variable ϕ is defined, the corresponding S_ϕ and Γ_ϕ follow. One consequence of the definition of the stream function is that the mass flow rates per unit area crossing the I and E surfaces, namely $\dot{m}_I''$ and $\dot{m}_E''$, are related to the stream functions ψ_I and ψ_E by

$$\frac{d\psi_I}{dx} = -\dot{m}_I'' \quad \text{and} \quad \frac{d\psi_E}{dx} = -\dot{m}_E'' \tag{2-38a,b}$$

For a boundary layer without transpiration at the wall, $\dot{m}_I'' = 0$. The entrainment rate at the edge $\dot{m}_E''$ is approximated by the equation (2-35) when the cross-stream gradient is close to the free-stream boundary. The entrainment calculation is based on the velocity profile and is controlled as part of the computation.

Figure 2-2(a) shows the region between the upstream location x_U and the next Δx-downstream location x_D. The region also bounded by I and E surfaces, i.e. the wall and the external free stream. Between them, the domain is composed of control volumes, each surrounding a grid point. In this work, a linearly-increasing non-uniform grid system (150 control volumes with 3% increase in ω direction) is used to enhance the resolution in the near-wall region. It is very reasonable because in the

outer region of the boundary layer all gradient properties are small in approaching the external conditions and a course grid is sufficient to describe the flow there.

The finite difference equation is derived by integrating the differential equation over a control volume. For ease of integration, equation (2-35) is further rewritten as

$$\frac{1}{\Delta\psi}\frac{\partial}{\partial x}(\Delta\psi\phi)+\frac{\partial}{\partial\omega}\left(b\omega\phi-c\frac{\partial\phi}{\partial\omega}\right)=d \tag{2-39}$$

In deriving the difference equation, it is assumed that the variation of ϕ is piecewise-linear between the grid points. This assumption simplifies the derivation and keeps the physical essence of the solutions. The marching procedure is to obtain the unknown values of ϕ at x_D by using known values at x_U. In each marching step, the equations are decoupled from one another. For example, the solving sequence is solving k_p first then k_t, ε_p, ε_t and U; thus the "old" upstream ε_p value is used in the k_p-equation, but the updated k_p value will be used in the ε_p-equation. This procedure requires that the marching step be kept small in order to reduce the accumulation of errors. In this work, the step size $\Delta x = 0.25\delta_\theta$ (δ_θ is the momentum thickness) was found adequate to have step-size-independent solutions.

In dealing with the nonlinear convection-diffusion terms, the "hybrid-scheme" technique is used, thus yielding an implicit set of coupled algebraic equations for a typical control volume (see Figure 2-2(b)). The detailed derivation of this difference equation is explained in Patankar (1988). The final expression are as follows:

$$a_P\phi_P = a_N\phi_N + a_S\phi_S + b \tag{2-40}$$

where $b = S_c \Delta x (\Delta y)_P + a_{PU} \phi_{PU}$ (2-41a)

$$a_{PU} = (\Delta \psi)_U (\Delta \omega)_P \tag{2-41b}$$

$$a_N = \Delta x \cdot \max\left[0., -\dot{m}''_n, \frac{\Gamma_n}{\Delta y_n} - \frac{1}{2}\dot{m}''_n\right] \tag{2-41c}$$

$$a_S = \Delta x \cdot \max\left[0., \ \dot{m}''_s, \frac{\Gamma_s}{\Delta y_s} + \frac{1}{2}\dot{m}''_s\right] \tag{2-41d}$$

and $a_P = a_N + a_S + a_{PU} - S_P \Delta x (\Delta y)_P$ (2-41e)

hence, the mass flow through four surfaces of the control volume is conserved to satisfy continuity.

$$(\Delta \psi)_U (\Delta \omega)_P = (\Delta \psi)_D (\Delta \omega)_P + \dot{m}''_n \Delta x - \dot{m}''_s \Delta x \tag{2-42}$$

Finally, with the specified boundary conditions, the discretized equation (2-42) can be easily solved by a Tri-Diagonal-Matrix Algorithm (TDMA) to have the solution ϕ in each control volume.

2.5 Initial Profiles and Boundary Conditions

2.5.1 Initial Profiles

Since the boundary layer equations are not valid at the leading edge of a flat plate ($x = 0$), the initial profiles of all dependent variables must be specified at some distance downstream of the leading edge ($x = x_i$). In addition, boundary conditions must be provided to describe the wall and free stream conditions as the computation marches forward.

Mean Velocity:

The no-slip condition requires the velocity at the wall to be zero. The velocity at the free stream is specified as a function of x, $U = U_e(x)$. In this work, the external mean velocity is set constant to describe the zero-pressure flat plate boundary layer flow. The starting location is far upstream of boundary layer transition, thus the flow is a laminar boundary layer. The Blasius profile is used to represent the variation of U with y. The profile is the numerical solution of the Blasius equation

$$2f''' + ff'' = 0 \tag{2-43}$$

with boundary conditions $f = f' = 0$ at $\eta = 0$ and $f' = 1$ as $\eta = \infty$. Here, the prime denotes the derivative with respect to the Blasius similarity variable $\eta = y\sqrt{U_e / \nu x}$.

Total Enthalpy:

The total enthalpy in the free stream is assumed to remain constant for all the cases considered. At the wall, the temperature or heat flux is prescribed. For the case of a specified wall temperature, the initial profiles are derived by similarity transformation using the similarity variable η and stream function ψ. The non-dimensional temperature is expressed as

$$\theta'' + \frac{1}{2}\Pr f\theta' = -2\Pr f''^2 \tag{2-44}$$

where Pr is the molecular Prandtl number, and θ is the non-dimensional temperature, defined by

$$\theta = \frac{T - T_e}{U_e^2 / 2C_p} \tag{2-45}$$

The total enthalpy is computed through equation (2-4) and solution of (2-44) with $\theta = \theta_w$ at wall and $\theta = 0$ at free stream.

Partial Turbulent Kinetic Energy:

Exactly at the wall, there is no fluctuation of turbulent velocities; both values of the partial turbulent kinetic energy must be zero. At the free stream, the partial kinetic energies are specified as

$$k_p = S_g k_e, \qquad k_t = (1 - S_g) k_e \tag{2-46a,b}$$

where $S_g = 1/\left(1+k_t/k_p\right)_e$ is a spectrum shape factor which indicates how much energy is contained in the production region. In order to compare with the experimental data, it is assumed that the free stream turbulence is isotropic, so that the total kinetic energy is given as

$$k_e = 1.5\overline{(u')^2} = 1.5(Tu)^2 U_e^2 \tag{2-47}$$

Two different initial profiles of total turbulent kinetic energy were proposed respectively by Rodi (1987) and Reshotko (1990). Both considered the effects of the elevated free-stream turbulence; they are

Rodi: $$\frac{k}{k_e} = f'^2 \tag{2-48}$$

Reshotko: $$\frac{k}{k_e} = \left(f' + \frac{1}{2}\eta f''\right)^2 \tag{2-49}$$

and shown in Figure 2-3. Rodi's profile simply assumes that the amplitude of turbulent fluctuations inside the boundary layer is linear with respect to the local mean velocity. However, the Reshotko's profile presents an overshoot characteristic in the laminar boundary layer which is reflected in the experimental evidence of Klebanoff (1964, see Reshotko 1994) and Dyban et al. (1976) by measuring the streamwise fluctuating component. In Figure 2-3, the peak of the profile is at $\eta \approx 3.2$, and is much less than the experimental data. This under-prediction is due to the isotropic assumption and the use of the two dimensional Blasius profile in estimating the fluctuation component

u'. A more proper treatment of the "Klebanoff mode" would require three-dimensionality and anisotropy. A derivation of Reshotko's profile can be found in Appendix C.

After defining the partition of the free-stream energy spectrum by S_g, we have another difficulty in partitioning the kinetic energy inside the boundary layer. Although Klebanoff indicated that the overshoot structure is largely from low frequency fluctuations, the fraction of the turbulent kinetic energy k inside the boundary layer that comes from the low frequency part (i.e. in production region k_p) is still unknown. Here, we assume that the initial energy distribution across the boundary layer also has the same ratio S_g. That is

$$k_p = S_g k \qquad \text{and} \qquad k_t = (1 - S_g)k \tag{2-50a,b}$$

Later calculation shows that the friction coefficient C_f is not sensitive to the initial turbulent kinetic energy profile (whether Rodi's or Reshotko's profile) but the transition location will be changed due to how much energy is initially contained in the large eddies.

Turbulent Kinetic Energy Transfer Rate:

The initial profile of the dissipation is introduced by Rodi and Scheuerer (1985) in assuming local equilibrium

$$\varepsilon = \varepsilon_p + \varepsilon_t = a_1 (k_p + k_t) \frac{\partial U}{\partial y} \tag{2-51}$$

where a_1, the structure parameter (defined as $-\overline{uv}/k$), depends on the free-stream turbulence intensity. A limit must be imposed on ε which prevents the turbulent length scale inside the boundary layer from exceeding its free-stream value. Thus, we define the initial profiles as the following

$$\varepsilon_p = a_1 k_p \frac{\partial U}{\partial y} \qquad \text{for } \varepsilon_p \geq (\varepsilon_p)_e \tag{2-52a}$$

$$\varepsilon_t = a_1 k_t \frac{\partial U}{\partial y} \qquad \text{for } \varepsilon_t \geq (\varepsilon_t)_e \tag{2-52b}$$

2.5.2 Boundary Conditions

The boundary conditions at the wall are $U = 0$, $V = 0$, $k_p = 0$ and $k_t = 0$ due to the no slip condition. From the near-wall asymptotic analysis, the boundary conditions for ε_p and ε_t are suggested as

$$\varepsilon_p = 2\nu\left(\frac{\partial\sqrt{k_p}}{\partial y}\right)^2 \quad \text{and} \quad \varepsilon_t = 2\nu\left(\frac{\partial\sqrt{k_t}}{\partial y}\right)^2 \tag{2-53a,b}$$

At the edge of the boundary layer, the velocity is given by its free-stream value and all the turbulent quantities are there determined from solving equations (2-12) to (2-16) in the isotropic grid-generated turbulent flow (see Appendix B)

$$U_e \frac{\partial k_p}{\partial x} = -\varepsilon_p \tag{2-54}$$

$$U_e \frac{\partial k_t}{\partial x} = -\varepsilon_t \tag{2-55}$$

$$U_e \frac{\partial \varepsilon_p}{\partial x} = -C_{p2} f_{p2} \frac{\varepsilon_p^2}{k_p} \tag{2-56}$$

$$U_e \frac{\partial \varepsilon_t}{\partial x} = C_{t1} f_{t1} \left(\frac{k_t}{k_p} \right)^{3/2} \frac{\varepsilon_p^2}{k_p} - C_{t2} f_{t2} \frac{\varepsilon_t^2}{k_t} \tag{2-57}$$

The initial values of k_p, k_t, ε_p and ε_t in free-stream are given by experimental data and the specified S_g.

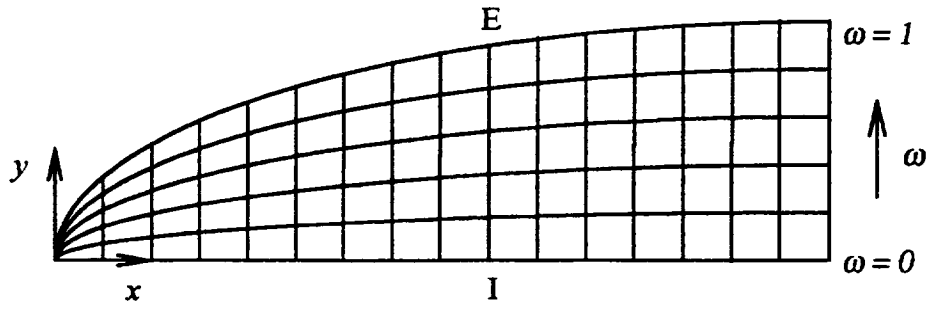

Figure 2-1 Grid system.

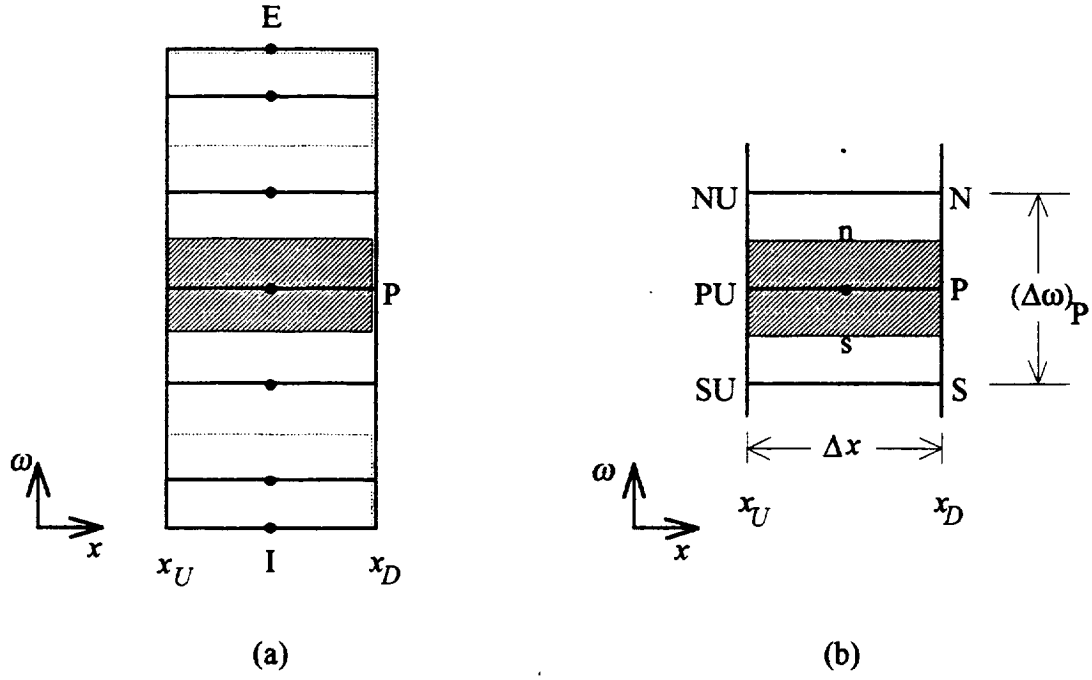

Figure 2-2 (a) Control volumes and grid points; (b) A typical control volume around a grid point.

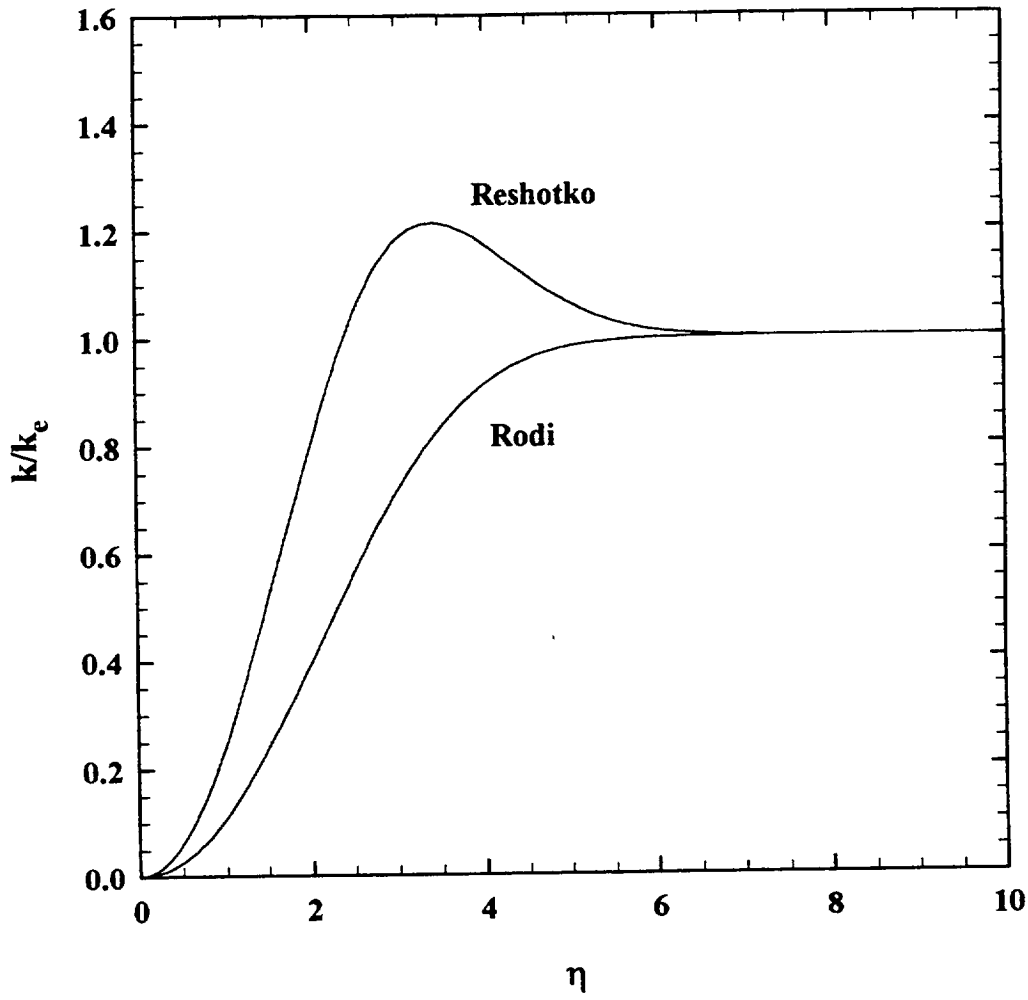

Figure 2-3 Initial profiles of turbulent kinetic energy.

CHAPTER THREE

NUMERICAL SIMULATION OF TRANSITION

3.1 Evaluation of the Two-Scale Turbulence Model

This section presents a series of computational tests which evaluate the effects of the starting location and initial profiles for numerical computation. These are the factors which must be known before using the turbulence model in computation. The importance of this evaluation to the transition prediction has been addressed by Rodi and Scheuerer (1985), Schmidt (1985) and Stephens and Crawford (1990). After this evaluation, the proper starting location and initial profiles can be used in computation with known influence on transition prediction. From the results we can also distinguish the sensitivities to these two factors from that of the turbulence model.

3.1.1 Sensitivity of the Starting Location

The sensitivity of starting location was evaluated by maintaining the following conditions in computation

- Tu = *2.3%*
- The mean velocity is the Blasius solution
- The turbulent kinetic energy is the Reshotko's profile
- The structure coefficient of dissipation rate a_1 is *0.3*

- The spectrum shape parameter S_g is maintained at *0.8*

The initial profiles of these tests were generated by equations (2-49) to (2-52). In these tests, the starting location was placed at length Reynolds numbers of 10^1, 10^2, 10^3 and 10^4. Because the local skin-friction coefficient C_f is an important measure of transitional behavior, it was used as the major parameter in evaluation. Figure 3-1 plots the computed local friction coefficient with starting Reynolds number. Also shown are the analytical solutions for the laminar boundary layer and Prandtl's correlation for the turbulent boundary layer

$$\text{laminar:} \qquad C_f = \frac{0.664}{\sqrt{\mathrm{Re}_x}} \tag{3-1}$$

$$\text{turbulent:} \qquad C_f = \frac{0.058}{\mathrm{Re}_x^{0.2}} \tag{3-2}$$

It appears that the friction coefficient is enhanced by the elevated free-stream turbulence level. Figure 3-1 also shows that the computed friction coefficient is not sensitive to starting location up to $\mathrm{Re}_x = 10^4$. Thus the starting location is set at $\mathrm{Re}_x = 10^2$ in any following computation.

3.1.2 Sensitivity to the Initial profiles

The initial profiles examined here are the Rodi profile and Reshotko's profile for turbulent kinetic energy and Rodi's profile for energy dissipation rate. For this set of numerical tests, the following conditions are maintained:

- Tu = *2.3%*
- The starting location is at Re_x = *100*
- The mean velocity is the Blasius solution
- The spectrum shape parameter S_g is kept at *0.8*

First, for the two different initial kinetic energy profiles, figure 3-2 shows that the prediction is not sensitive to the differences between these profiles. All subsequent computations use the Reshotko's profile. Although only the Rodi profile is used for initial turbulent energy dissipation rate, it is necessary to examine the sensitivity to the structure coefficient a_1 in equation (2-51). Figure 3-3 shows that the influence is very limited in transitioning boundary layer prediction. With increase in the coefficient a_1, that is more dissipation inside the boundary layer at the starting location, the transition has a slightly delayed onset. In the following calculation, the structure coefficient a_1 is set at *0.3*. From figures 3-1 to 3-3, we may conclude that the initiating computation has very little effect in transition prediction.

3.2 Comparison with the Experimental Data

Direct comparison with experimental data is necessary in the development of the turbulence model so that the capabilities and failures of the model can be assessed. In this section, calculations will be compared with five different sets of experimental data for the flow over a flat plate (zero pressure gradient). All of these experiments are subjected to the influence of elevated free-stream turbulence levels. The

turbulence intensity considered at the leading edge ranges from *1%* to *9%*. In some experiments, the transition is given in terms of heat transfer by constant heat flux or constant temperature at the flat plate, thus the local Stanton number is measured. The Stanton number is defined as

$$\mathrm{St} = \frac{\dot{q}_w}{\rho U_e C_p (T_w - T_e)} \tag{3-3}$$

Since the experimental data sets used here are from different facilities and since the wind tunnels are of different design with different instrumentation and ways of generating free-stream turbulence, the results obtained in the different experiments are not fully consistent. The experimental data could also be affected by a lot of factors, such as the area ratio of the contraction section, location of grid system, the measuring technique, flat plate leading edge radius, carefulness of the observer etc. For example, even though Sohn and Reshotko (1991) and Blair and Werle (1980) have similar facilities and similar grid designs, the transition locations are different. Therefore, agreement with all of the experimental data is not expected.

3.2.1 The Data of Blair and Werle

Blair and Werle (1980) conducted their experiments in a low speed wind tunnel with air at ambient conditions. The mean velocity in the test section was kept at *30.3* m/s. Various turbulence intensities (up to *6%*) were generated by inserting square-array biplane grids constructed from rectangular bars at the entrance of a two-dimensional *2.8:1* contraction. At the leading edge, a bleed system provided spanwise uniformity and prevented local separation and premature transition. The turbulent

quantities were measured by hot wire anemometry for all three components. The flat plate was heated by a uniform heat flux of *850* W/m^2 following a *42.9* mm unheated starting length. The turbulence in the test section was nearly homogeneous and isotropic and approximately followed the decay law

$$Tu_e = 0.78\left(\frac{x+132}{b}\right)^{-5/7} \tag{3-4}$$

where x is in cm; and b=*0.48, 1.27* and *3.81* for grids 1, 2 and 3 respectively. The test results of grid 4 will not be considered here because all the recorded data are already fully turbulent and so there is no transition information. Table 3-1 gives the values of turbulent kinetic energy k, dissipation rate ε and turbulent intensity Tu at leading edge that are used in the computation.

Parameter	Grid 1	Grid 2	Grid 3
Tu_e at x=0	*1.12%*	*2.33%*	*5.75%*
k_e (m^2/s^2) at x=0	*0.175*	*0.757*	*4.60*
ε_e (m^2/s^3) at x=0	*2.75*	*19.5*	*150*

Table 3-1 Free-stream turbulence conditions in computing the flows of Blair and Werle (1980).

Figure 3-4 shows the comparison between calculated Stanton numbers and experimental data. The transition is predicted late for grid 1 but early for grid 3. It should be noted that Blair and Werle reported that the transition is shifted upstream by wall effects in the flow without a grid. It is possible that the grid 1 case is also slightly affected in the same way. Also included in figure 3-4 are (*i*) the laminar boundary layer analytical solution of Reshotko (1995) for zero pressure gradient with uniform wall heat flux

$$\mathrm{St} = 0.453\,\mathrm{Pr}^{-2/3}\,\mathrm{Re}_x^{-1/2}\left[1-(x_0/x)\right]^{-1/3} \tag{3-5}$$

where x_0 is the unheated starting length and (*ii*) a correlation suggested by Kays and Crawford (1980) for fully turbulent boundary layer flow

$$\mathrm{St} = 0.03\,\mathrm{Pr}^{-0.4}\,\mathrm{Re}_x^{-0.2}\left[1-(x_0/x)^{0.9}\right]^{-1/9} \tag{3-6}$$

It is shown in the figure that the heat transfer is enhanced by free-stream turbulence level in both experiments and computations.

In figure 3-5, the effect of free-stream energy spectrum on the onset of transition is examined. The spectrum depends on the wind tunnel and on the grid used in generating the free-stream turbulence. If the production of turbulent kinetic energy is coming from most of the spectrum (S_g is large), the transition location is moved upstream. In other words, if there is more energy contained in the large eddies, the energy could penetrate more effectively into the boundary layer. Thus the onset of

transition is earlier. However, there are no experimental data available to confirm this prediction.

3.2.2 The Data of Rued and Wittig

These experiments were carried out in a wind tunnel with various free-stream turbulence intensities ($Tu = 1.6 \sim 11$ percent), zero and favorable pressure gradient and various cooling intensities ($T_w/T_e = 1.0 \sim 0.53$) (see Rued, 1985 and Rued and Wittig, 1985). The turbulence was generated by installing a calibrated grid located *170* mm upstream of the plate's leading edge. The air is heated before it enters the test section whereas the flat plate is cooled after a *15* mm uncooled leading edge region. In contrast to the experiments of Blair and Werle, the wall temperature in the cooled region is kept nearly constant ($T_w = 305$ K) under all conditions. The turbulence quantities are measured by Laser-Doppler-Anemometry and the turbulent skin friction is determined by a Preston-tube technique. Only two components, $\overline{u'^2}$ and $\overline{v'^2}$, of fluctuating velocities are measured at different locations and the ratio between them is from *0.7* to *0.9* in the zero pressure gradient condition. Therefore, the free-stream is not exactly isotropic. Since the third component $\overline{w'^2}$ was not measured, we assumed that the free-stream is isotropic and $\overline{w'^2} = \overline{v'^2}$ to set the level of k in the computations.

Here, we consider the zero-pressure-gradient, wall-cooling case only. In this case, the free-stream velocity is kept constant at $U_e = 47$ *m/s* and the turbulence intensities are varied from *1.6* to *8.7* percent at the leading edge. The free-stream flow conditions at the start of the test section are summarized in Table 3-2.

Parameter	No Grid	Grid 1	Grid 2	Grid 3	Grid 4
Tu_e at x=0	*1.71%*	*2.80%*	*4.65%*	*7.40%*	*10.8%*
k_e (m^2/s^2) at x=0	*0.969*	*2.60*	*7.16*	*18.14*	*38.6*
ε_e (m^2/s^3) at x=0	*62.3*	*480*	*1600*	*9530*	*24000*

Table 3-2 Free-stream turbulence conditions in computing the flows of Rued and Wittig (1985).

Figure 3-6 shows the comparison between experimental Stanton numbers and computation for flow without grid (grid 0) and with grids 1, 2 and 3. The predicted onset of transition is good for grids 0, 1 and 2 but too far upstream for grid 3. In general, the transition length is short for all cases.

3.2.3 The Data of Savill

The experimental data are from the test cases T3A and T3B of the European Special Interest Group on transition presented in the first ERCOFTAC (European Research Community On Flow Turbulence And Combustion) workshop (Savill, 1990). These two tests were performed on a flat plate at free-stream velocities U_0 of *5.2* m/s and *9.6* m/s with turbulence intensities at the leading edge of *2.8%* and *5.7%* respectively. The objective of these experiments is to provide data for the examination of various turbulence models in the prediction of transition for zero pressure gradient boundary layers.

The tests were conducted in a low speed wind tunnel with air. As a result of careful design, the test section free-stream turbulence intensity is within *0.2%* over the operating velocity range of *0* to *25* m/s, and the air temperature is controlled within *0.1* degree C during operation. Hot wire anemometry was extensively used in the turbulence measurements. Free-stream turbulence is generated by parallel arrays of round rods and square bars in T3A and T3B respectively. The grid is installed right after the *2.5:1* contraction section and *610* mm ahead of the leading edge of the flat plate. The leading edge has a *0.75* mm radius with a *5* degree chamfer on the other side of the test surface. Earlier studies (Roach, 1987) reveal that the turbulence generated by such grids is indeed isotropic and obeys the following decay law

$$\frac{u'}{U_0} = C(x+610)^{-5/7} \tag{3-7}$$

where $C = 2.74$ for the T3A grid; $C = 5.60$ for the T3B grid; and x is the distance from leading edge in mm. Figures 3-7 and 3-8 show the friction coefficient and shape factor, respectively, compared with the experimental data. Good agreement is obtained for both cases except that the transition length of T3A is short. The model also produces good prediction of the mean velocity profiles development, as illustrated by figures 3-9 and 3-10 for T3A and T3B respectively.

In order to further characterize the transition process, we integrate the turbulent kinetic energy equation (equation 2-13 plus 2-14) across the boundary layer with respect to y from the wall to the free-stream. Thus, we have

$$\frac{d}{dx}\left[\int_0^\infty U\left(k_p + k_t\right)dy\right] = \overline{P}_k - \overline{\varepsilon} \tag{3-8}$$

where $\overline{P}_k = \int_0^\infty P_k dy$ and $\overline{\varepsilon} = \int_0^\infty \left(\varepsilon_p + \varepsilon_t\right)dy$ (3-9a,b)

Figure 3-11 shows that the ratio of $\overline{P}_k/\overline{\varepsilon}$ increases from the leading edge of the flat plate. More and more energy is produced inside the boundary layer and the rate of production also increase until the ratio reaches a maximum. Finally, the ratio decreases and the boundary layer reaches the equilibrium condition where the flow is fully turbulent. From this figure, we see that the present model simulates the transitional boundary layer flow development as a gradual process that begins far-upstream of the increase of skin friction. The velocity profiles reflecting this process are shown in Figure 3-12. The logarithmic layer is gradually generated during the transition.

Figures 3-13 and 3-14 plot the partial turbulent kinetic energy $k_p^+ \ (= k_p/U_\tau^2)$ and $k_t^+ \ (= k_t/U_\tau^2)$ as a function of the wall unit coordinate y^+ in the T3A case with $S_g = 0.9$. The turbulent energy is penetrating the boundary layer by diffusion and convection from the free-stream. During the transition process, the turbulent energy level is rapidly elevated for the whole boundary layer. It should be noted that the transfer zone turbulent kinetic energy k_t^+ is two orders-of-magnitude lower than that in the production zone k_p^+. However, close to the free-stream, the role of k_t^+ becomes more and more important until it behaves as the spectrum parameter S_g in free-stream. In other words, the production region of the energy spectrum is more effective when approaching the wall. Note that although the initial profile has little influence, the Reshotko profile appears at $\mathrm{Re}_x = 1 \times 10^5$. Figures 3-15 and 3-16

represent the net energy transfer function ε_p^+ (= $\nu\varepsilon_p/U_\tau^4$) and ε_t^+ (= $\nu\varepsilon_t/U_\tau^4$) of the transitional boundary layer. As expected, the quantity of ε_t^+ is small because the energy is just transferred through this transfer region. Figure 3-17 shows that the Reynolds stress gradually increases throuth transition until it reaches equilibrium.

For high free-stream turbulence intensity, such as the T3B case (figure 3-18), the ratio $\overline{P}_k/\overline{\varepsilon}$ is very rapidly increasing, thus the transition location is much earlier. However, the flow does not reach equilibrium boundary layer until well after transition. This is because the dissipation rate is also high in this case.

3.2.4 The Data of Kim and Simon

Kim and Simon (1991a,b) have studied the transitional boundary layer flow over flat plate and concave surfaces and tabulated the results for any further study. Only the flat plat cases are considered here. The experiment was performed in a low-speed, open-return wind tunnel with high contraction (area ratio *10.6:1*) two-dimensional (aspect ratio *6:1*) nozzle installed right before the test section. Up to *8%* free-stream turbulence intensity is generated by using an insert section after the contraction nozzle. They use hot-wire anemometry with single-, double- and triple-wires probes in measuring various turbulence quantities. Stanton numbers were measured using thermocouples embedded in the wall and the intermittencies were obtained by conditional sampling technique. They investigated three different turbulent intensities, 0.32%, 1.5% and 8.3%, in flat plate boundary layer flow; the latter two are presented in Table 3-3 for computation.

Parameter	Case 2	Case 3
Mean velocity (m/s)	*16.7*	*9.2*
Tu_e at x=0	*1.5%*	*8.91%*
k_e (m^2/s^2) at x=0	*0.0941*	*1.008*
ε_e (m^2/s^3) at x=0	*0.10*	*11.86*

Table 3-3 Free-stream turbulence conditions in computing the flows of Kim and Simon (1991).

Figures 3-19 and 3-20 show the skin-friction coefficient and shape factor of case 2, as a function of Reynolds number respectively. The present model predicts the transition is very abrupt at the onset, but it behaves well thereafter. In figure 3-21 the velocities from calculation (figure 3-21(a)) are compared with the experimental data (figure 3-21(b)) in wall coordinates. The agreement is quiet good. However, the computed Reynolds stresses are generally lower than the experimental data as shown in figure 3-22.

Kim and Simon applied $190\ W/m^2$ heat flux at the wall in the high turbulence intensity case. For this case (figures 3-23 and 3-24), the computed skin-friction coefficient and shape factor compare favorably with experiment. Transition occurs upstream of the experimental data taken. Figure 3-25 shows the Stanton number as a function of Reynolds number. In contrast to the experimental data, the calculated heat transfer is augmented slightly over the standard turbulent correlation (equation 3-6).

3.2.5 The Data of Sohn and Reshotko

The experiment was conducted in a low speed wind tunnel at the NASA Lewis Research Center (Sohn and Reshotko, 1991). The wind tunnel is similar in design to that of Blair et al. (1981) but with a higher contraction nozzle (area ratio 3.6:1) and a smaller test area cross-section. The grid system, similar in design to that of Blair et al. (1981), is installed upstream of the contraction. A bleed system is also used at the plate leading edge to prevent local separation. The mean velocity inside the test section is kept constant ($30.5\ m/s$) and the turbulent intensities are varied from *1%* to *7%* at the leading edge. A constant heat flux ($350\ W/m^2$) is applied after the *1.375* inch unheated length. This wind tunnel was used by Suder et al. (1988) who claimed that the test section turbulence was isotropic. Sohn and Reshotko used the same grids as Suder et al. but obtained slightly higher turbulence intensities for each grid. Since only the stream wise free-stream turbulence quantities were measured, it is assumed that the flow is homogeneous and isotropic in computation. The free-stream flow conditions at the leading edge for each grid are summarized in Table 3-4.

Parameter	Grid 1	Grid 2	Grid 3
Tu_e at x=0	*1.12%*	*2.85%*	*6.14%*
k_e (m^2/s^2) at x=0	*0.175*	*1.137*	*5.253*
ε_e (m^2/s^3) at x=0	*0.647*	*39.8*	*290.7*

Table 3-4 Free-stream turbulence conditions in computing the flows of Sohn and Reshotko (1991).

Similar to Blair's results, the measured flow for grid 4 is fully turbulent so that we consider grids 1, 2 and 3 only. Figure 3-26 documents the decay of free-stream turbulence intensities for each of the grids. Note that the agreement between the computation and experimental results verifies the simplified power-law equation for grid turbulence flow. Figure 3-27 shows that the calculated onset of transition calculation is delayed for grid 1 but very early for grid 3. These computational results are similar to those calculated for the Blair and Werle data. The computed Stanton number variations are shown in figure 3-28. Since the present model assumes the momentum equation to be uncoupled from the energy equation, it should not show any lag (or lead) of the heat transfer quantities. Recently, Madavan and Rai (1995) simulated the experiment by a Direct Numerical Simulation (DNS) technique and their results show that the transition in skin friction leads the transition in heat transfer. Figure 3-29 shows the comparison of the Reynolds analogy factor, $2\mathrm{St}/C_f$, between experimental data, DNS result and the present model prediction. The reference laminar and turbulent curves are obtained from the combination of equations (3-1), (3-5) and (3-2), (3-6) respectively. The model predicts the early transiton but agrees well in the fully turbulent flow.

Figures 3-30 and 3-31 show the development of mean velocity and temperature profiles respectively. Both profile sets change from the laminar profiles until they reach the log law. In figure 3-30, two reference curves represent the viscous sublayer $U^+ = y^+$ and the logarithmic layer $U^+ = 2.5 \ln y^+ + 5$. As obtained in the experiment, a small wake region is clearly seen at $\mathrm{Re}_x = 5 \times 10^5$, however, it is diminished in DNS result (see figure 8 of Madavan and Rai, 1995). Also shown in figure 3-31 are the laminar solution $T^+ = \mathrm{Pr}\, y^+$ and the turbulent correlation:

$$T^+ = 13.2\,\mathrm{Pr} + \frac{\mathrm{Pr}_t}{0.41}\ln\left(\frac{y^+}{13.2}\right) \tag{3-10}$$

where T^+ is defined as $(T_w - T)/T_\tau$ and T_τ is the friction temperature, defined as $\dot{q}_w/\rho C_p U_\tau$.

Figure 3-32 shows the normal mean velocity profiles at various stream wise locations. Since the transition is so abrupt, the normal mean velocity becomes negative not only in near-wall region but also in the outer layer by a very small amount at $\mathrm{Re}_x = 2.2\times 10^5$. Also noted is that the mean normal velocity is of the same order-of-magnitude as the DNS results (Rai, 1994). However, the experimental data have higher values, are felt to be in error. This is because the experimental values of V at the edge of the boundary layer are much larger than the experimental values of $d\delta^*/dx$.

Figures 3-33(a) and 3-33(b) plot the turbulent intensity evolution of the transitional boundary layer in wall coordinate $y^+$and outer variable y/δ respectively. Here, the turbulent intensity $<u'>/U_e$ is defined as

$$\frac{<u'>}{U_e} = \frac{1}{U_e}\sqrt{\frac{2}{3}k} \tag{3-11}$$

Both figures shows that the peak value increases in the stream wise direction and reaches a maximum in the transition region before reaching and maintaining an equilibrium in the fully turbulent flow. The maximum is moving forward the wall as Reynolds number increases. The variable $<u'>$ is not the real fluctuation quantity

since the flow inside the boundary layer is not isotropic. It is less than the actual stream wise turbulence quantity u' as shown in figure 3-34(a) and (b), because u' is always the largest component experimentally. However, the general trend of $<u'>/U_e$ is similar to the trend of u'/U_e. Figure 3-35 shows the turbulent kinetic energy in fully turbulent flow. In the near wall region, the model does not have the high peak value as the DNS data but in the same y/δ^* location. The difference in outer region could be due to the errors in DNS results because all three components of the turbulent intensities in DNS data are still in obviously decay at $y/\delta = 1$.

3.3 Summary

In this chapter, five different sources of experimental data have been used to evaluate the transition prediction capability of the multiple-scale turbulence model. The prediction is insensitive to the starting computation location and the initial profiles of turbulent kinetic energy k and dissipation rate ε. Figure 3-36 shows the comparison of the predictions with the correlation suggested by Abu-Ghannam and Shaw (1980). The correlations for the start and end of transition are:

$$\mathrm{Re}_{\theta,S} = 163 + \exp(6.91 - 100\ \mathrm{Tu}) \tag{3-12}$$

$$\mathrm{Re}_{\theta,E} = 2.667\,\mathrm{Re}_{\theta,S} \tag{3-13}$$

Also shown in the figure are the experimental data in their report from various facilities. The multiple-scale k-ε predictions are reasonably good for the start of

transition but are too early in general for the end of transition. It should be noted in the experimental data that the Reynolds number Re_θ has a very wide range at the same freestream turbulence intensity especially for the end of transition.

Since the turbulence model is calibrated from the freestream, a spectrum parameter S_g $(= k_p/(k_p + k_t)$ in freestream) is generated in describing the influence of the energy spectrum of freestream. The parameter S_g is the percentage of the freestream turbulent kinetic energy as the boundary condition of k_p equation. Thus the value of S_g is always less than one. The flat plate transitional boundary layer is then described by two parameters; (*i*) turbulent intensity Tu which represents the amplitude of the fluctuation and (*ii*) spectrum parameter S_g which characterizes the frequency feature of turbulence. Figure 3-37 shows the map of optimal values of S_g in the simulation of various experiments if the start of transition is close to the experiment results. From figure 3-37, S_g decreases as the freestream turbulence intensity increases although the data are somewhat scattered. This trend means that the energy production corresponding to the transition is less for higher elevated freestream turbulence. However, the predictions have an early start of transition for Tu > 6% and have numerical difficulty for $S_g < 0.4$. Further validations are required for these high freestream turbulence levels.

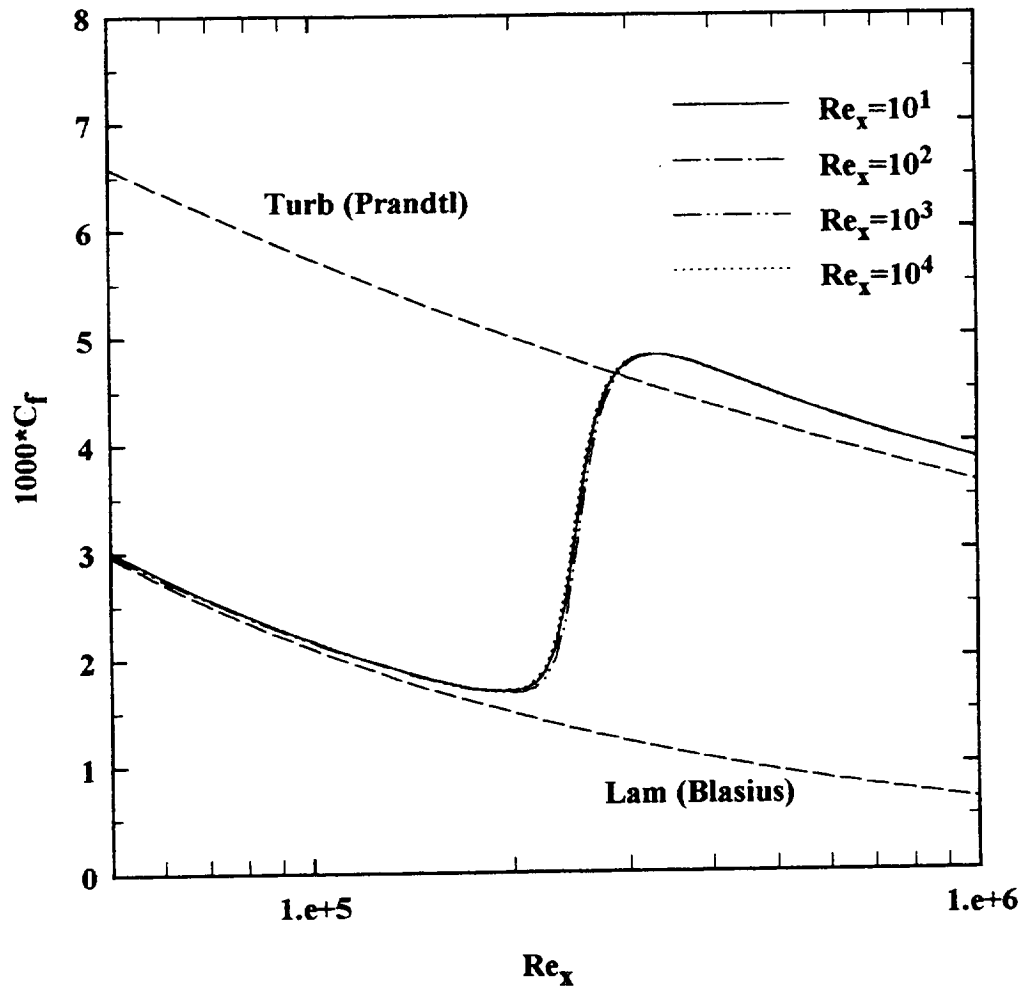

Figure 3-1 Local friction coefficient versus Reynolds number for the sensitivity of starting location; (Tu = 2.3%, S_g = 0.8).

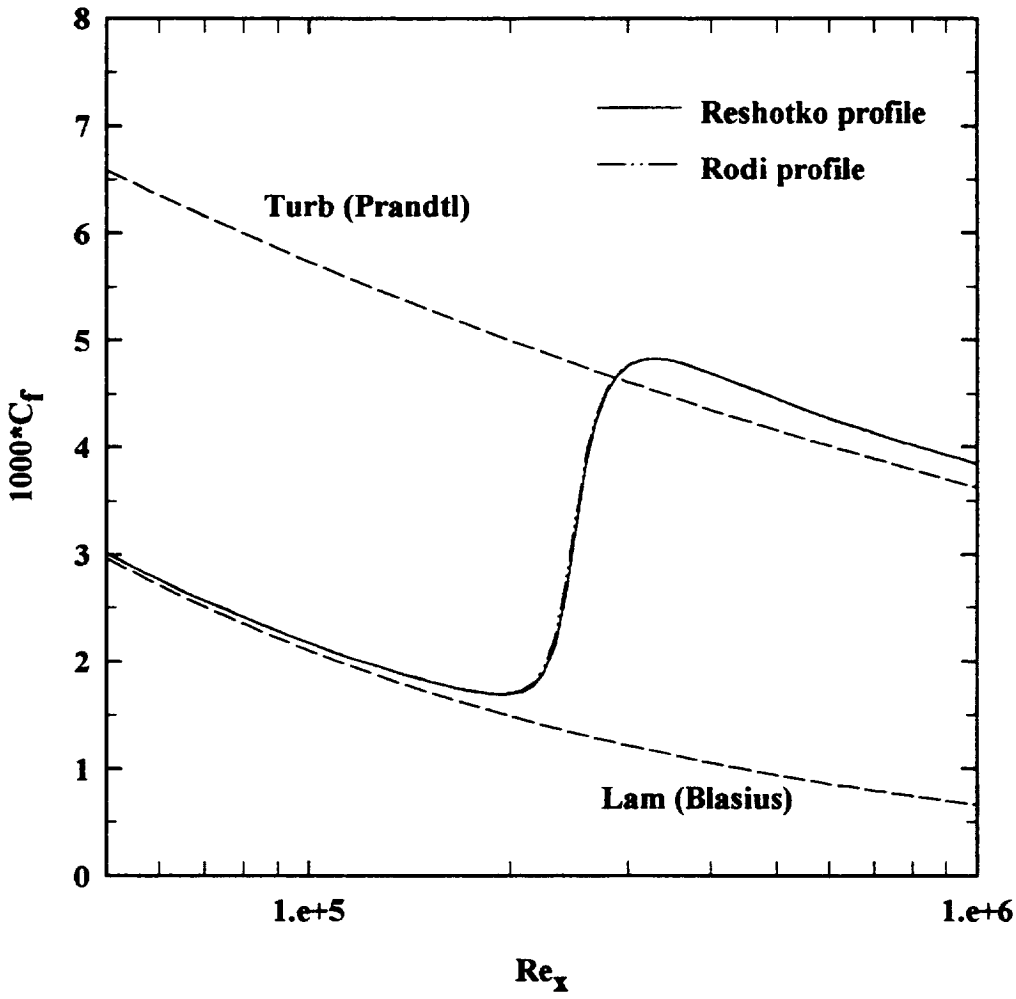

Figure 3-2 Local friction coefficient versus Reynolds number for the sensitivity of initial turbulent kinetic energy profile; (Tu = 2.3%, S_g = 0.8).

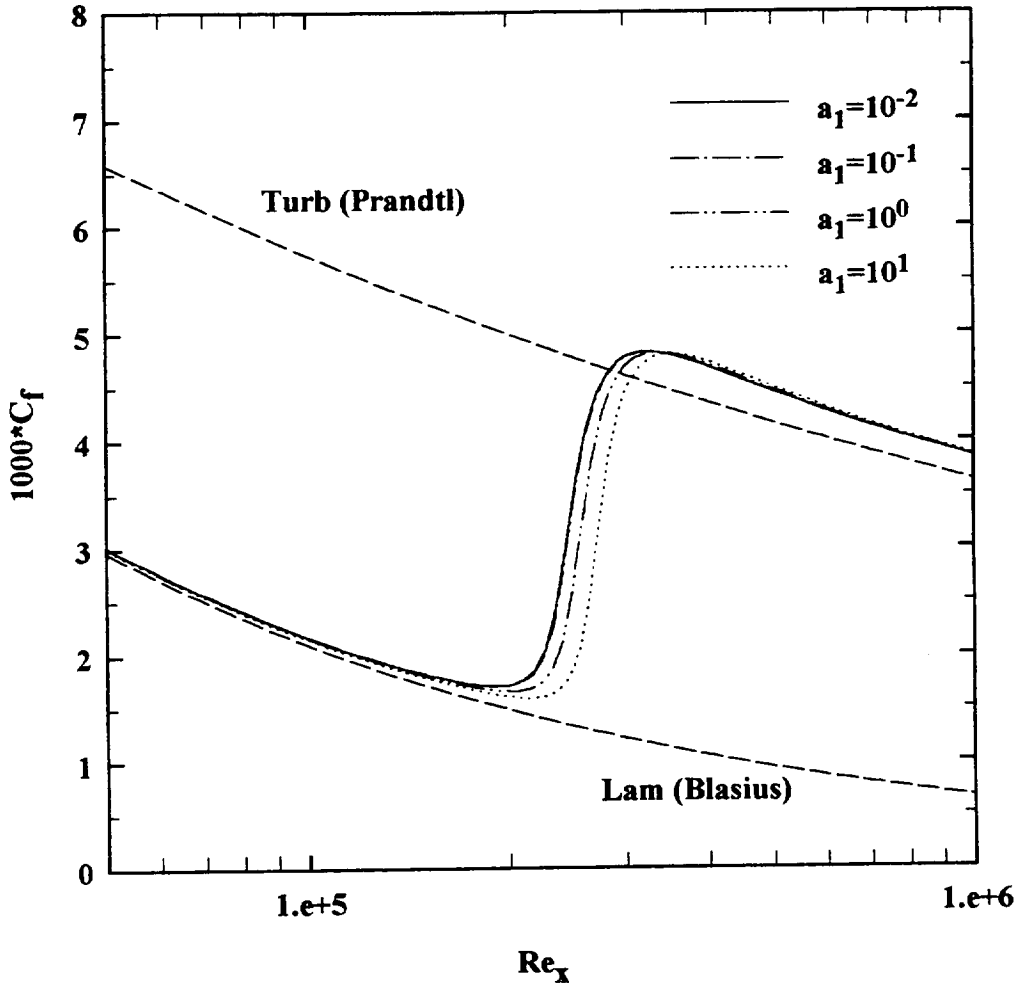

Figure 3-3 Local friction coefficient versus Reynolds number for the sensitivity of initial turbulent dissipation rate profile; (Tu = 2.3%, S_g = 0.8).

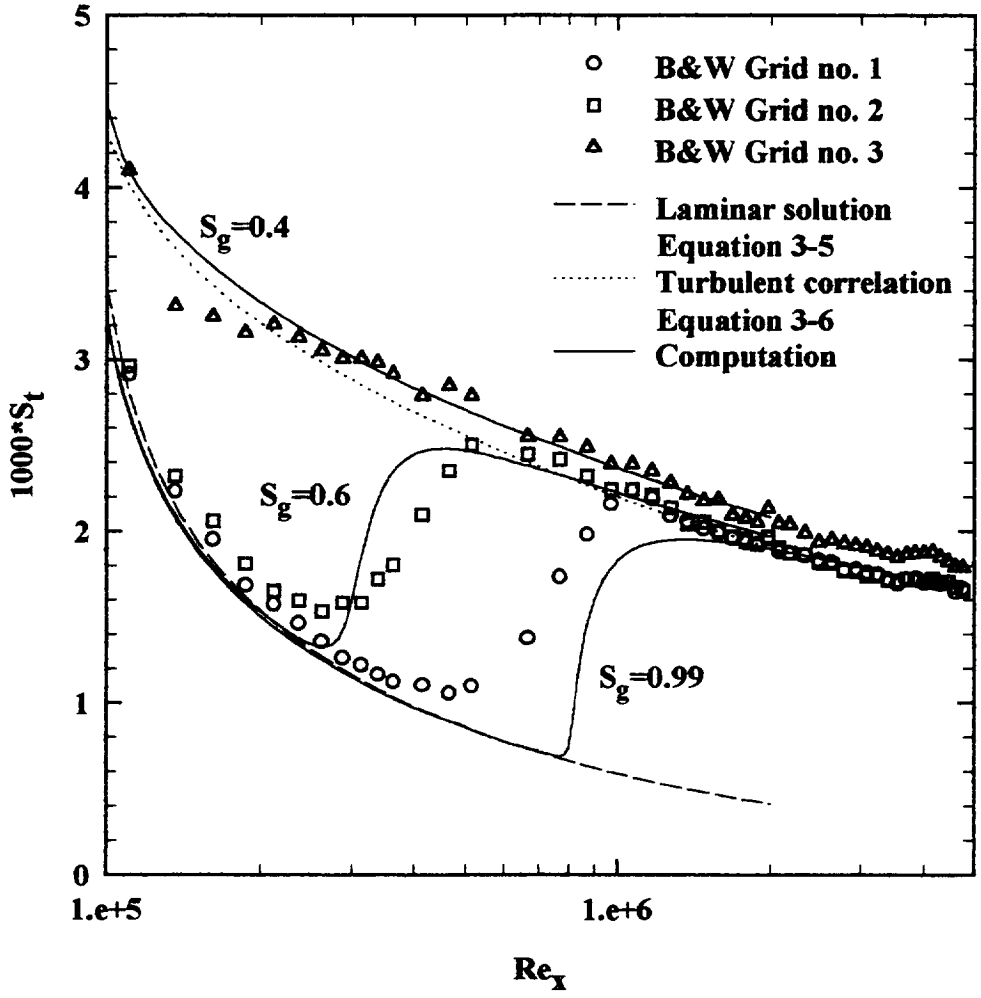

Figure 3-4 Comparison of the predicted heat transfer during transition with the data of Blair and Werle (1980).

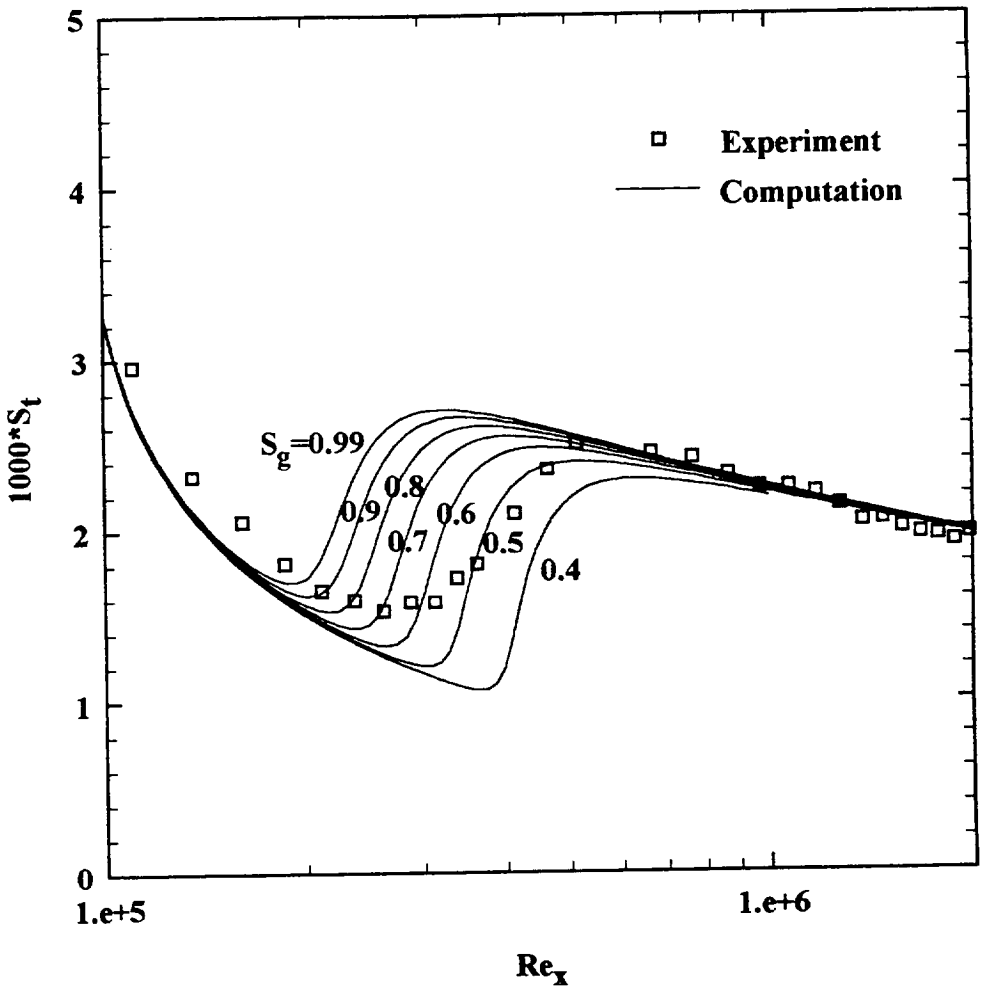

Figure 3-5 Free-stream spectrum factors of the experimental data of Blair and Werle (1980) grid 2.

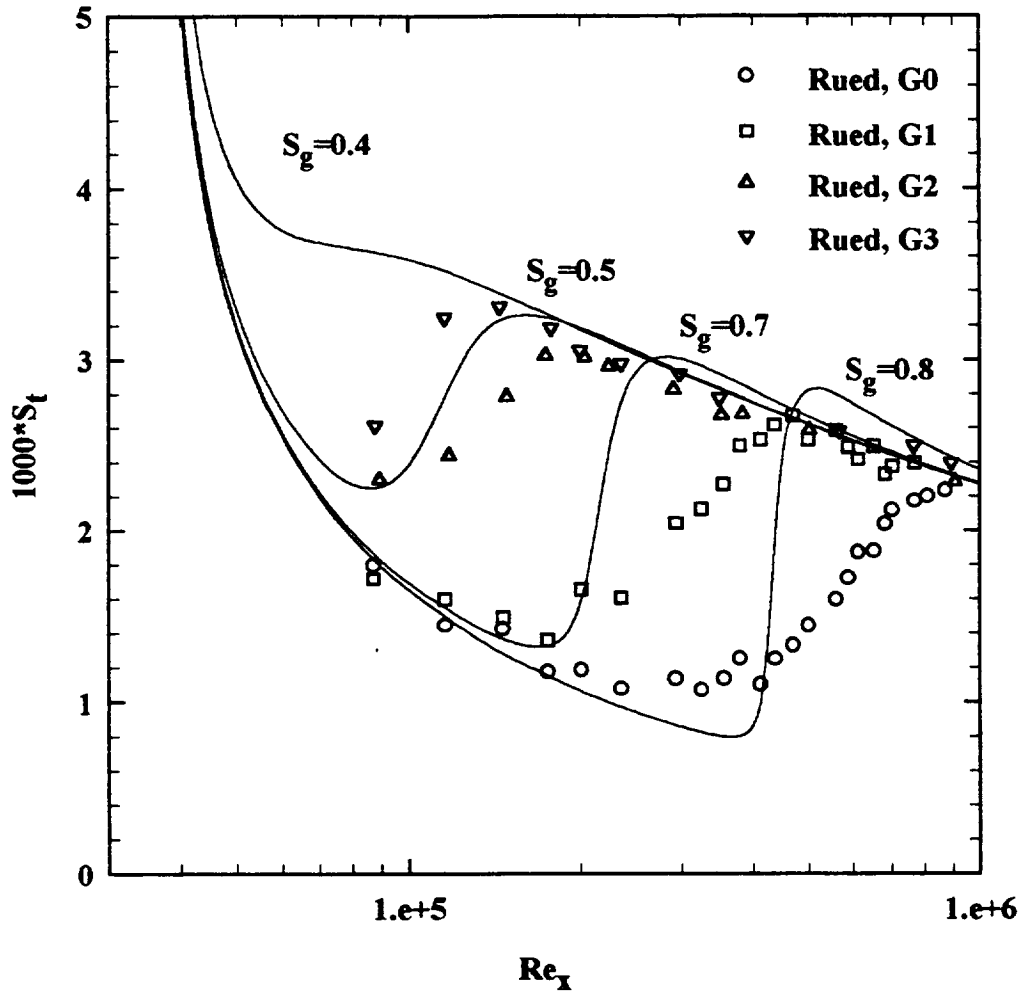

Figure 3-6 Comparison of the predicted heat transfer during transition with the data of Rued (1985).

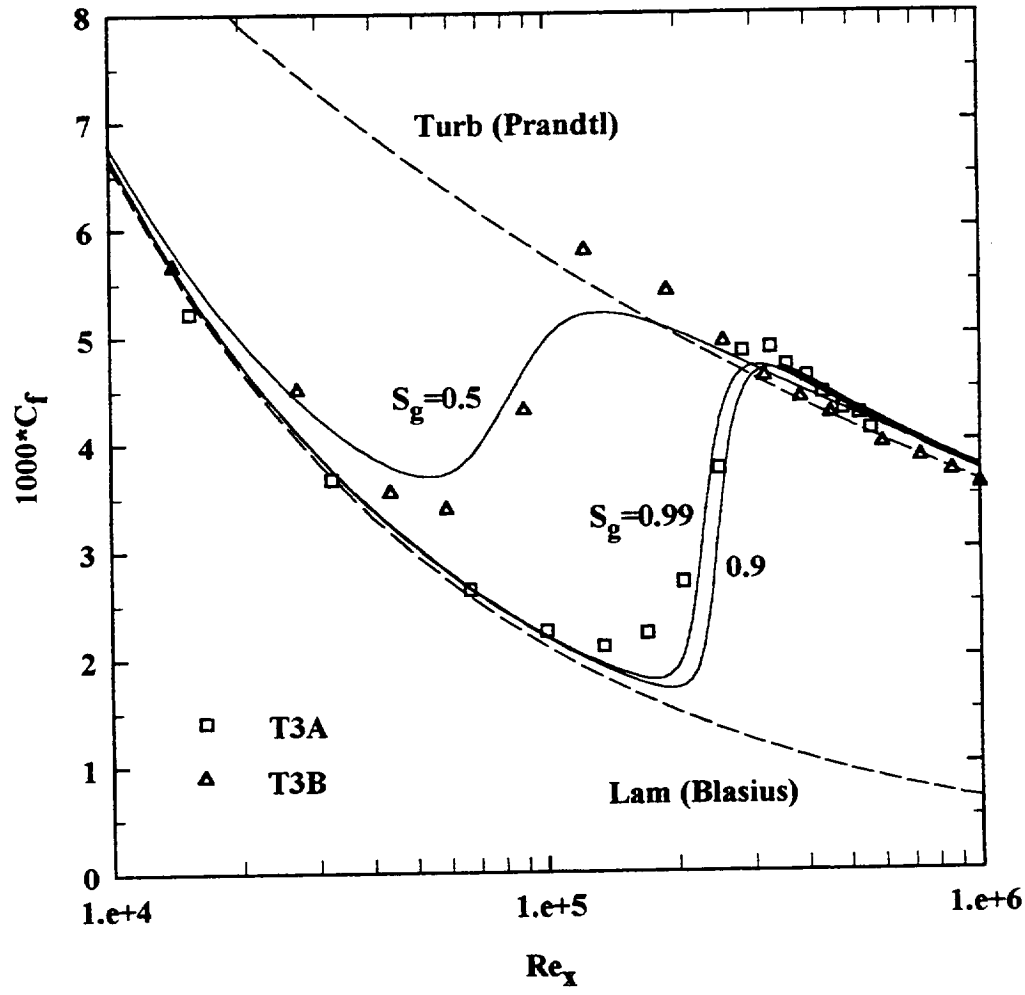

Figure 3-7 Comparison of the predicted friction coefficient during transition with the data of T3A and T3B.

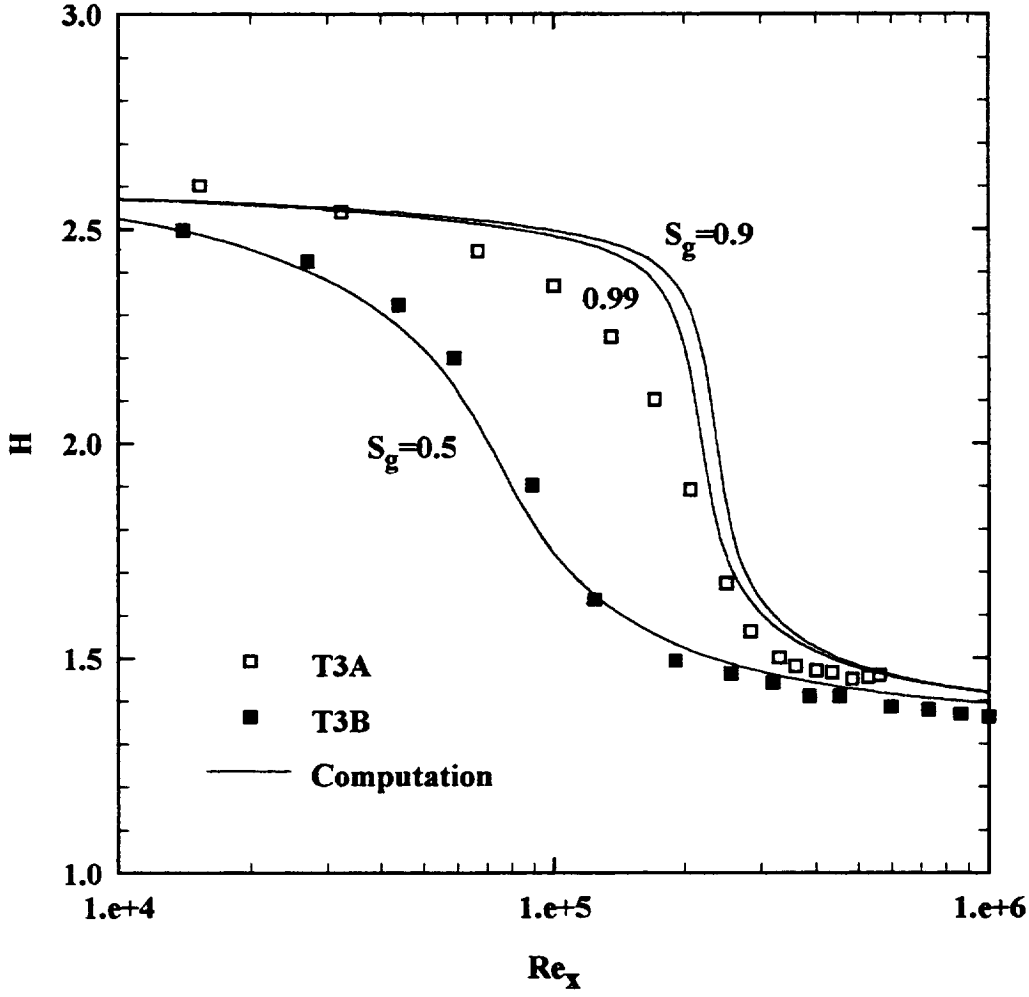

Figure 3-8 Comparison of the predicted shape factor during transition with the data of T3A and T3B.

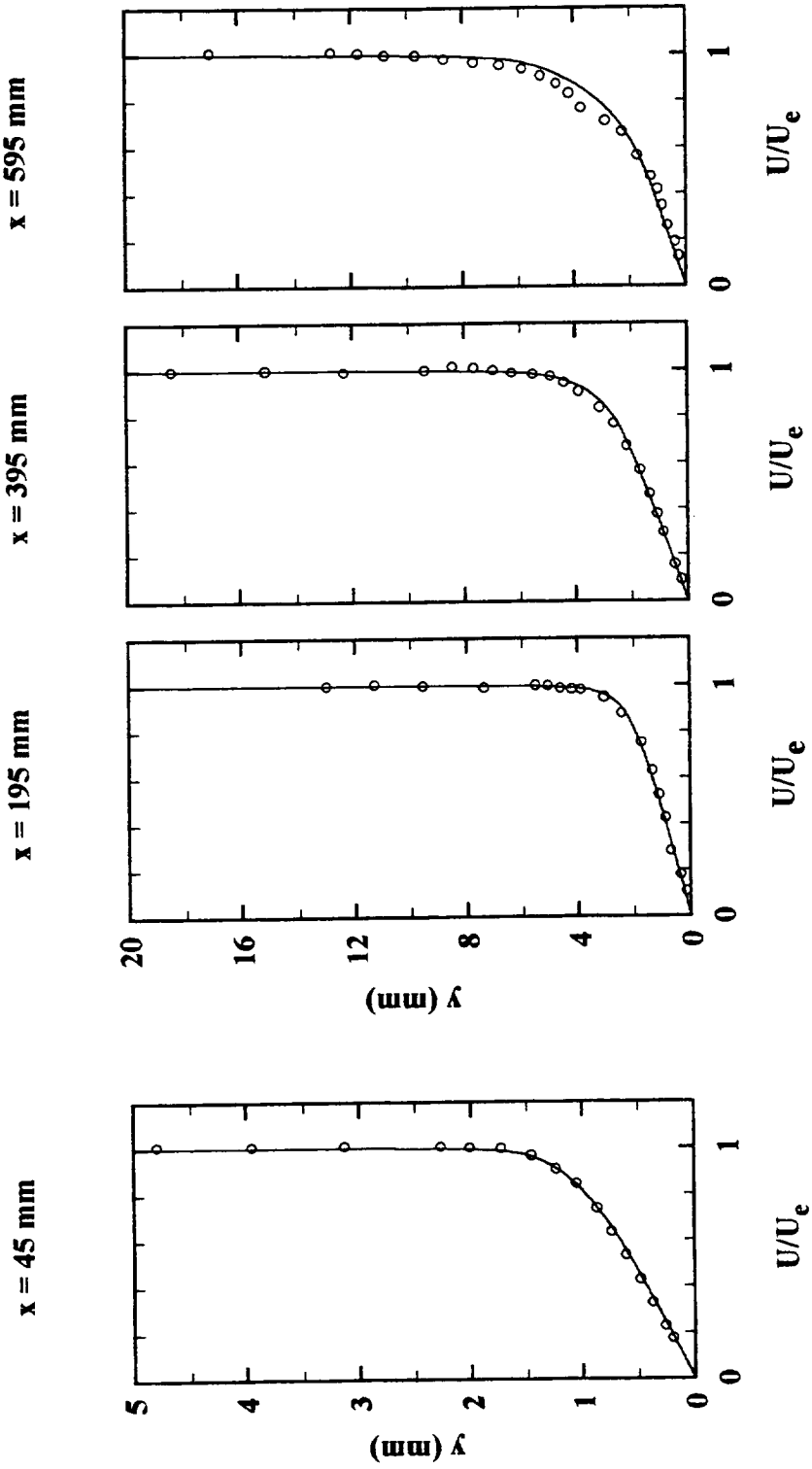

Figure 3-9(a) Comparison of predicted mean flow profiles with experimental data for T3A; (Symbol: experimental data, Solid line: computation, S_g=0.99)

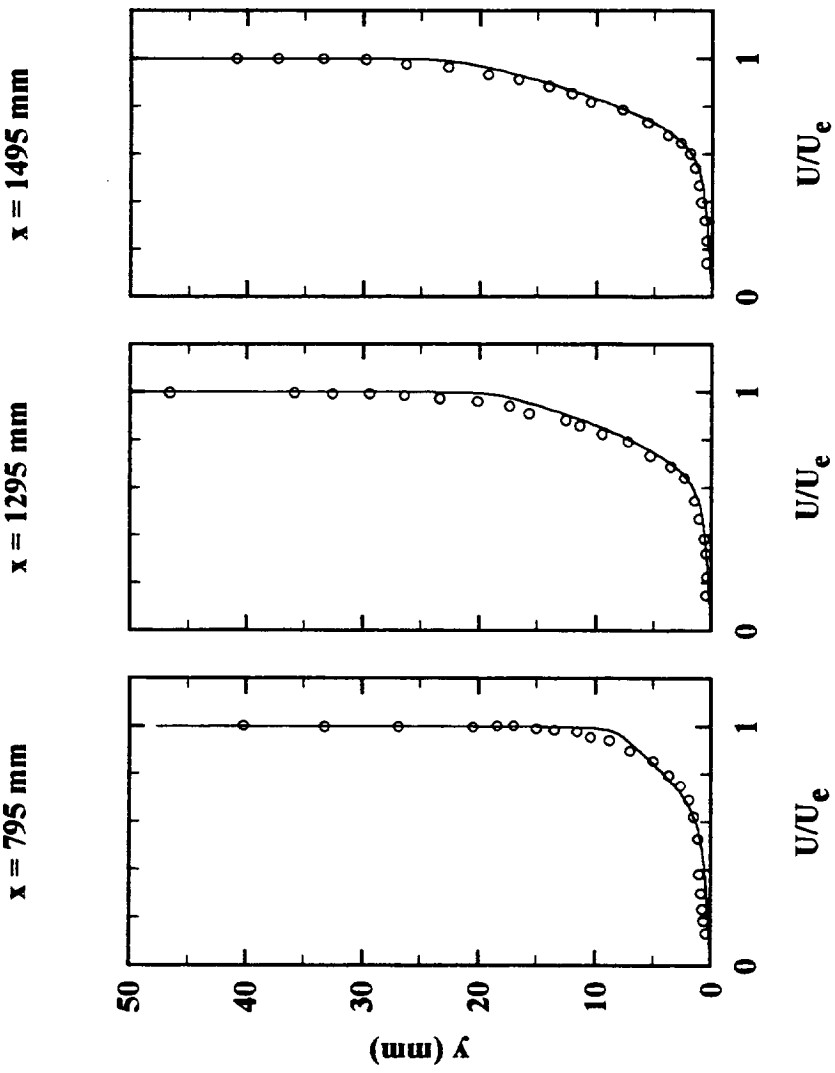

Figure 3-9(b) Comparison of predicted mean flow profiles with experimental data for T3A; (Symbol: experimental data, Solid line: computation, S_g=0.99)

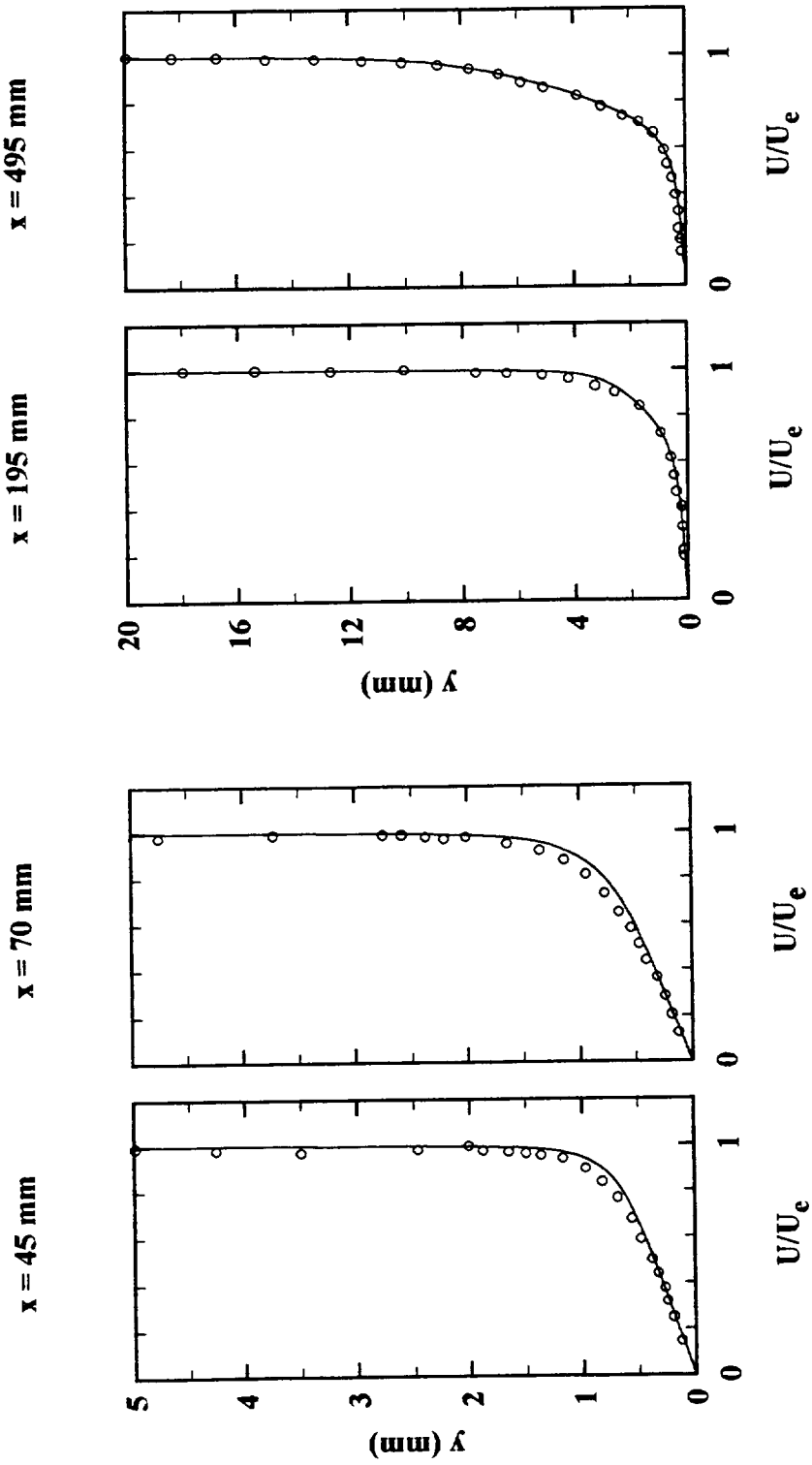

Figure 3-10(a) Comparison of predicted mean flow profiles with experimental data of T3B; (Symbol: experimental data; Solid line: computation, S_g=0.5)

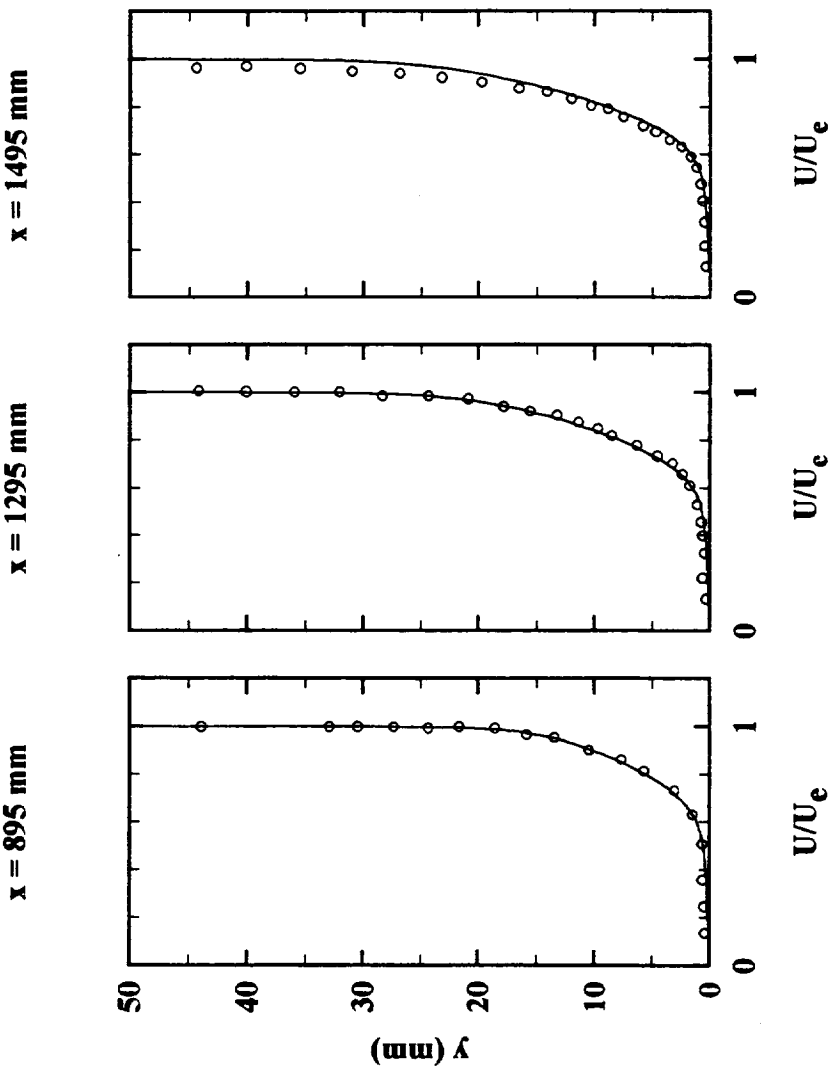

Figure 3-10(b) Comparison of predicted mean flow profiles with experimental data of T3B; (Symbol: experimental data; Solid line: computation, S_g=0.5)

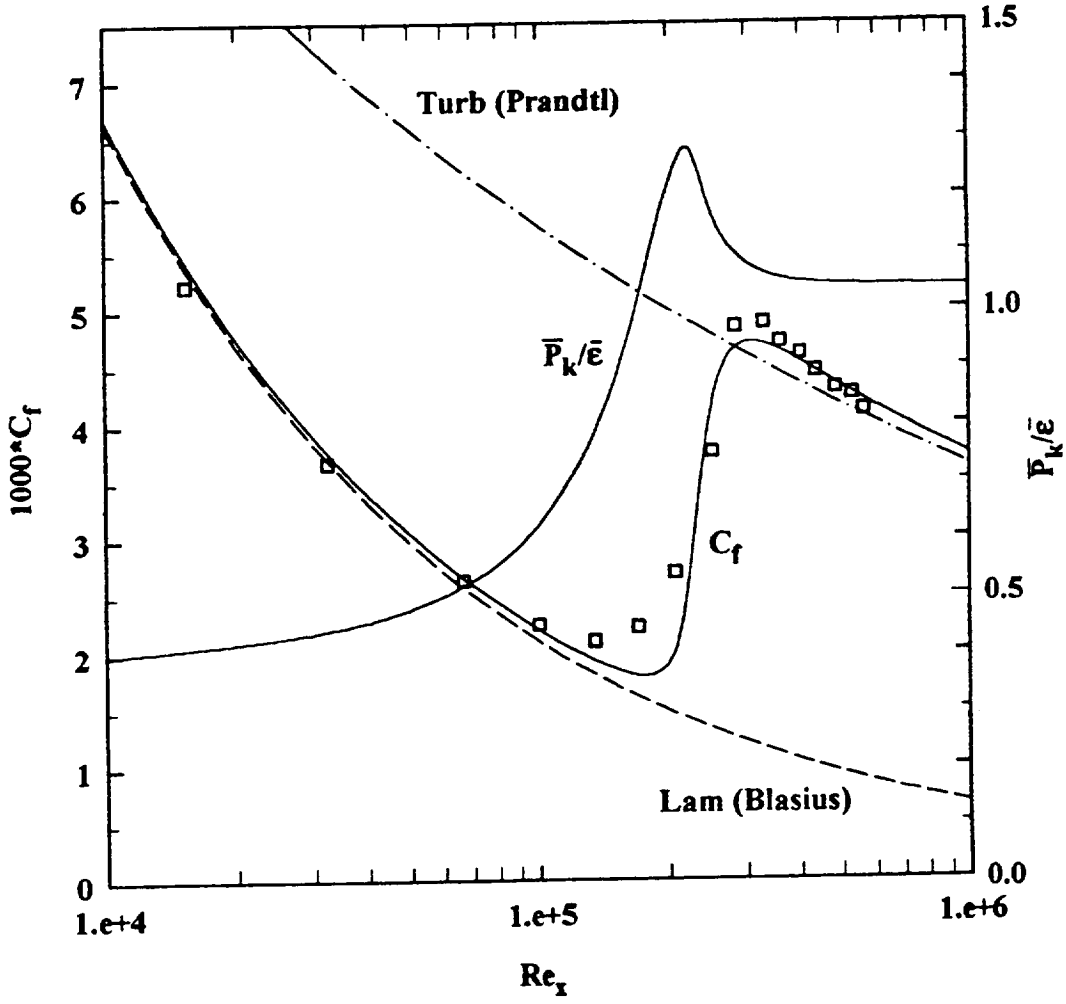

Figure 3-11 Computed local friction coefficient and $\overline{P}_k/\bar{\varepsilon}$ versus Reynolds number for T3A test case; ($S_g = 0.99$)

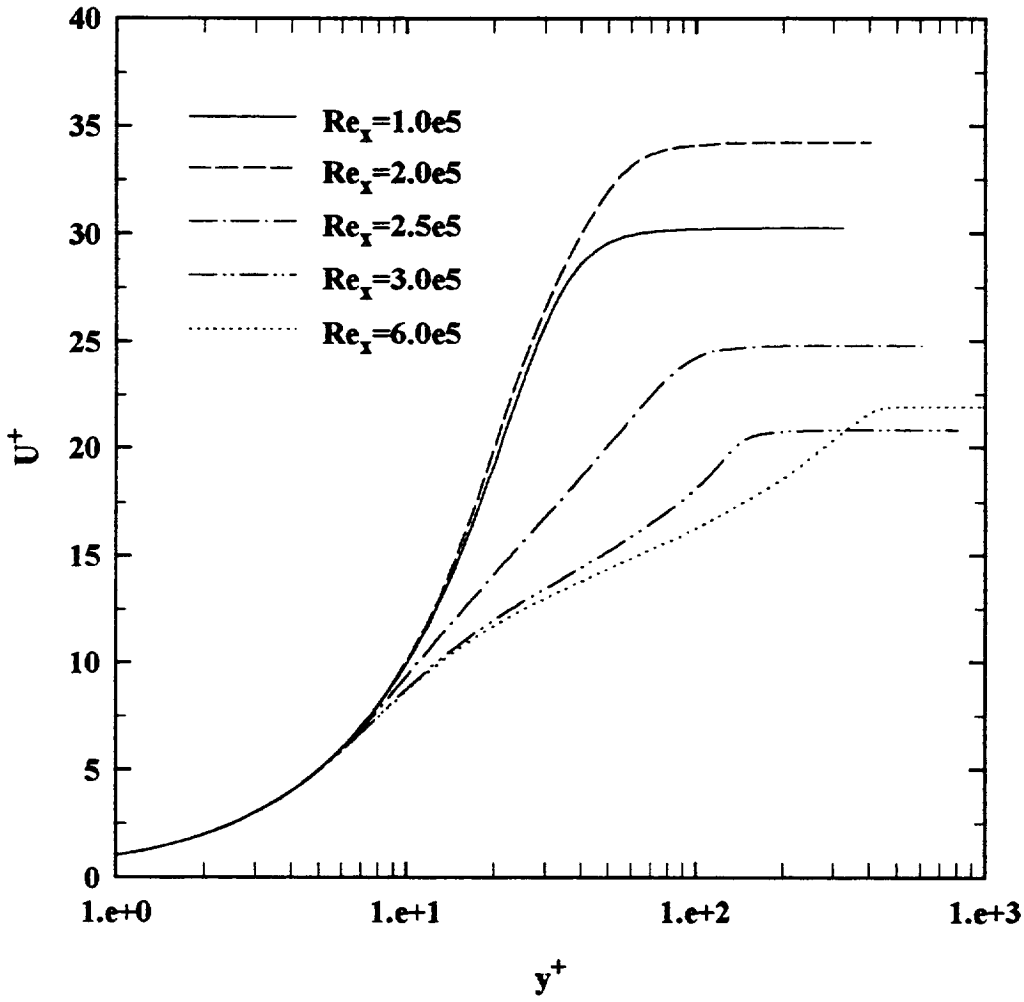

Figure 3-12 Computed mean velocity profiles for T3A test case; (S_g = 0.9).

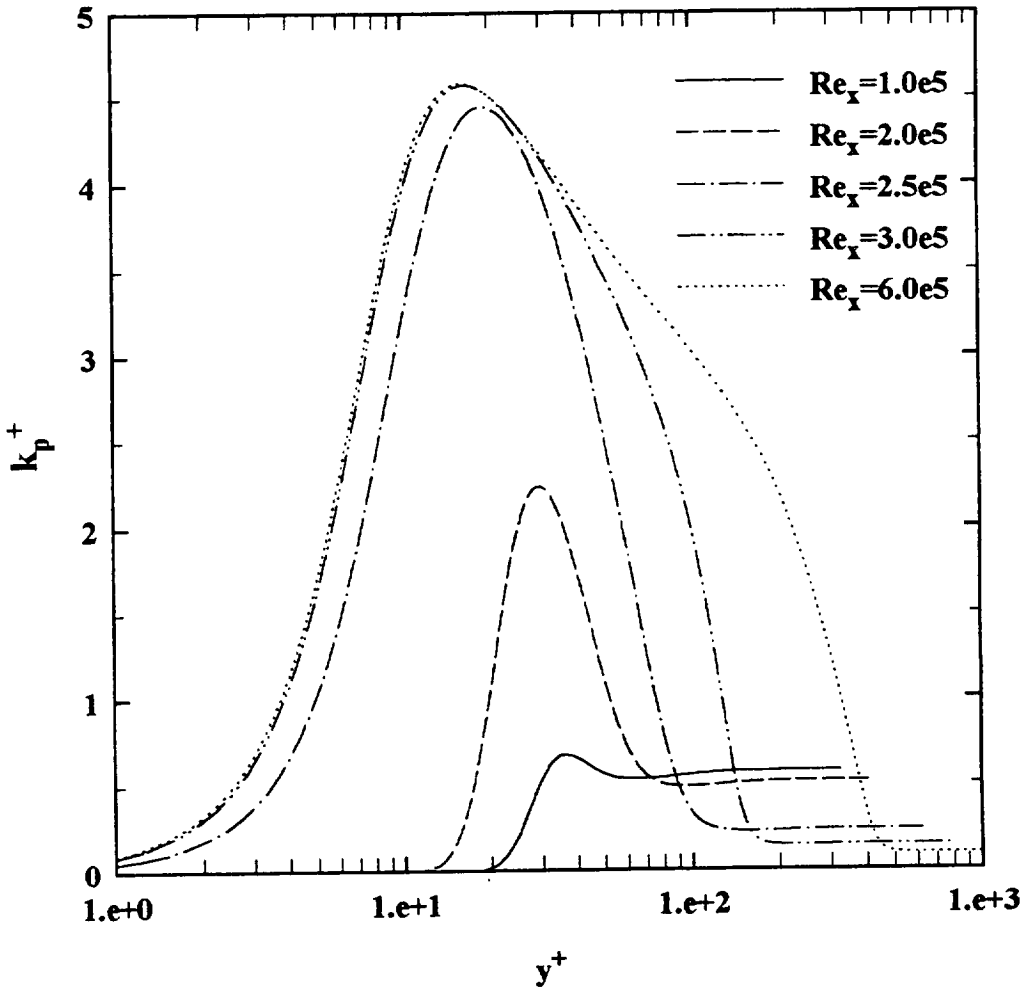

Figure 3-13 Computed turbulent kinetic energy of production region k_p for T3A test case; (S_g = 0.9).

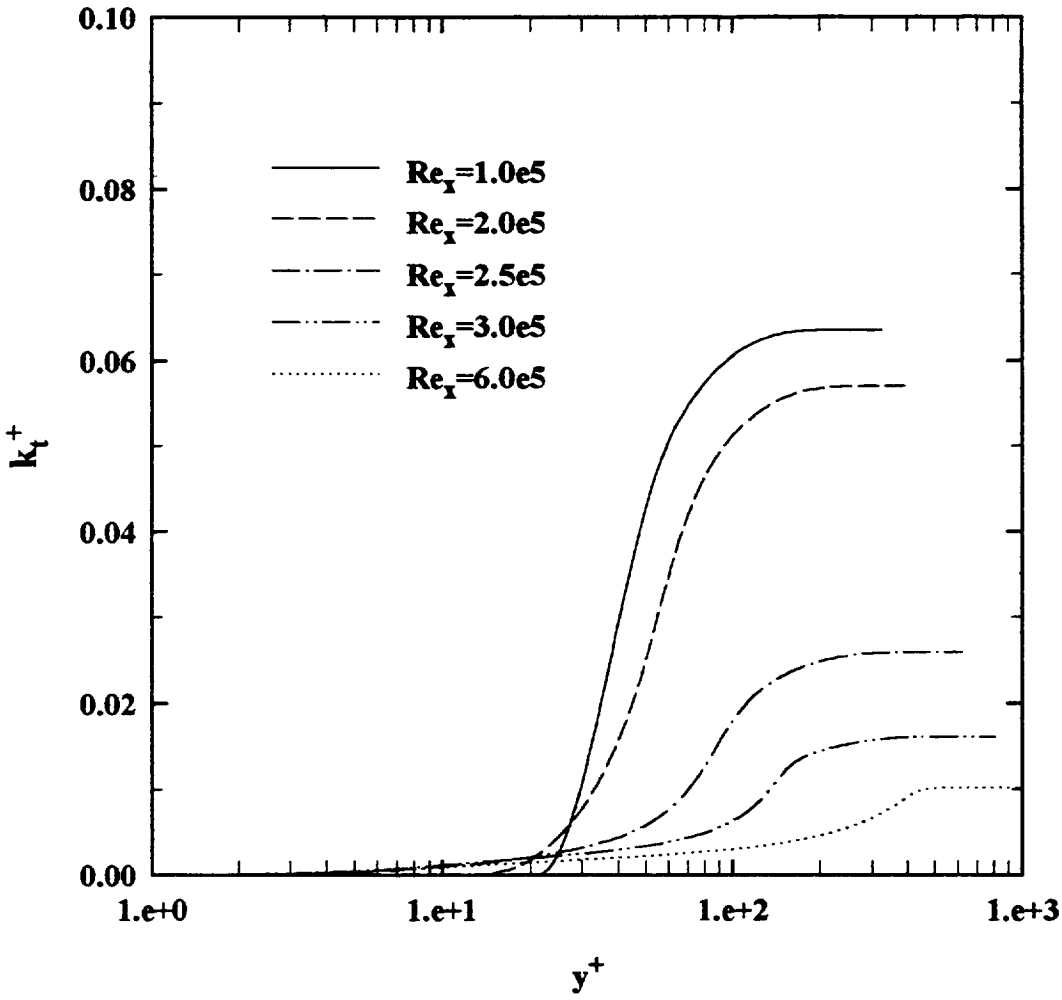

Figure 3-14 Computed turbulent kinetic energy of transfer region k_t for T3A test case; (S_g = 0.9).

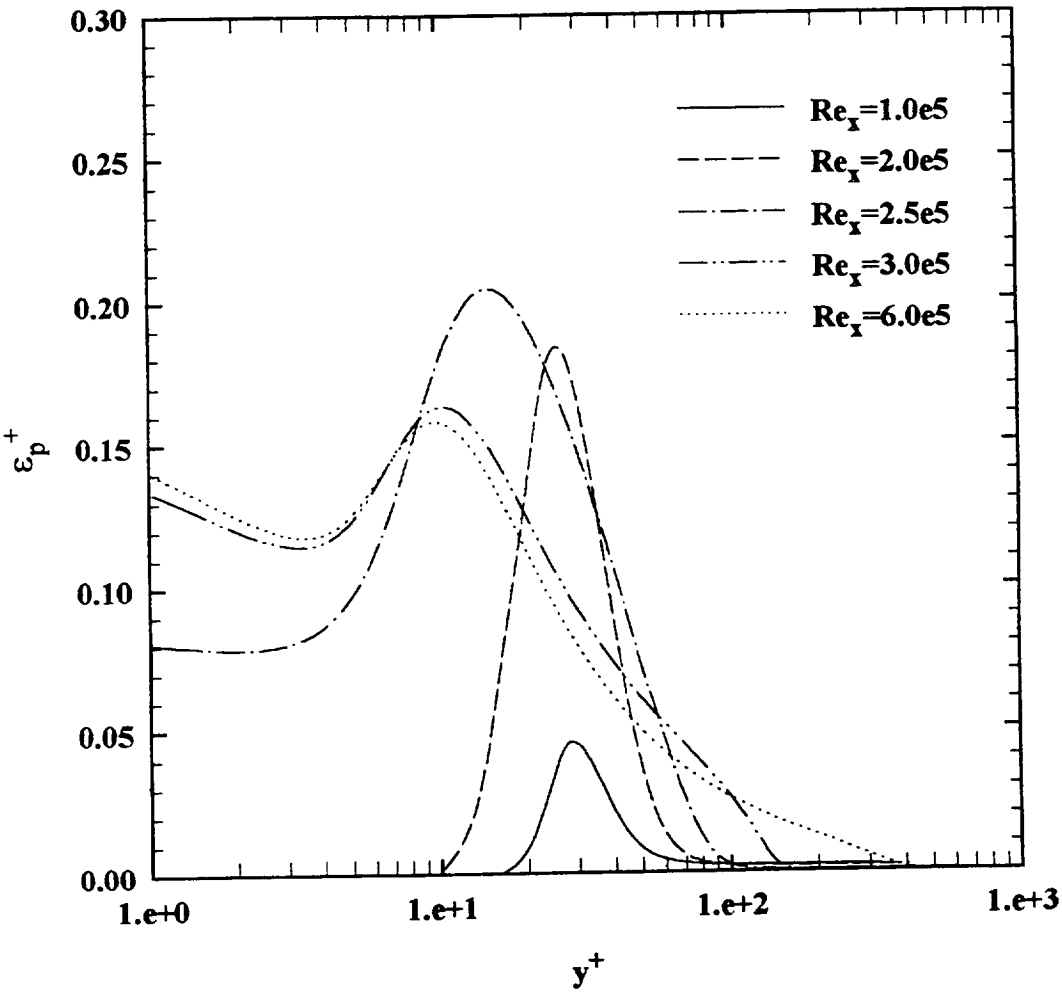

Figure 3-15 Computed energy transfer function ε_p for T3A test case; (S_g = 0.9).

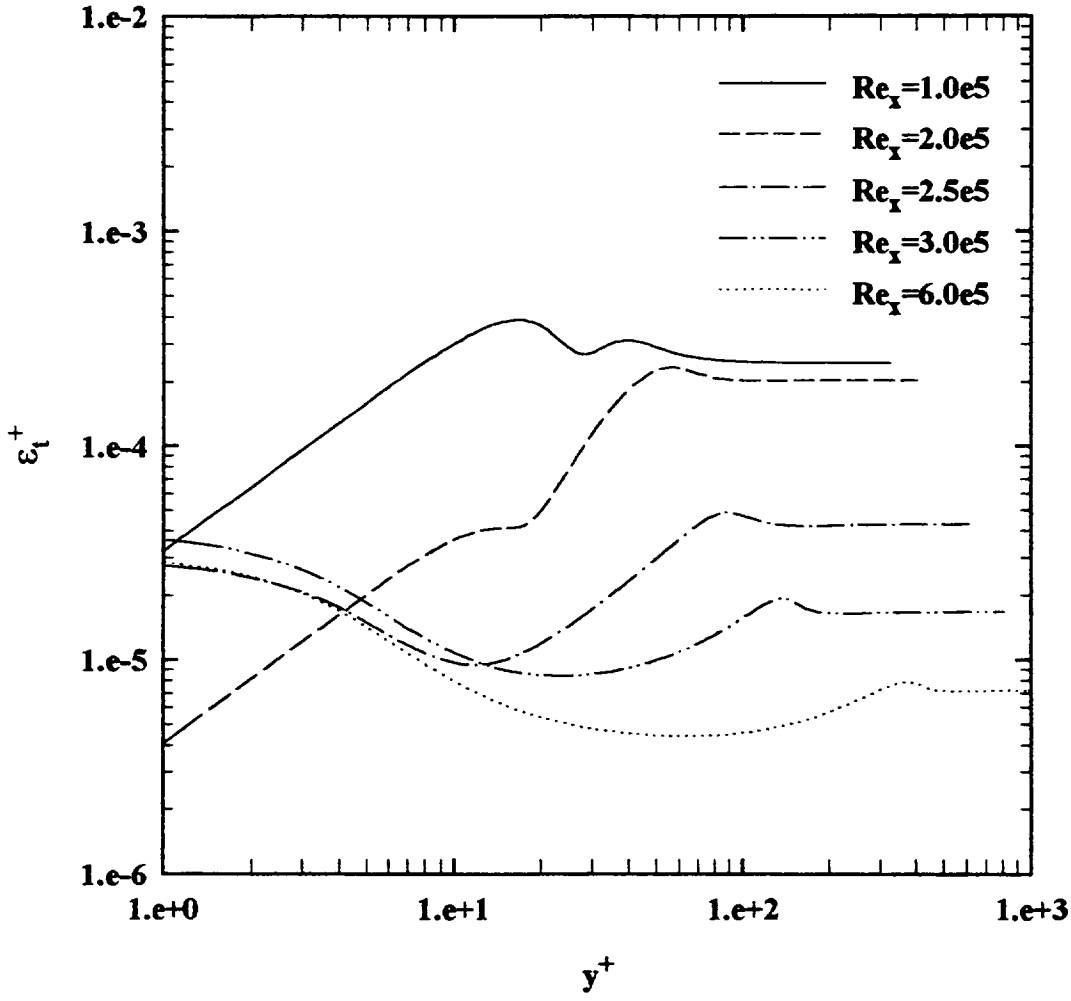

Figure 3-16 Computed energy transfer function ε_t for T3A test case; (S_g = 0.9).

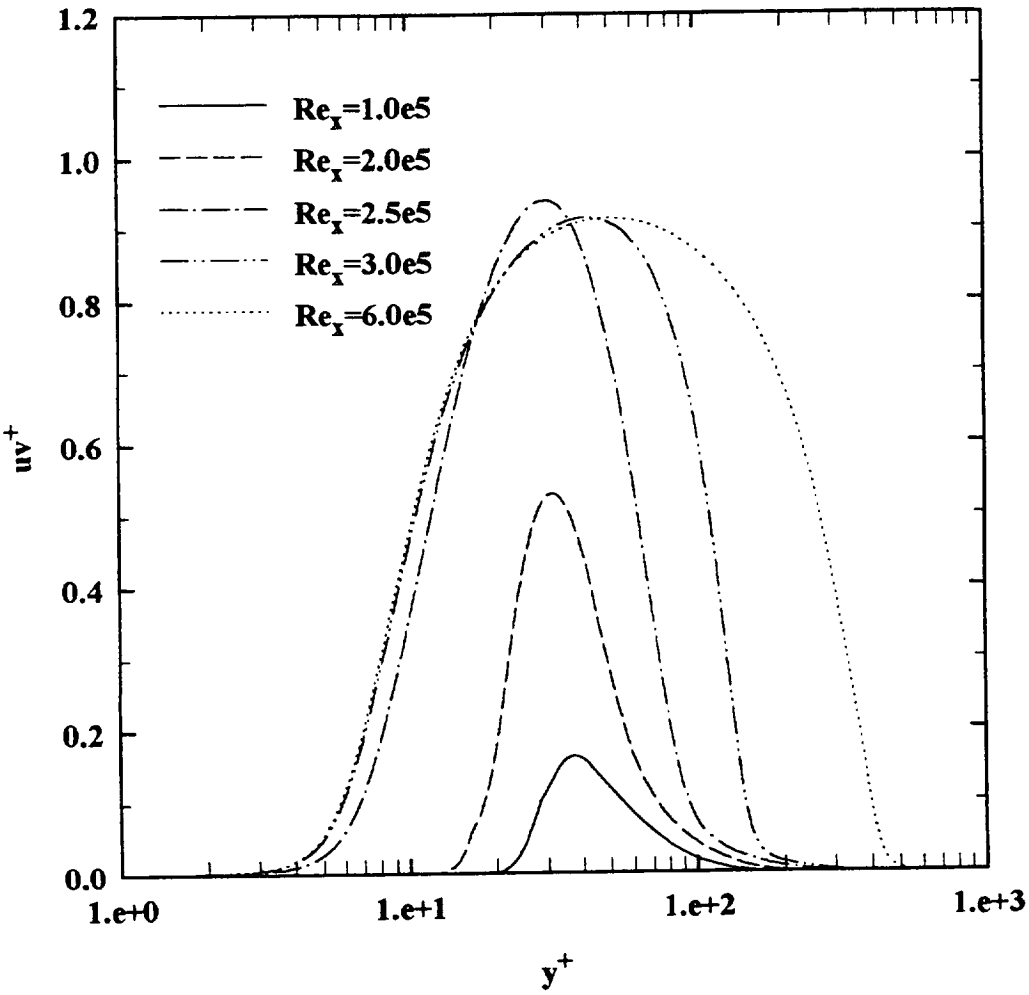

Figure 3-17 Computed Reynolds stress distribution for T3A test case; (S_g = 0.9).

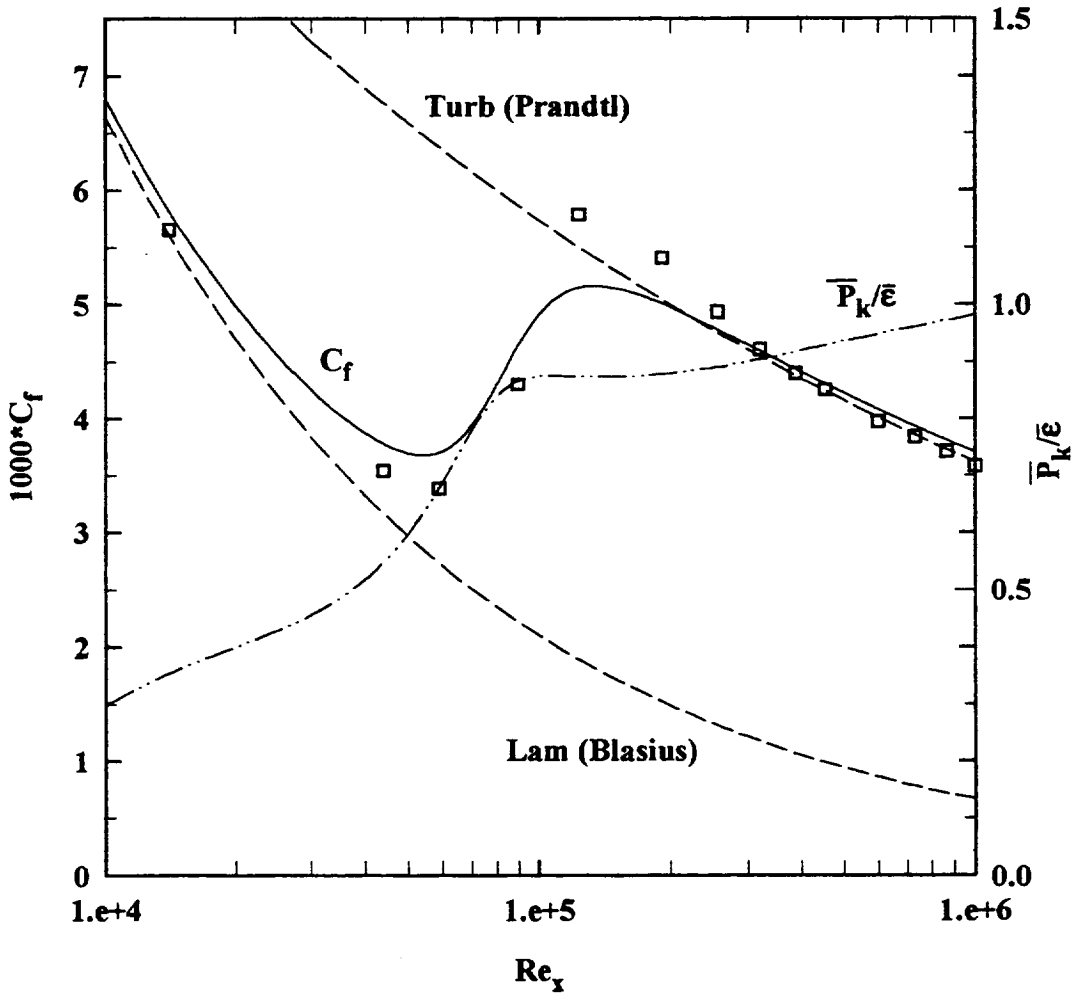

Figure 3-18 Computed local friction coefficient and $\overline{P}_k/\overline{\varepsilon}$ versus Reynolds number for T3B test case; (S_g = 0.5).

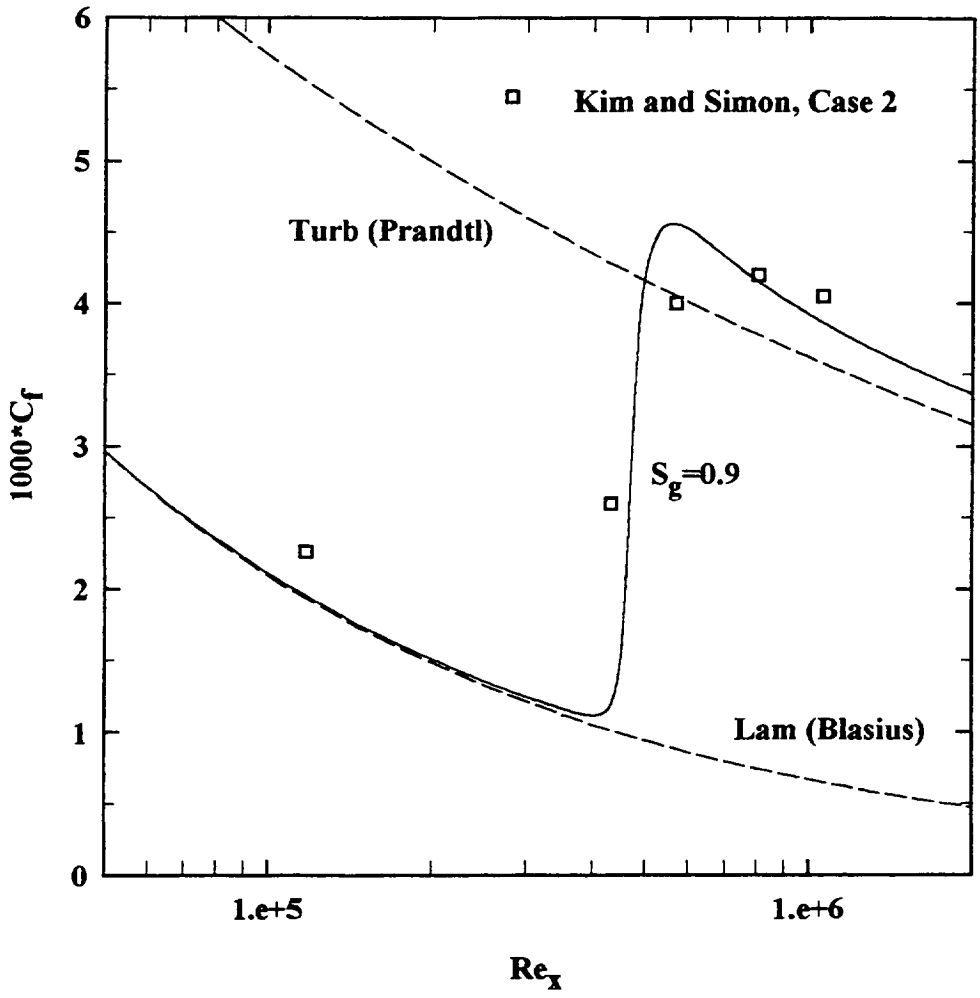

Figure 3-19 Comparison of the predicted friction coefficient with the experimental data of Kim and Simon (1991) case 2.

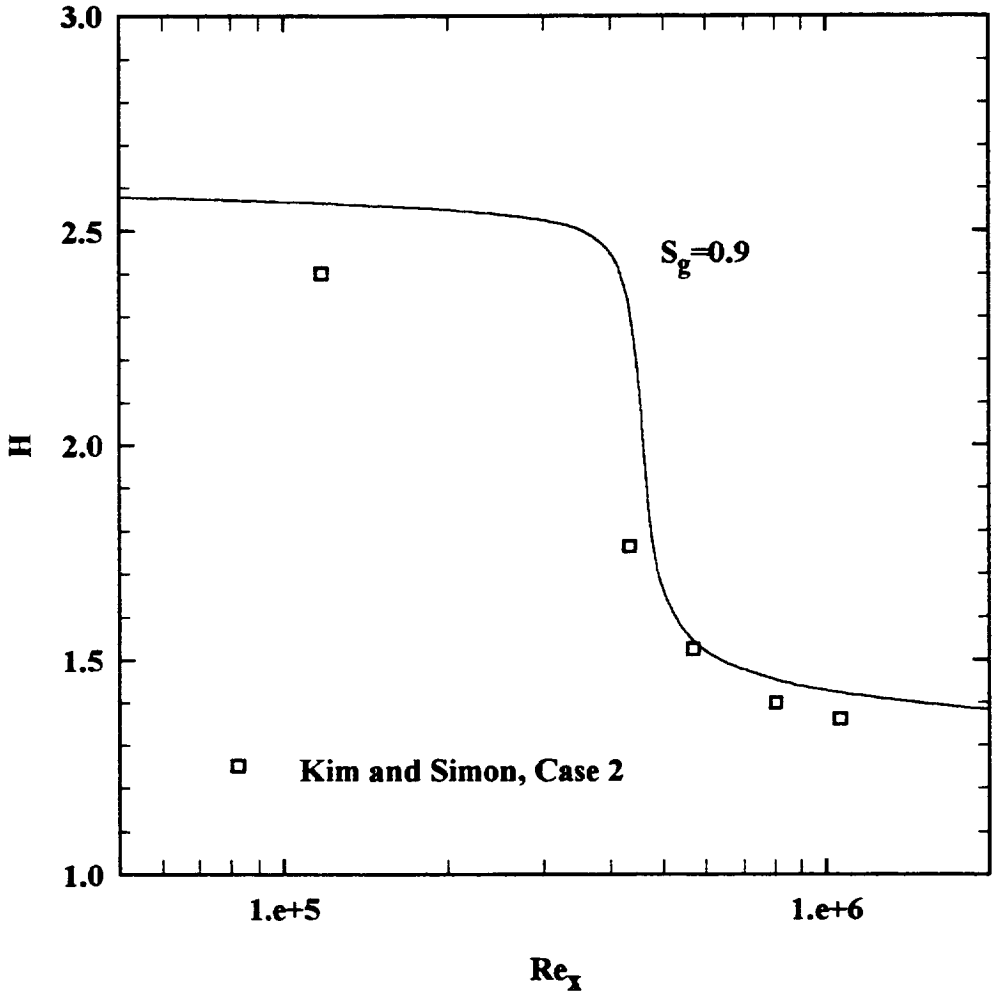

Figure 3-20 Comparison of the shape factor with the experimental data of Kim and Simon (1991) case 2.

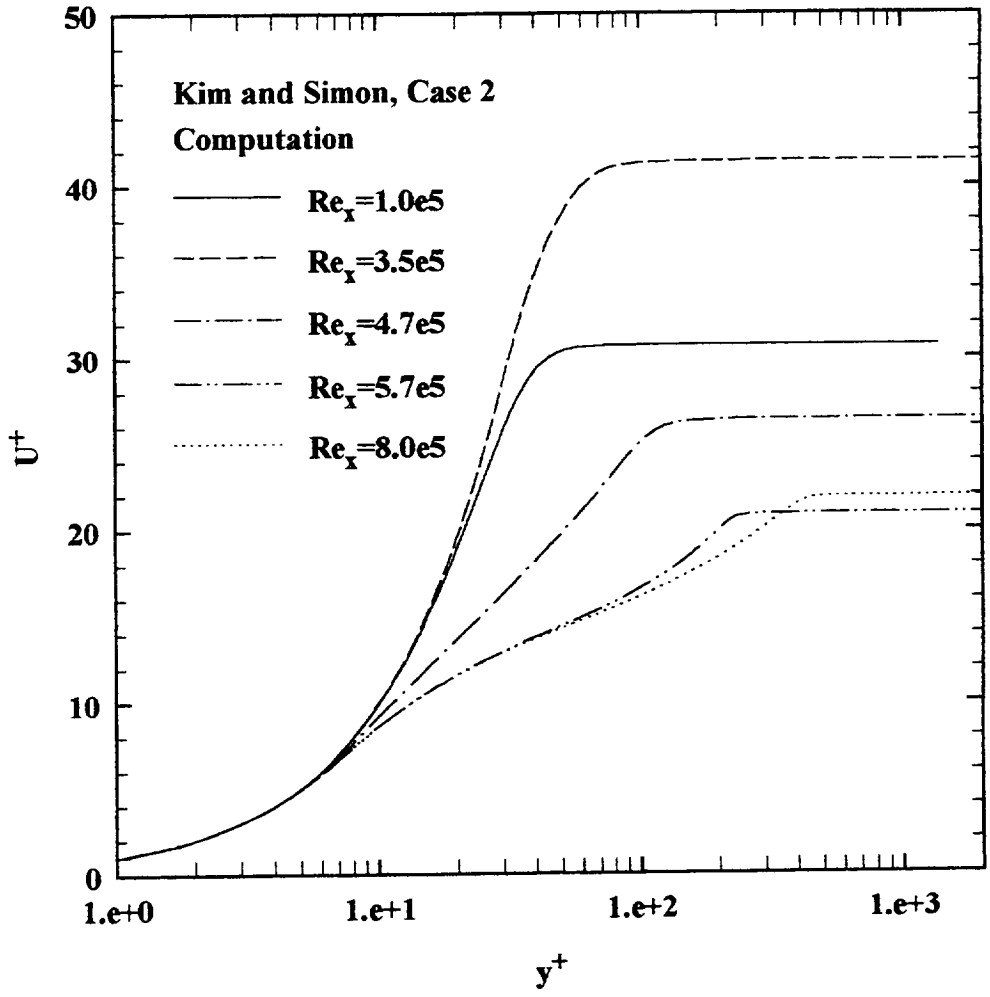

Figure 3-21(a) Computed mean velocity profiles; the experiment of Kim and Simon (1991) case 2.

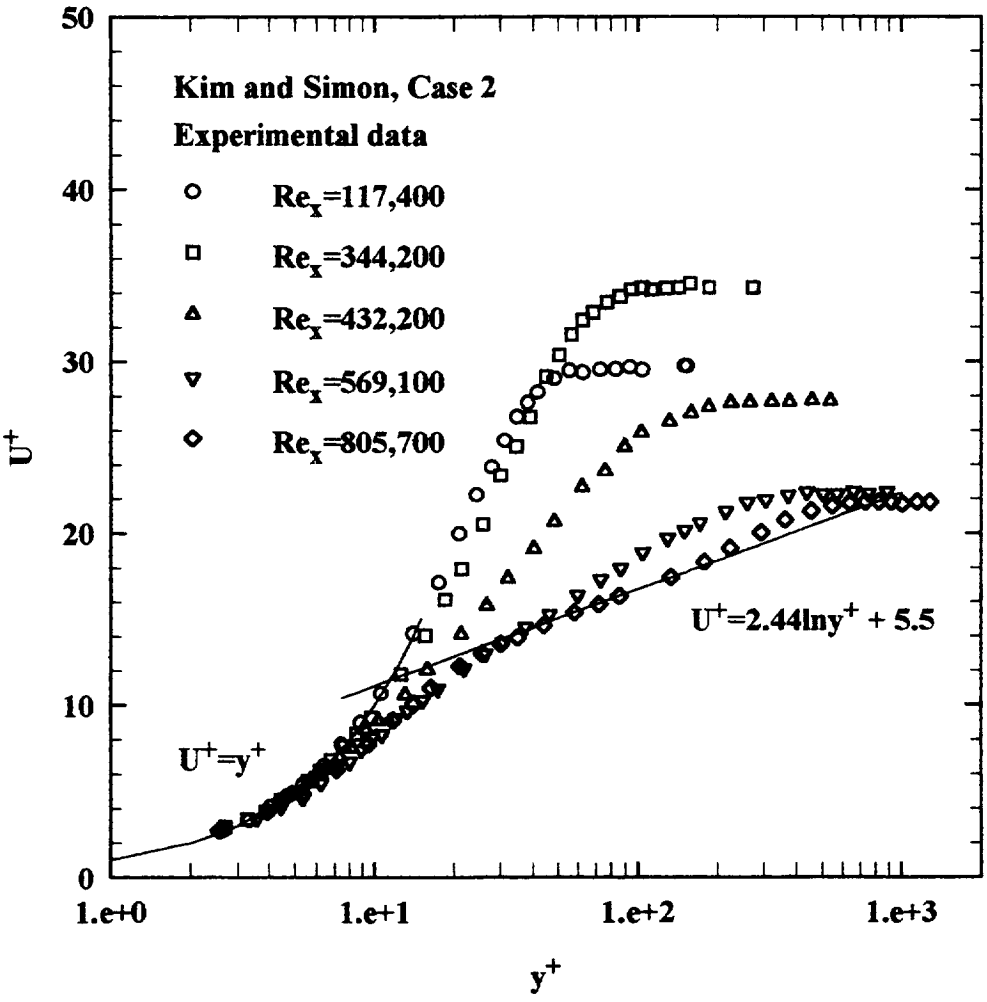

Figure 3-21(b) Mean velocity profiles; the experimental data of Kim and Simon (1991) case 2.

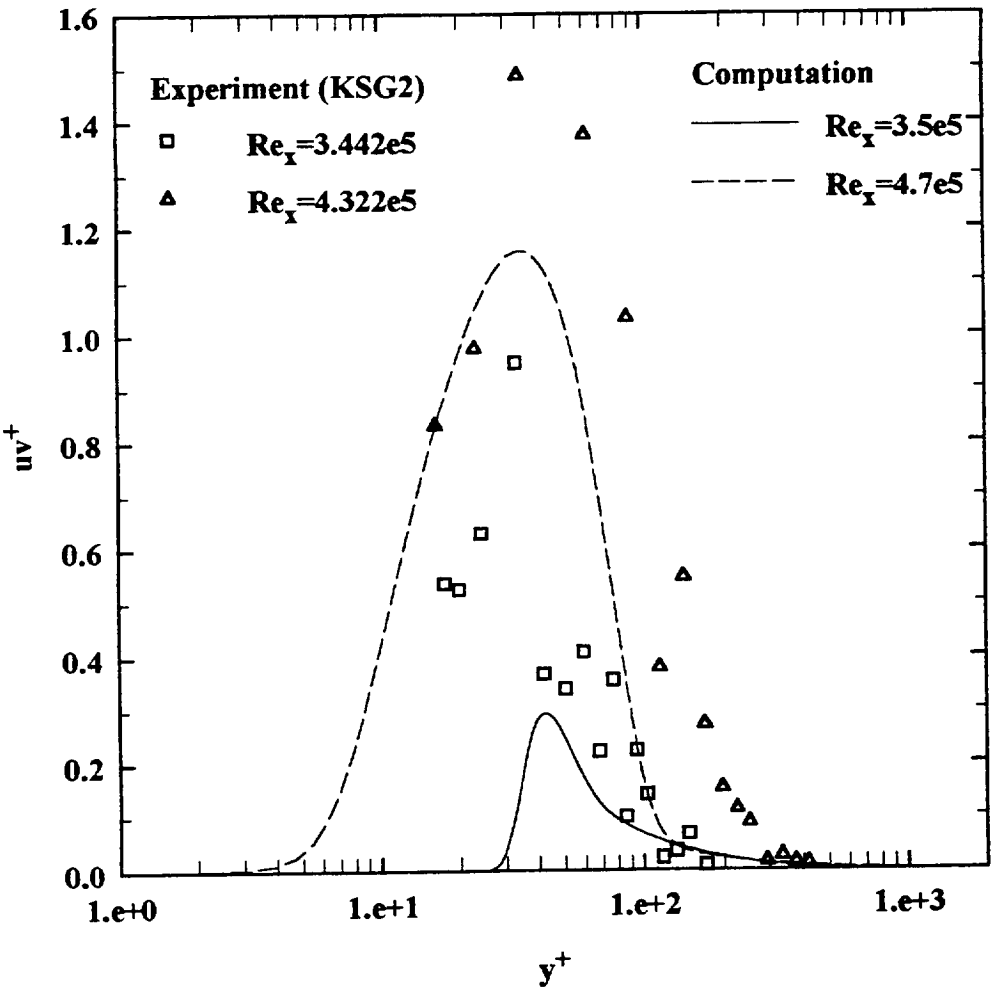

Figure 3-22(a) Reynolds stress development (before transition); comparison of the model with the experimental data of Kim and Simon (1991) case 2.

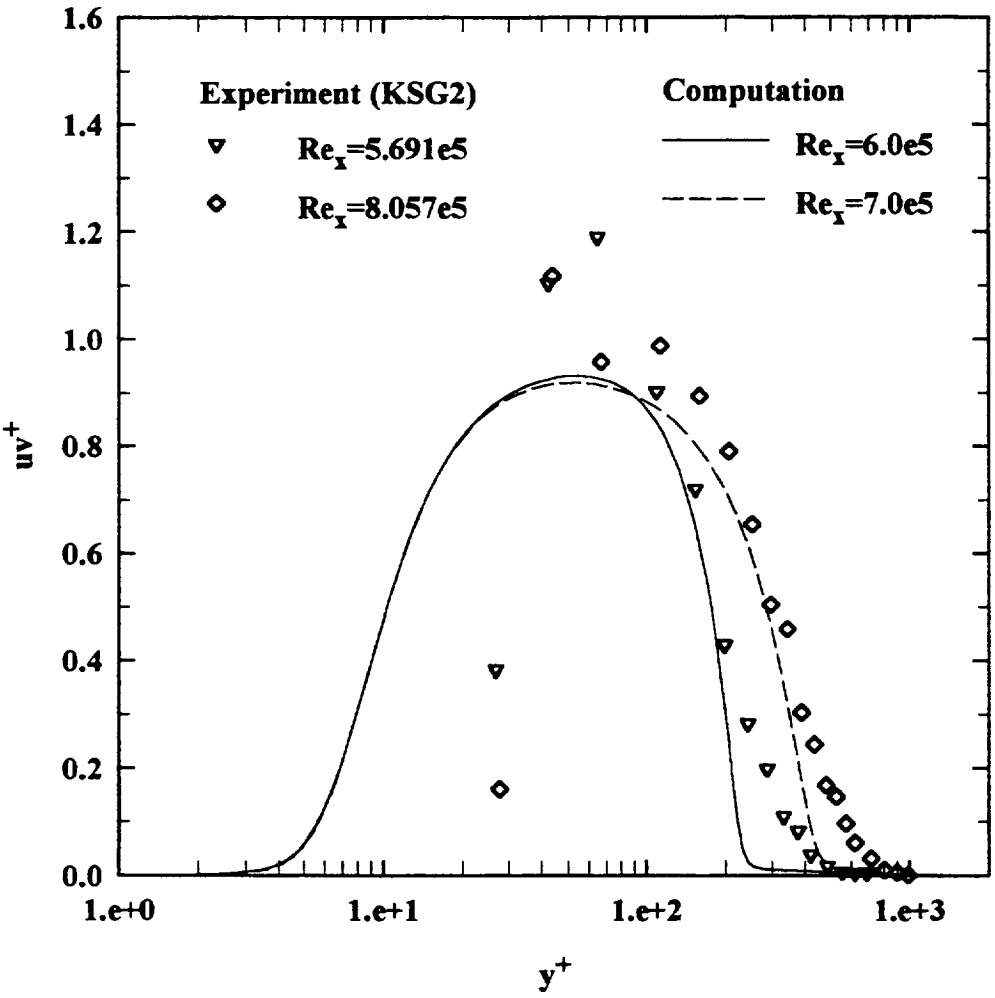

Figure 3-22(b) Reynolds stress development (in transition); comparison of the model with the experimental data of Kim and Simon (1991) case 2.

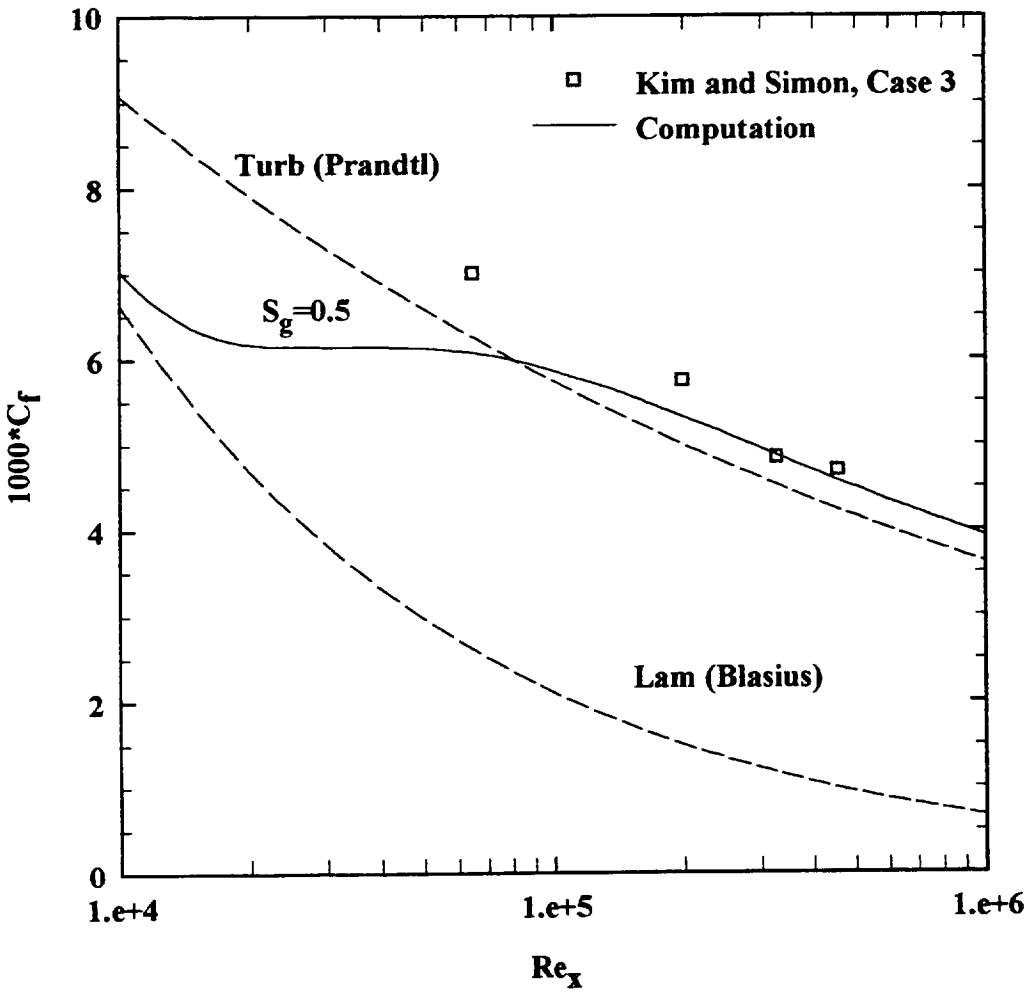

Figure 3-23 Comparison of the predicted friction coefficient with the experimental data of Kim and Simon (1991) case 3.

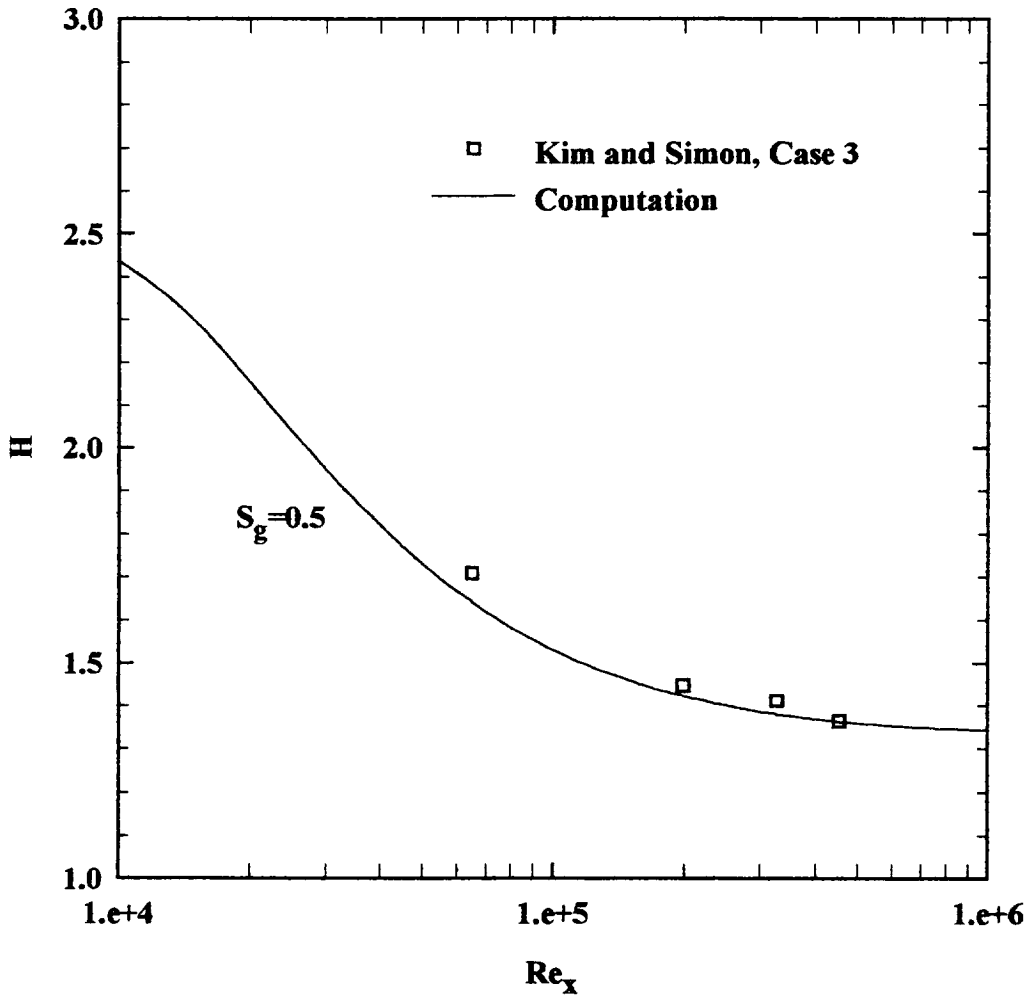

Figure 3-24 Comparison of the shape factor with the experimental data of Kim and Simon (1991) case 3.

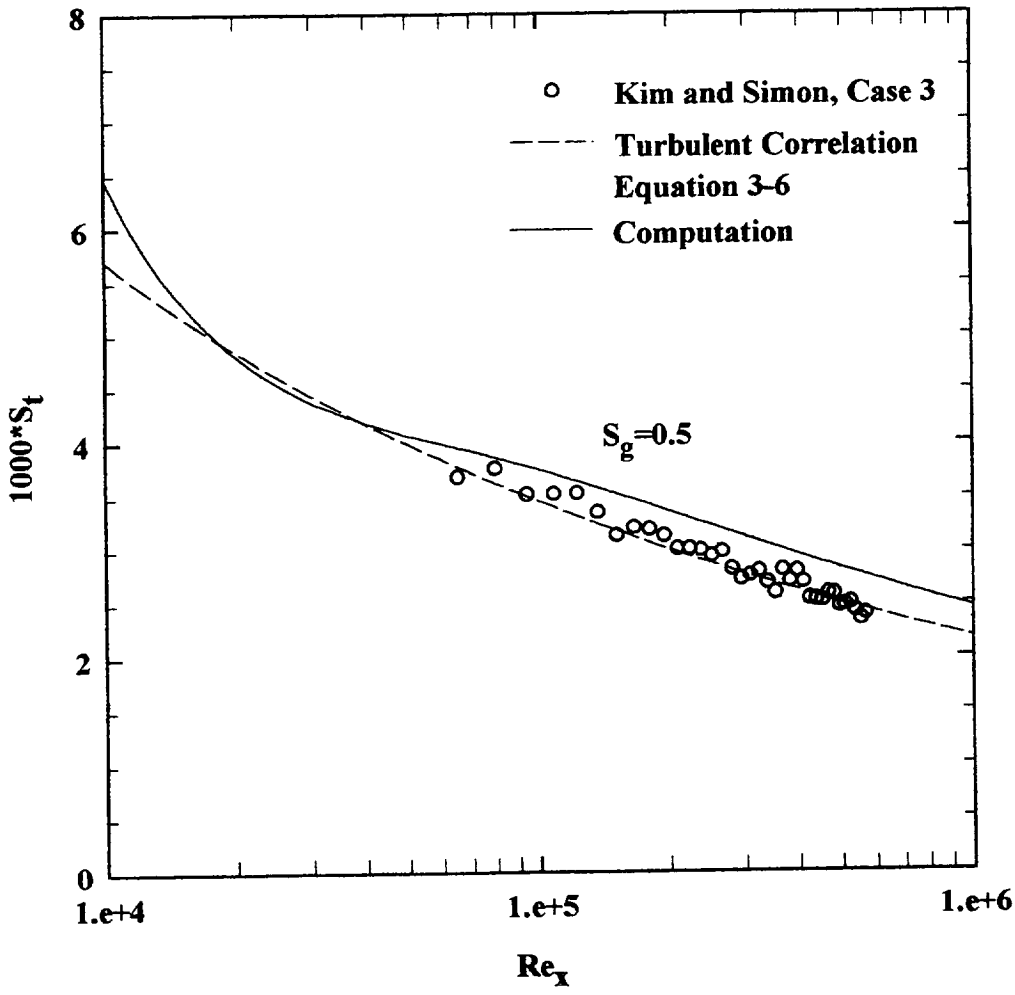

Figure 3-25 Comparison of the predicted heat transfer with the experimental data of Kim and Simon (1991) case 3.

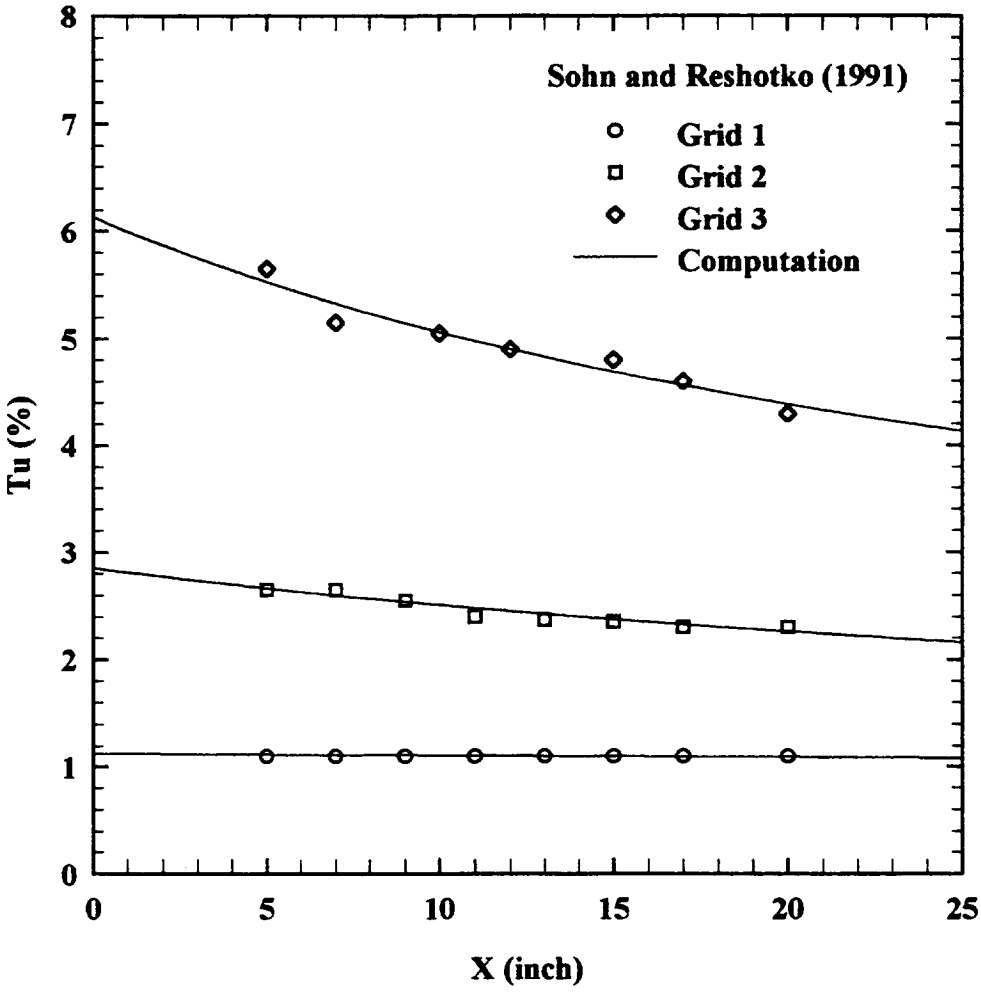

Figure 3-26 Comparison of the predicted freestream turbulent intensities with the experimental data of Sohn and Reshotko (1991).

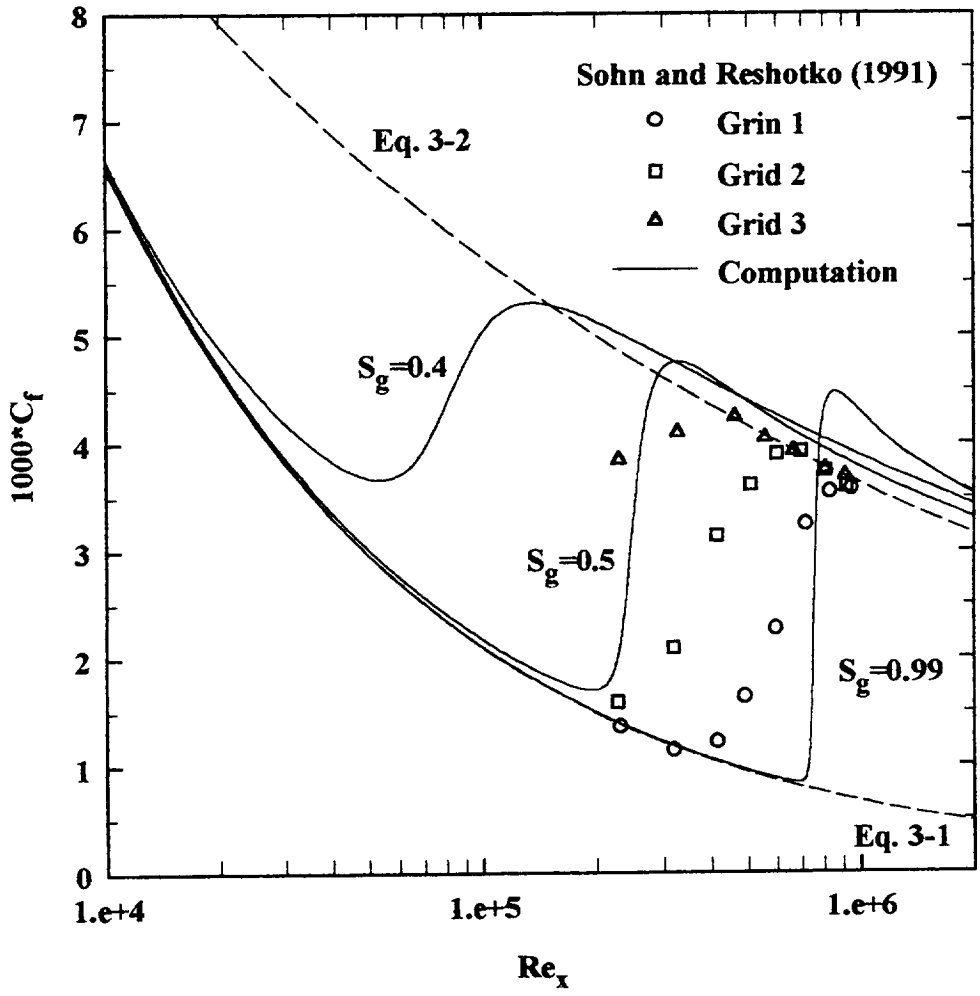

Figure 3-27 Comparison of the predicted friction coefficient with the experimental data of Sohn and Reshotko (1991).

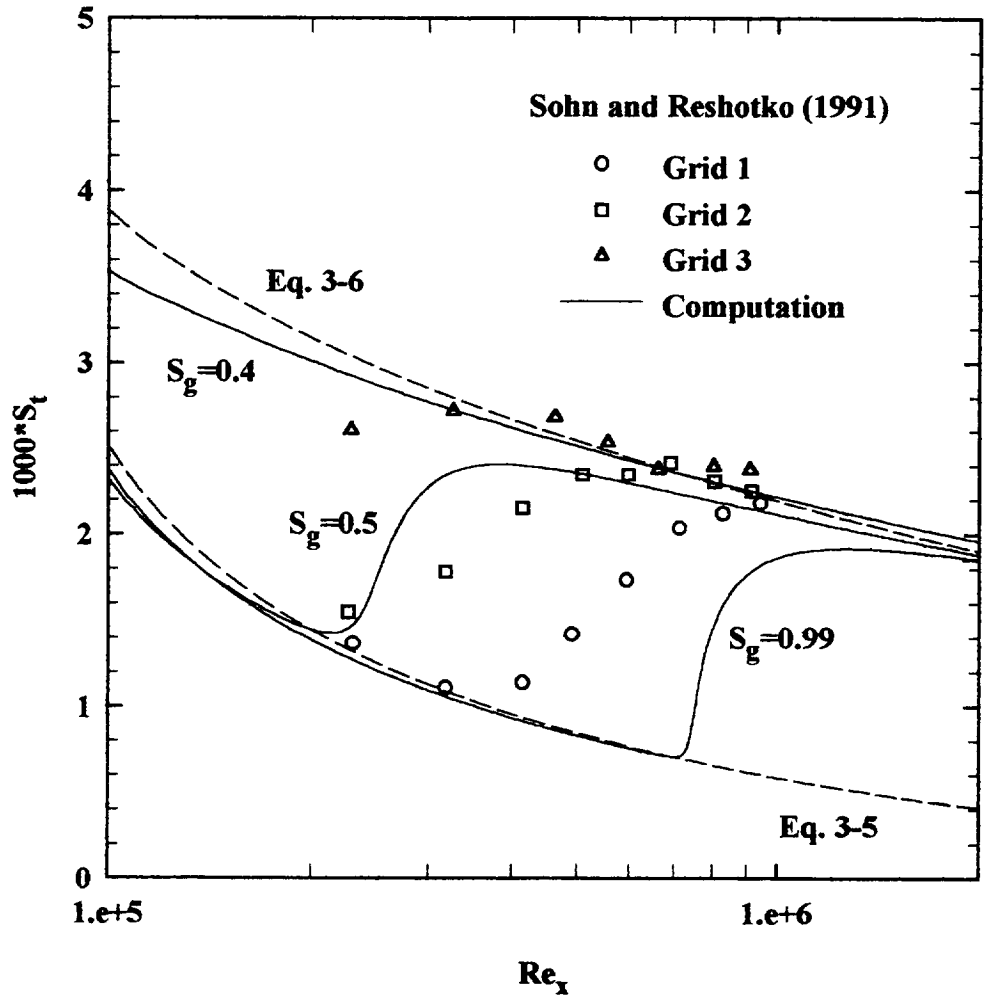

Figure 3-28 Comparison of the predicted heat transfer with the experimental data of Sohn and Reshotko (1991).

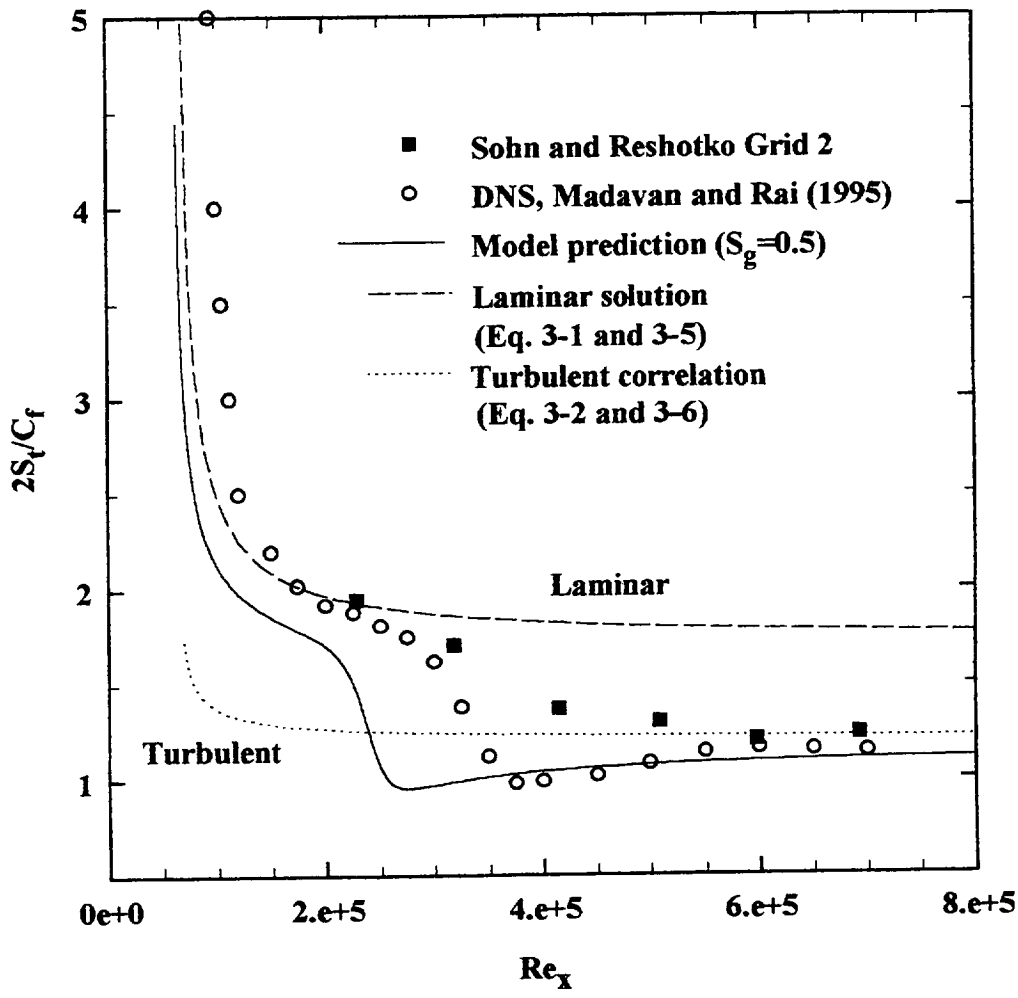

Figure 3-29 Comparison of the predicted Reynolds analogy factors with the experimental data of Sohn and Reshotko (1991) and the DNS results of Madavan and Rai (1995).

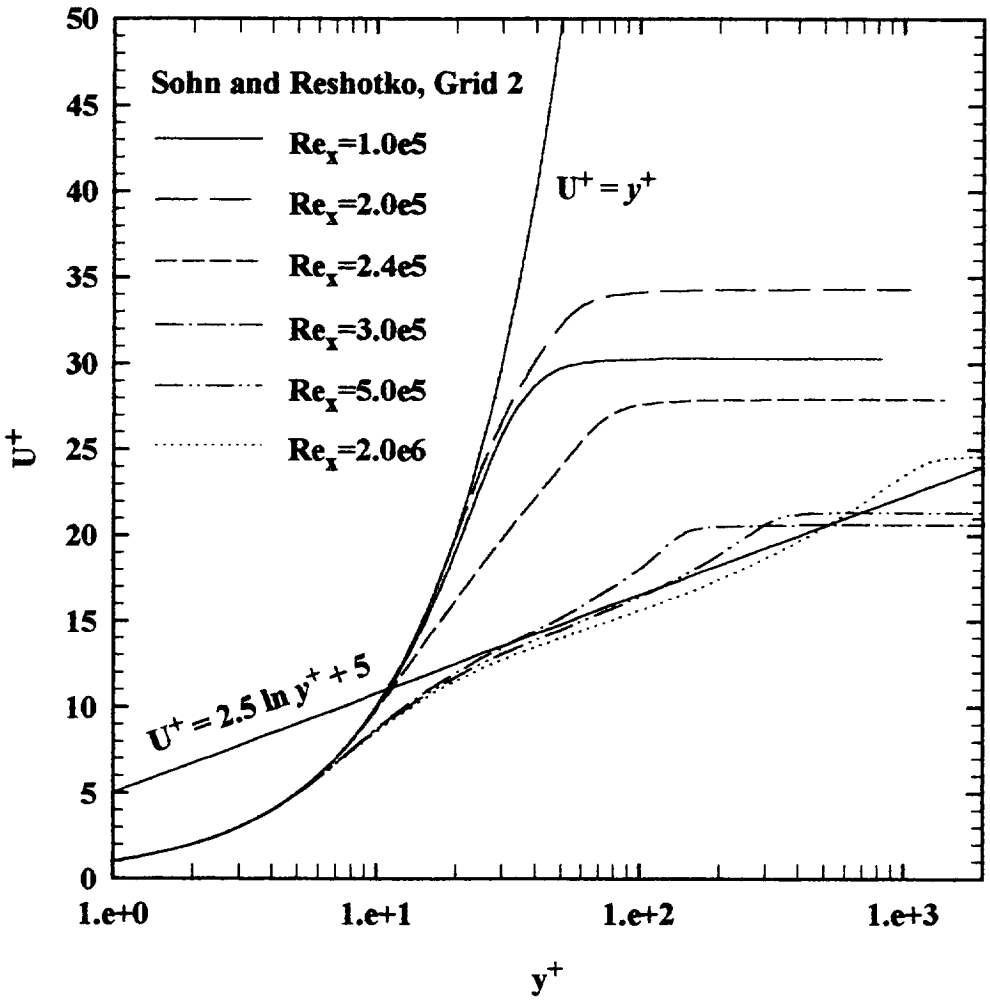

Figure 3-30 Predicted mean velocity profiles at various streamwise locations, in wall units (S_g = 0.5); Sohn and Reshotko (1991) grid 2.

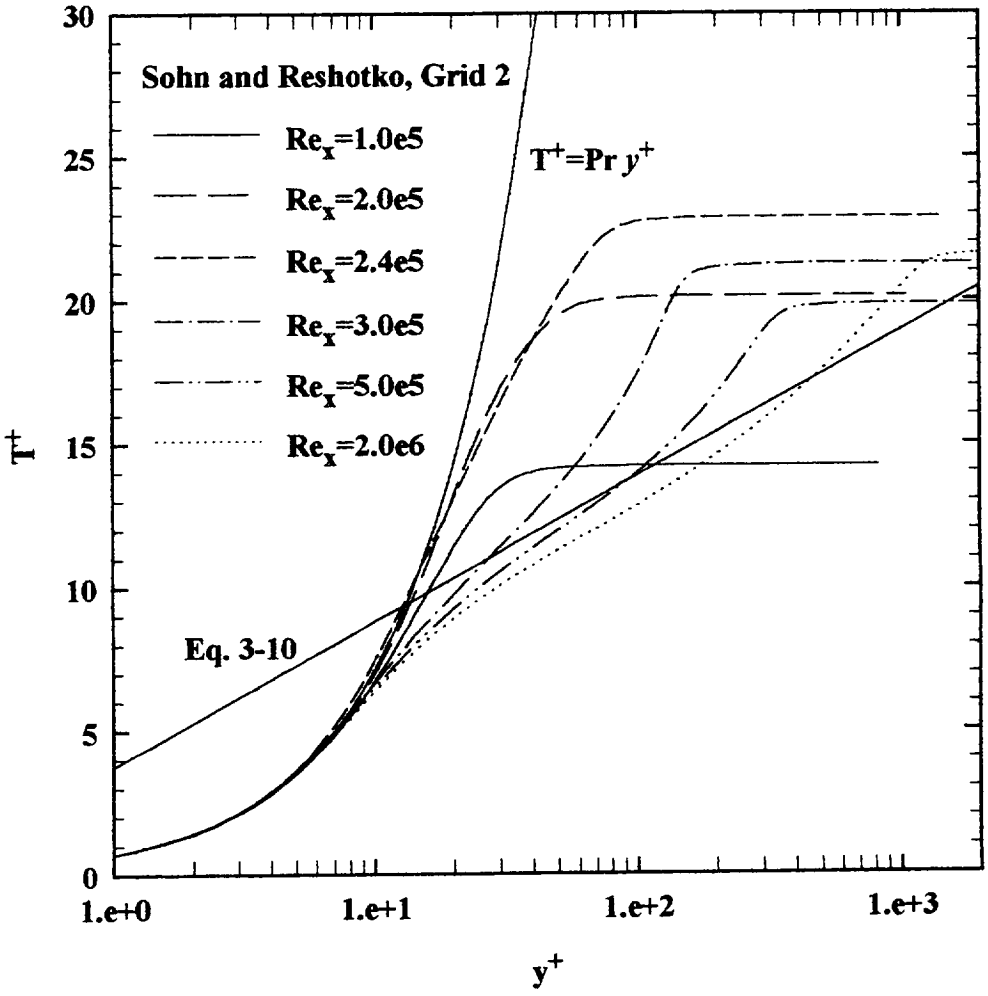

Figure 3-31 Predicted mean temperature profiles at various streamwise locations, in wall units (S_g = 0.5); Sohn and Reshotko (1991) grid 2.

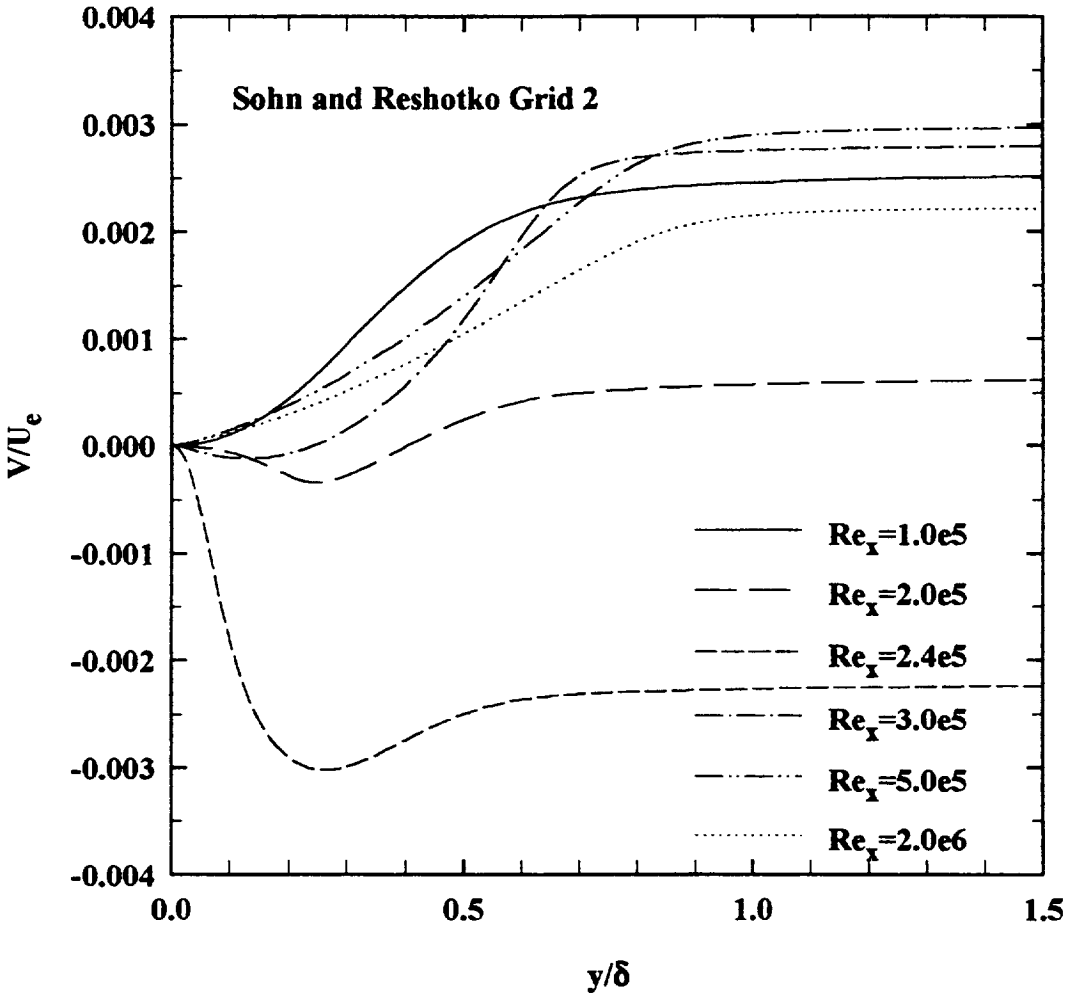

Figure 3-32 Predicted mean normal velocity profiles at various streamwise locations (S_g = 0.5); Sohn and Reshotko (1991) grid 2.

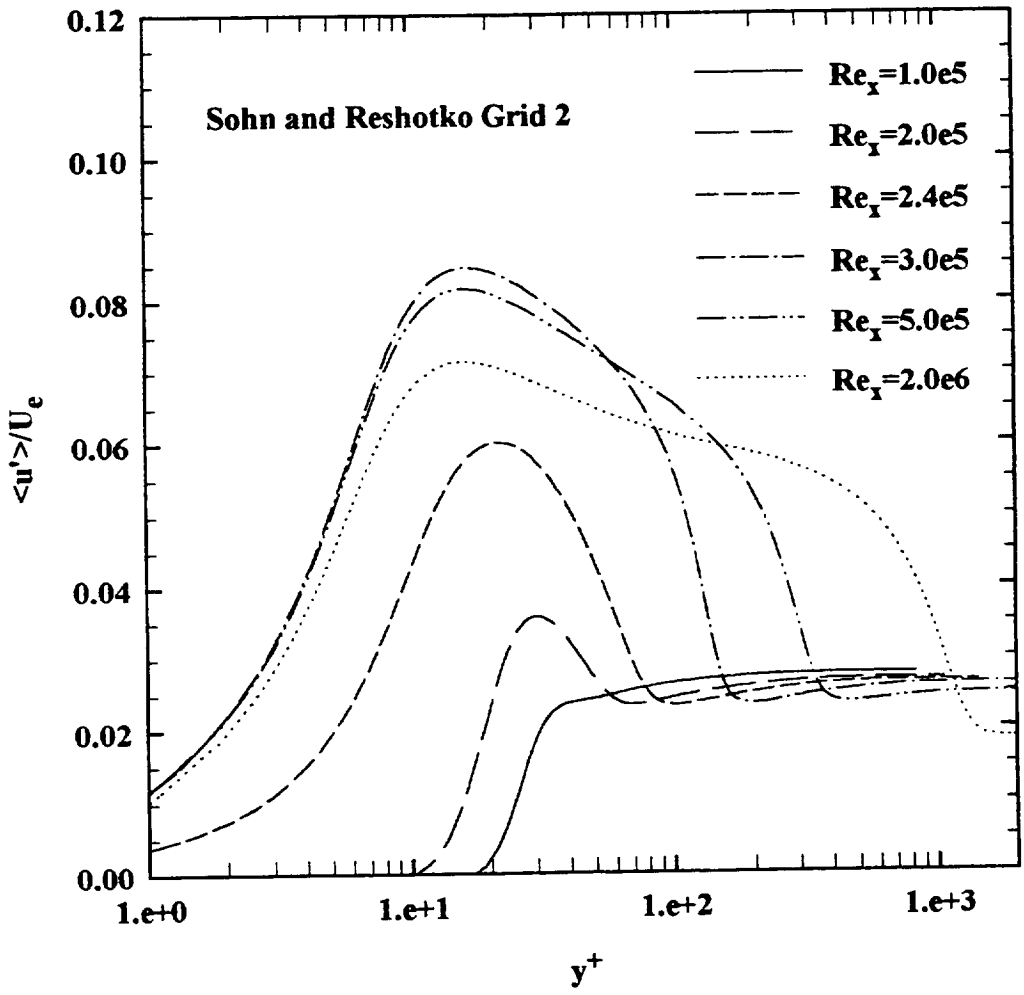

Figure 3-33(a) Predicted turbulent intensity $< u' > / U_e$ at various streamwise locations, in wall units (S_g = 0.5); Sohn and Reshotko (1991) grid 2.

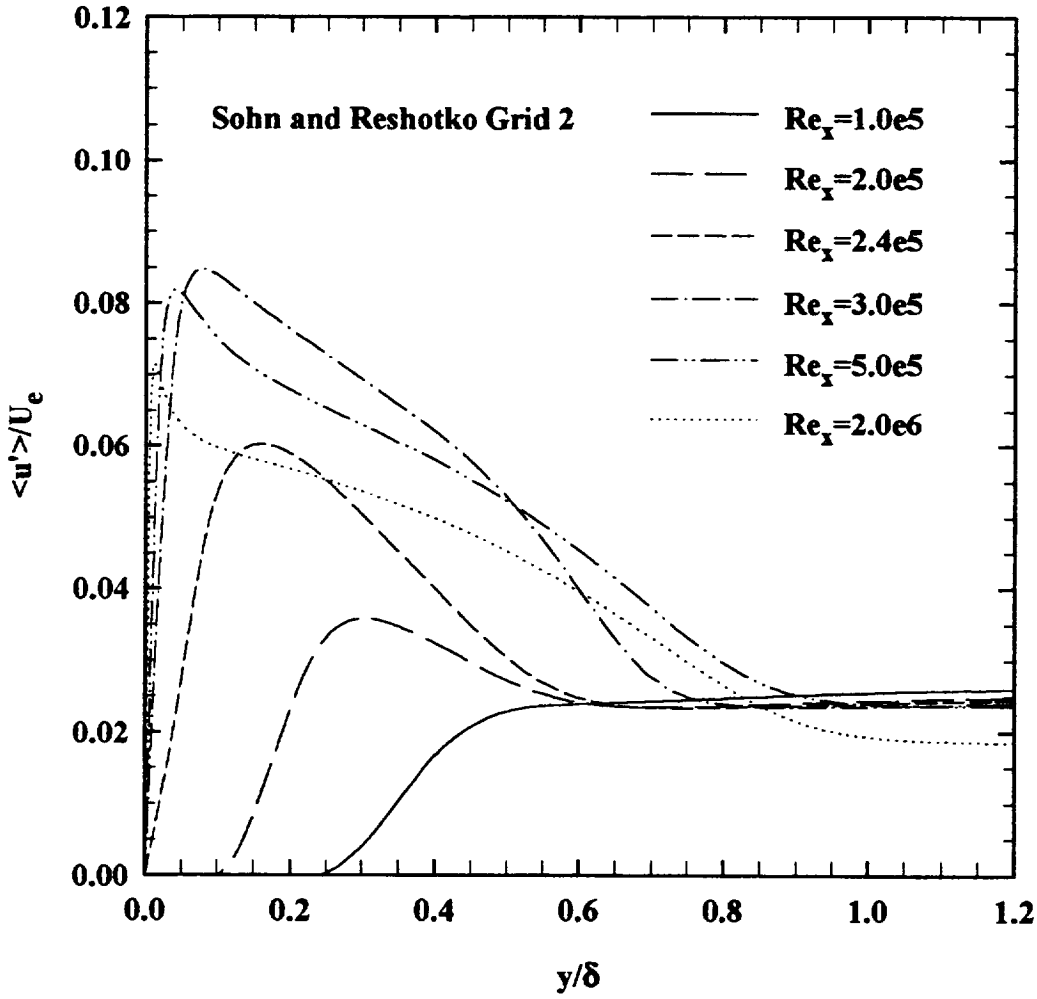

Figure 3-33(b) Predicted turbulent intensity $< u' > / U_e$ at various streamwise locations, in outer variable y/δ ($S_g = 0.5$); Sohn and Reshotko (1991) grid 2.

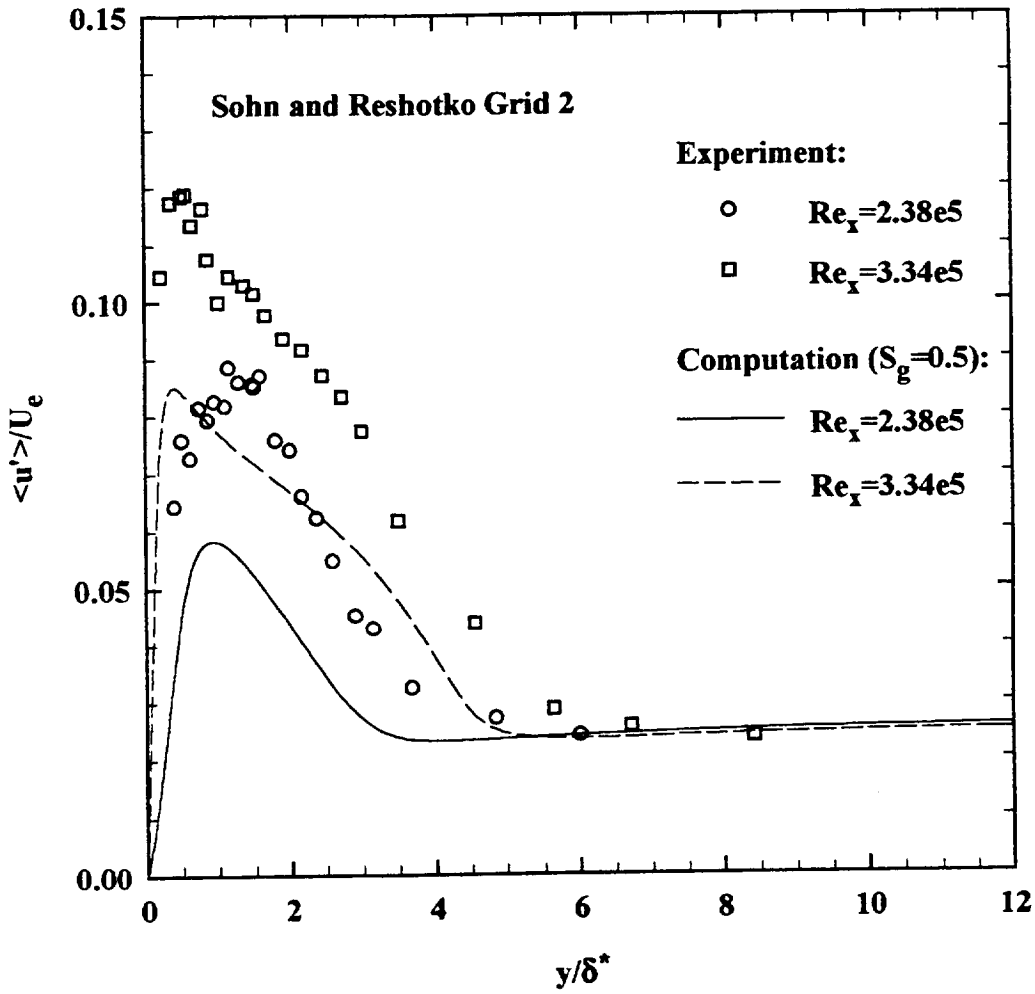

Figure 3-34(a) Comparison of the turbulent intensity $< u' > / U_e$ at streamwise location Re_x = 2.38e5 and 3.34e5 with the experimental data of Sohn and Reshotko (1991) grid 2.

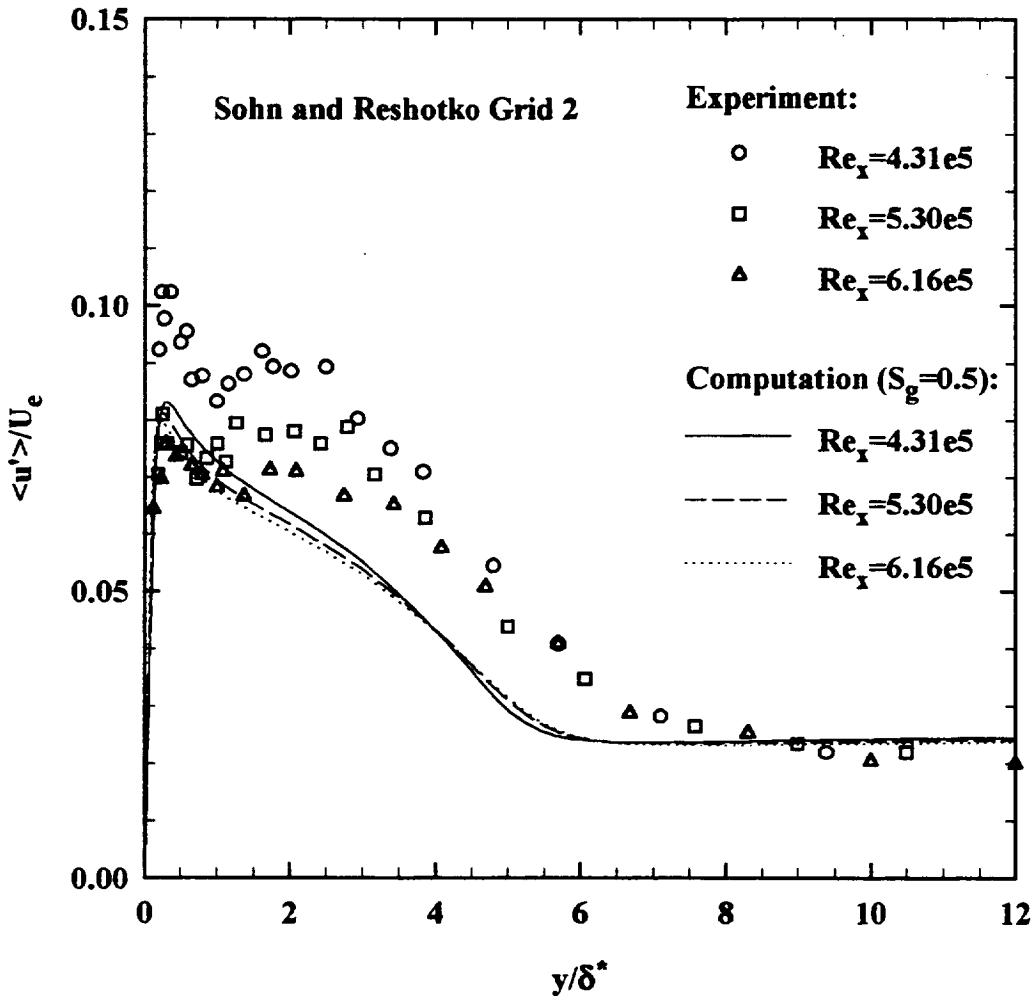

Figure 3-34(b) Comparison of the turbulent intensity $< u' > / U_e$ at streamwise locations Re_x = 4.31e5, 5.30e5 and 6.16e5 with the experimental data of Sohn and Reshotko (1991) grid 2.

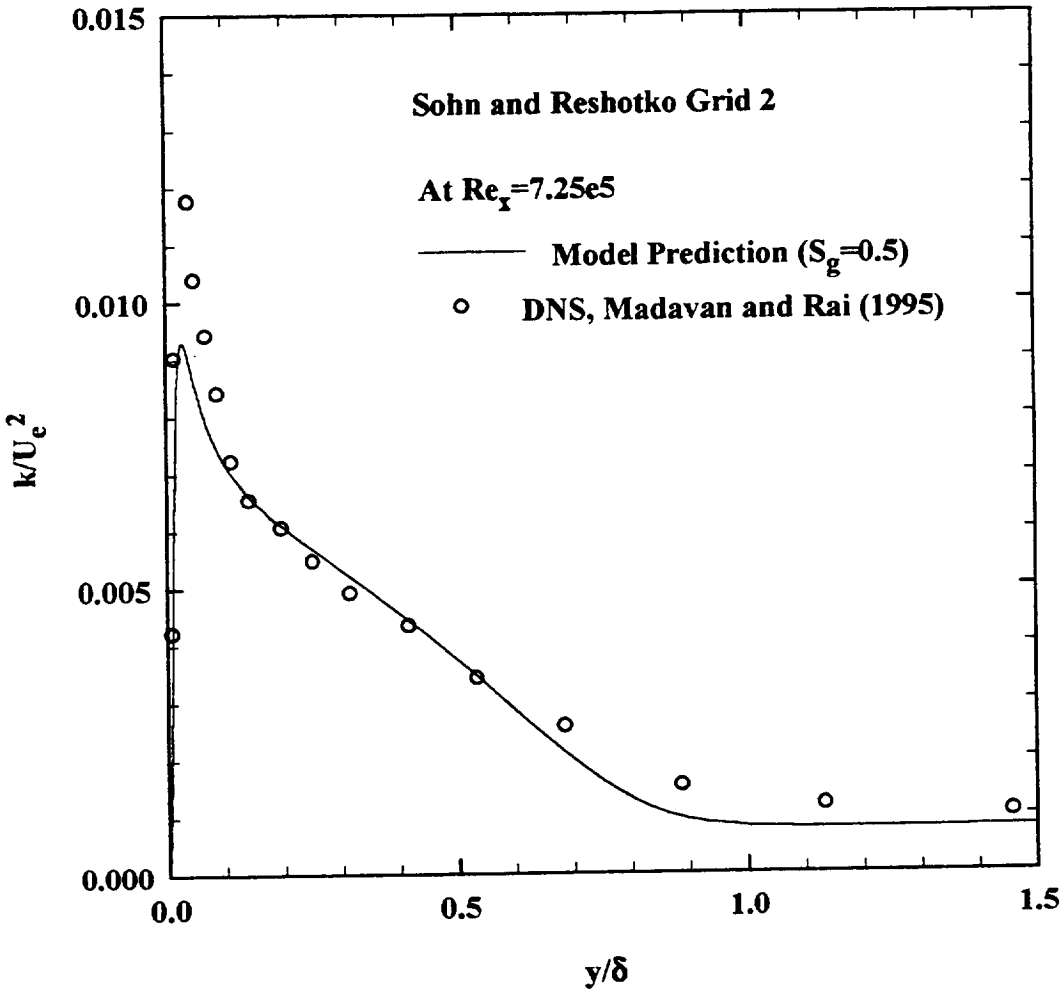

Figure 3-35 Comparison of the turbulent kinetic energy k at Re_x = 7.25e5 with the DNS data of Madavan and Rai (1995).

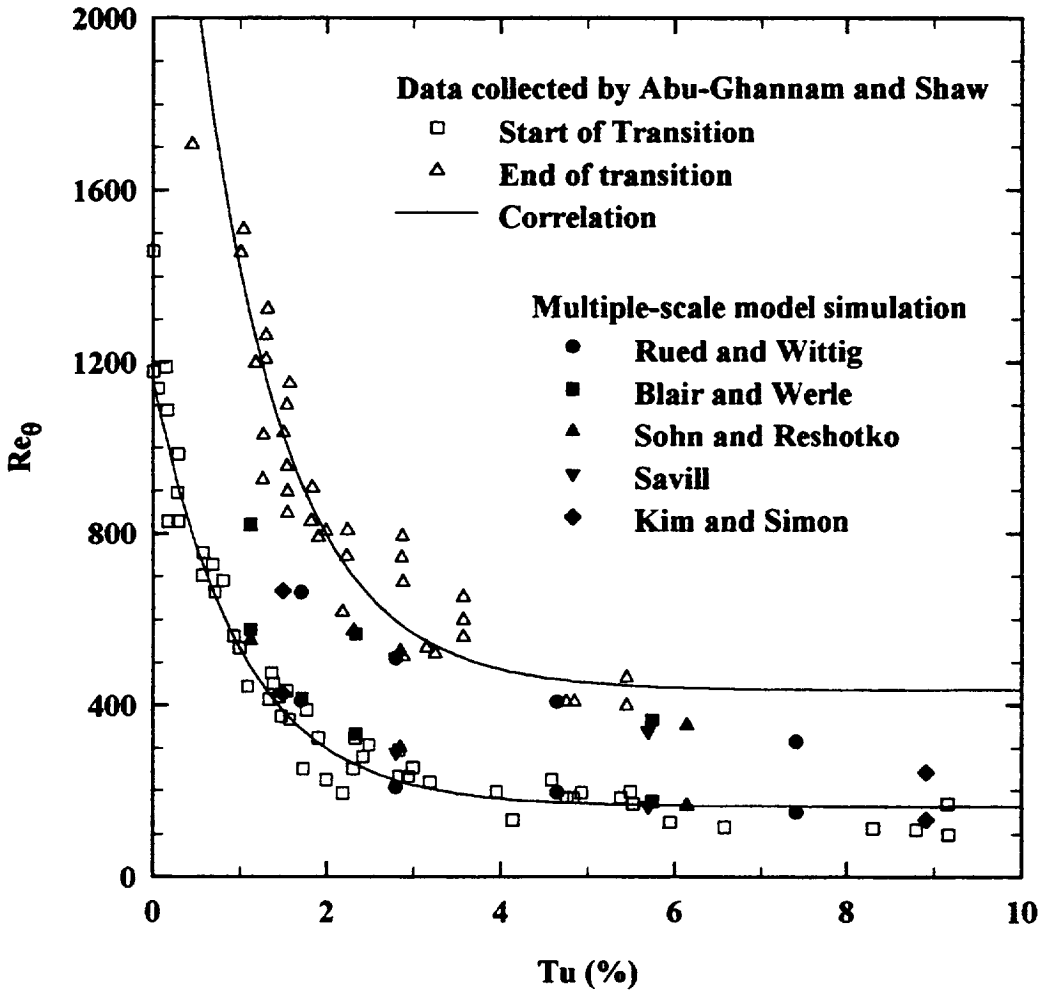

Figure 3-36 Comparison of the calculated momentum thickness Reynolds number at the start and end of transition with the correlation and experimental data of Abu-Ghannam and Shaw (1980).

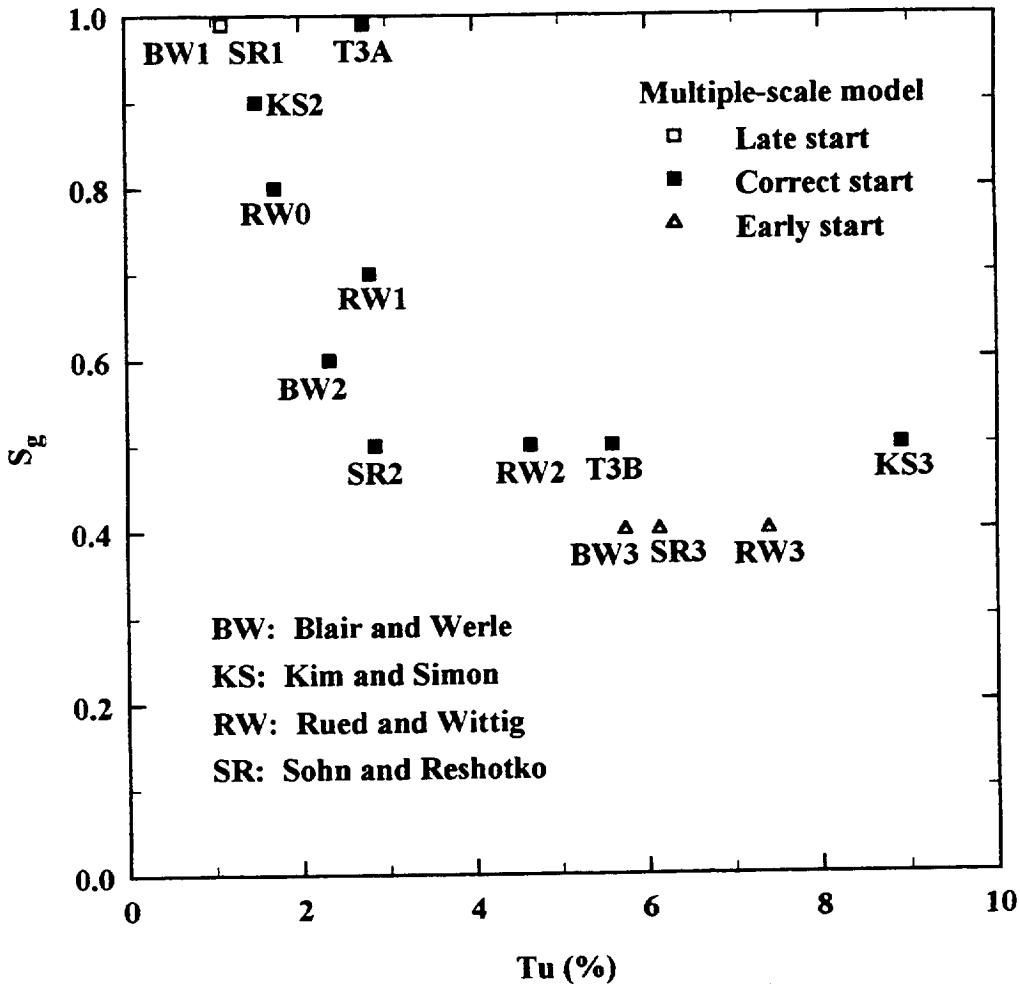

Figure 3-37 The map of spectrum parameter S_g in various experiments.

CHAPTER FOUR

CONCLUDING REMARKS

This study contributes to the development and application of multiple-scale k-ε turbulence modeling to the transitional boundary layer with elevated freestream turbulence levels. The conclusions of this work can be summarized as the following:

(1) A multiple-scale k-ε turbulence model is developed from the split spectrum concept and the eddy viscosity formulation. In the energy spectrum, the turbulent kinetic energy is divided into production, transfer and dissipation regions by wave number. The energy can be described by the cascading process from the production region through the transfer region to the dissipation region. The multiple-scale model models the first two regions and assumes that all the energy is dissipated in the third region. Thus the low and high frequency turbulent fluctuation are modeled respectively with and without coupling of the mean flow. Unlike previous multiple-scale models, the present model uses the *net* energy transfer function of turbulent energy spectrum as the variable corresponding to the length scale in each region. In the limit, the model becomes the single-scale k-ε turbulence model if one considers the first region only.

(2) The model constants are calibrated from the exact solutions of the simplified multiple-scale model for grid turbulence, for homogeneous shear flow and for

the near-wall fully turbulent equilibrium flow. In the homogeneous shear flow calculation, the ratio between two partial kinetic energies, k_t/k_p, is kept constant so that the flow can be simulated for different mean shear rates. From these calculations, the model constants then depend on the partitioning of the energy spectrum which is characterized by S_g $(=k_p/(k_p+k_t))$. Thus, in boundary layer applications, the present multiple-scale k-ϵ model constants could be automatically tuned to the energy spectrum of the freestream. This feature is not available in other turbulence modeling. Damping functions with the proper magnitude variations normal to the wall are used in order to accommodate the near-wall and transitional behavior.

(3) The Patankar-Spalding method is used in this work and the calculations show that the solutions are independent of the starting location and initial profiles. Five different sets of experimental data from different wind tunnels are used in evaluation of the turbulence model. The results show that the model can capture most of the features of transition, such as (*i*) progressive change from laminar to fully turbulent flow in each variable; (*ii*) as freestream turbulence level increases, the onset of transition moves upstream; (*iii*) enhanced heat transfer is obtained at elevated freestream turbulence intensity and (*iv*) negative normal mean velocities are obtained in the near-wall region during transition. However the model yields earlier than experimental transition at high freestream turbulence levels (Tu > 6%) and transition-lengths that are too short.

(4) In the multiple-scale model, the influence of elevated freestream turbulence level for transitional boundary layers is categorized by two parameters, the turbulence intensity Tu and the spectrum parameter S_g. The former has been used in representing the effect of freestream turbulence intensity. The introduction of S_g is the first attempt to involve the frequency spectrum in k-ε type turbulence modeling. However, the actual value of S_g is difficult to determine since it could be affected by many factors. These factors can be (*i*) from the facility, such as the location of the turbulence-generating grid, the contraction ratio of settling chamber, etc. and (*ii*) from the environment, such as roughness of plate, acoustic wave and the shape of leading edge, etc. Further investigation is necessary to understand those factors in the improvement of multiple-scale turbulence modeling.

REFERENCES

Abu-Ghannam, B.J. and Shaw, R. (1980), "Natural Transition of Boundary Layers - The Effects of Turbulence, Pressure Gradient, and Flow History," Journal of Mechanical Engineering Science, Vol. 22, pp. 213-228.

Bardina, J., Ferziger, J.H. and Reynolds, W.C. (1983), "Improved Turbulence Models Based on Large-Eddy Simulation of Homogeneous, Incompressible Turbulent Flows," *Stanford University Tech. Rep. TF-19.*

Barlow, R.S. and Johnston, J.P. (1988a), "Structure of a Turbulent Boundary Layer on a Concave Surface," Journal of Fluid Mechanics, Vol. 191, pp. 137-176.

Barlow, R.S. and Johnston, J.P. (1988b), "Local Effects of Large-Scale Eddies on Bursting in a Concave Boundary Layer," Journal of Fluid Mechanics, Vol. 191, pp. 177-195.

Batchelor, G.K. and Townsend, A.A. (1948a) "Decay of Isotropic Turbulence in the Initial Period," Proceeding Royal Society of London, Series A, Vol. 193, pp. 539-558.

Batchelor, G.K. and Townsend, A.A. (1948b) "Decay of Isotropic Turbulence in the Final Period," Proceeding Royal Society of London, Series A, Vol. 194, pp. 527-543.

Blackwelder, R.F. and Kovasznay, L.S.G. (1972), "Time Scales and Correlations in a Turbulent Boundary Layer," Physics of Fluids, Vol. 15, No. 9, pp. 1545-1554.

Blair, M.F. (1981a), "Final Data Report - Vol. I - Velocity and Temperature Profile Data for Zero Pressure Gradient, Fully Turbulent Boundary Layers," United Technologies Research Center report R81-914388-15.

Blair, M.F. (1981b), "Final Data Report - Vol. II - Velocity and Temperature Profile Data for Accelerating Transitional Boundary Layers," United Technologies Research Center report R81-914388-16.

Blair, M.F. (1983a), "Influence of Free-Stream Turbulence on Turbulent Boundary Layer Heat Transfer and Mean Profile Development, Part I - Experimental Data," ASME Journal of Heat Transfer, Vol. 105, pp. 33-40.

Blair, M.F. (1983b), "Influence of Free-Stream Turbulence on Turbulent Boundary Layer Heat Transfer and Mean Profile Development, Part II - Analysis of Results," ASME Journal of Heat Transfer, Vol. 105, pp. 41-47.

Blair, M.F. (1992a), "Boundary-Layer Transition in Accelerating Flows with Intense Freestream Turbulence: Part 1 - Disturbances Upstream of Transition Onset," ASME Journal of Fluid Engineering, Vol. 114, pp. 313-321.

Blair, M.F. (1992b), "Boundary-Layer Transition in Accelerating Flows with Intense Freestream Turbulence: Part 2 - The Zone of Intermittent Turbulence," ASME Journal of Fluid Engineering, Vol. 114, pp. 321-332.

Blair, M.F. and Werle, M.J. (1980), "The Influence of Freestream Turbulence on the Zero Pressure Gradient Fully Turbulent Boundary Layer," United Technology Research Center report R80-915388-12.

Byggostoyl, S. and Kollmann, W. (1981), "Closure Model for Intermittent Turbulent Flows," Int. Journal of Heat and Mass Transfer, Vol. 24, No. 11, PP. 1811-1822.

Byggostoyl, S. and Kollmann, W. (1986), "A Closure Model for Conditioned Stress Equations and Its Application to Turbulent Shear Flows," Physics of Fluids, Vol. 29, No. 5, PP. 1430-1440.

Cebeci, T. and Smith, A.M.O. (1974), *Analysis of Turbulent Boundary Layers*, Academic Press, New York.

Champagne, F.H., Harris, V.G. and Corrsin, S. (1970), "Experiments on Nearly Homogeneous Turbulent Shear Flow," Journal of Fluid Mechanics, Vol. 41, pp. 609-638.

Chien, K.Y. (1982), "Predictions of Channel and Boundary-Layer Flows with a Low-Reynolds-Number Turbulence Model," AIAA Journal, Vol. 20, pp. 33-38.

Cho, J.R. and Chung, M.K. (1992), "A k-ε-γ Equation Turbulence Model," Journal of Fluid Mechanics, Vol. 237, pp. 301-322.

Comte-Bellot, G. and Corrsin, S. (1966) "The Use of a Contraction to Improve the Isotropy of Grid-generated Turbulence," Journal of Fluid Mechanics, Vol. 25, Part 4, pp. 657-682.

Comte-Bellot, G. and Corrsin, S. (1971) "Simple Eulerian Time Correlation of Full- and Narrow-band Velocity Signals in Grid-generated 'Isotropic' Turbulence," Journal of Fluid Mechanics, Vol. 48, Part 2, pp. 273-337.

Corrsin, S. and Kistler, A.L. (1955), "The Free-stream Boundaries of Turbulent Flows," NACA report 1244.

Crawford, M.E. and Kays, W.M. (1976), "STAN5 - A program for Numerical Computation of Two-Dimensional Internal and External Boundary Layer Flows," NASA CR-2742.

Daniels, L.D. and Browne, W.B. (1981), "Calculation of Heat Transfer Rates to Gas Turbine Blades," International Journal of Heat and Mass Transfer, Vol. 24, pp. 871-679.

Dhawan, S. and Narasimha, R. (1958), "Some Properties of Boundary Layer Flow during the Transition from Laminar to Turbulent Motion," Journal of Fluid Mechanics, Vol. 3, No. 5, pp. 418-436.

Duncan, B.S., Liou, W.W. and Shih, T.H. (1993), "A Multiple-Scale Turbulence Model for Incompressible Flow," AIAA Paper 93-0086.

Dyban, B.S., pik, E. Ya. and Suprun, T.T. (1976), "Characteristics of the Laminar Boundary Layer in the Presence of Elevated Free-stream Turbulence," Fluid Mechanics-Soviet Research, Vol. 5, No. 4, pp. 30-36.

Emmons, H.W. (1951), "The Laminar-Turbulent Transition in a Boundary Layer - Part I," Journal of Aeronautical Science, Vol. 18, pp. 490-498.

Fabris, G., Harsha, P.T. and Edelman, R.B. (1981), "Multiple-Scale Turbulence Modeling of Boundary Layer Flows for Scramjet Applications," NASA CR 3433.

Fiedler, H. and Head, M.R. (1966), "Intermittency Measurements in the Turbulent Boundary Layer," Journal of Fluid Mechanics, Vol. 25, pp. 719-735.

Fujisawa, N. (1990), "Calculations of Transitional Boundary-Layers with a Refined Low Reynolds Number Version of a k-ε Model of Turbulence," *Engineering Turbulence Modeling and Experiments*, Elsevier Science Publishing o., Inc.

Gostelow, J.P. and Blunden, A.R. (1989), "Investigations of Boundary Layer Transition in an Adverse Pressure Gradient," ASME Journal of Turbomachinery, Vol. 111, pp. 366-375.

Hall, D.J. and Gibbings, J.C. (1972), "Influence of Stream Turbulence and Pressure Gradient upon Boundary Layer Transition," Journal of Mechanical Engineering Science, Vol. 14, pp. 134-146.

Hanjalic, K., Launder, B.E. and Schiestel, R. (1980), "Multiple-Time-Scale Concepts in Turbulent Transport Modelling," *Turbulent Shear Flows, Vol. 2*, Springer-Verlag, New York.

Harris, V.G., Graham, A.H. and Corrsin, S. (1977), "Further Experiments in nearly Homogeneous Turbulent Shear Flow," Journal of Fluid Mechanics, Vol. 81, Part 4, pp. 657-687.

Hedley, T.B. and Keffer, J.F. (1974) "Some Turbulent/Non-turbulent Properties of the Outer Intermittent Region of a Boundary Layer," Journal of Fluid Mechanics, Vol. 64, pp. 645-678.

Johns, W.P. and Launder, B.E. (1972), "The Prediction of Laminarization with a Two-Equation Model of Turbulence," International Journal of Heat and Mass Transfer, Vol. 15, pp. 301-314.

Johns, W.P. and Launder, B.E. (1973), "The Calculation of Low Reynolds Number Phenomena with a Two-Equation Model of Turbulence," International Journal of Heat and Mass Transfer, Vol. 16, pp. 1119-1130.

Kays, W.M. and Crawford, M.E. (1980), *Convective Heat and Mass Transfer*, 2nd edition, McGraw-Hill, New York.

Keller, F.J. (1993), "Flow and Thermal Structures in Heated Transitional Boundary Layers with and without Streamwise Acceleration," Ph.D. Dissertation, Clemson University, Clemson, South Carolina.

Kim, J. and Simon, T.W. (1991a), "Free-Stream Turbulence and Concave Curvature Effects on Heated, Transitional Boundary Layers, Volume I - Final Report," NASA CR 187150.

Kim, J. and Simon, T.W. (1991b), "Free-Stream Turbulence and Concave Curvature Effects on Heated, Transitional Boundary Layers, Volume II - Program Listings and Tabulated Data," NASA R 187151.

Kim, J., Simon, T.W. and Russ, S.G. (1992), "Free-Stream Turbulence and Concave Curvature Effects on Heated, Transitional Boundary Layer," ASME Journal of Heat Transfer, Vol. 114, pp. 338-347.

Kim, S.W. (1988), "A Near-Wall Turbulence Model and Its Application to Fully Developed Turbulent Channel and Pipe Flows," NASA TM 101399.

Kim, S.W. (1991), "Calculation of Divergent Channel Flows with a Multiple-Time-Scale Turbulence Model," AIAA Journal, Vol. 29, No. 4, pp. 547-554.

Kim, S.W. and Benson, T.J. (1992), "Calculation of a Circular Jet in Crossflow with a Multiple-Time-Scale Turbulence Model," International Journal of Heat and Mass Transfer, Vol. 35, No. 10, pp. 2357-2365.

Kim, S.W. and Chen, C.P. (1987), "A Multiple-Time-Scale Turbulence Model Based on Variable Partitioning of Turbulent Kinetic Energy Spectrum," NASA CR 179222.

Kosorygin, and Polyakov (1985), "Laminar Boundary Layers in Turbulent Flows," in *Laminar-Turbulent Transition*, edited by Arnal, D. and Michel, R., Springer-Verlag, 1990.

Kovasznay, L.S.G., Kibens, V. and Blackwelder, R.F. (1970), "Large-Scale Motion in the intermittent Region of a Turbulent Boundary Layer," Journal of Fluid Mechanics, Vol. 41, pp. 283-325.

Kuan, C.L. (1987), "An Experimental Investigation of Intermittent Behavior in Transitional Boundary Layer," M.S. Thesis, Clemson University, Clemson, South Carolina.

Lam, C.K.G. and Bremhorst, K.A. (1981), "Modified Form of the k-ε Model for Predicting Wall Turbulence," ASME Journal of Fluid Engineering, Vol. 103, pp. 456-460.

Launder, B.E. and Sharma, B.I. (1974), "Application of the Energy-Dissipation Model to Turbulence to the Calculation of Flow Near a Spinning Disc," Letters in Heat and Mass Transfer, Vol. 1, pp. 131-138.

Maciejewski, P.K. and Moffat, R.J. (1992a), "Heat Transfer With Very High Free-Stream Turbulence: Part I - Experimental Data," ASME Journal of Heat Transfer, Vol. 114, pp. 827-833.

Maciejewski, P.K. and Moffat, R.J. (1992b) "Heat Transfer With Very High Free-Stream Turbulence: Part II - Analysis of Results," ASME Journal of Heat Transfer, Vol. 114, pp. 834-839.

Madavan, N.K. and Rai, M.M. (1995) "Direct Numerical Simulation of Boundary Layer Transition on a Heated Flat Plate with Elevated Freestream Turbulence," AIAA Paper 95-0771.

Mayle, R.E. (1991), "The Role of Laminar-Turbulent Transition in Gas Turbine Engines," ASME Journal of Turbomachinery, Vol. 113, pp. 509-537.

McDonald, H. and Fish, R.W. (1973), "Practical Calculation of Transitional Boundary Layers," International Journal of Heat and Mass Transfer, Vol. 16, pp. 1729-1744.

Moinn, A.S. and Yaglom, A.M. (1971), *Statistical Fluid Mechanics*, Vol. 1 and 2, MIT Press, Cambridge.

Morkovin, M.V. (1979), "On the Question of Stabilities Upstream of Cylindrical Bodies," NASA CR 3231.

Myong, H.K. and Kasagi, N. (1988), "A New Proposal for a k-ε Turbulence Model and Its Evaluation," JSME(B), Vol. 54, pp. 3003-3009.

Myong, H.K. and Kasagi, N. (1990), "Prediction of Anisotropy of the Near-Wall Turbulence with an Anisotropic Low-Reynolds-Number k-ε Turbulence Model, Journal of Fluid Engineering, Vol. 112, pp. 521-524.

Nagano, Y. and Hishida, M. (1987), "Improved Form of the k-ε Model for Wall Turbulent Shear Flows," ASME Journal of Fluids Engineering, Vol. 109, pp. 156-160.

Nagano, Y. and Tagawa, M. (1990), "An Improved k-ε Model for Boundary Layer Flows," ASME Journal of Fluids Engineering, Vol. 112, pp. 33-39.

Narasimha, R. (1985), "The Laminar-Turbulent Transition Zone in the Boundary Layer," Progress of Aeronautical Science, Vol. 22, pp. 29-80.

Nisizima, S. and Yoshizawa, A. (1987), "Turbulent Channel and Couette Flows Using an Anisotropic k-ε Model," AIAA Journal Vol. 25, No. 3, pp. 414-420.

Patankar, S.V. (1988), "Parabolic Systems: Finite-Difference Method I," in *Handbook of Numerical Heat Transfer*, edited by Minkowycz, W.J., Sparrow, E.M., Schneider, G.E. and Pletcher, R.H., John Willey and Sons, Inc.

Patankar, S.V. (1980), *Numerical Heat Transfer and Fluid Flow*, Hemisphere Publishing Co.

Patel, V.C., Rodi, W. and Scheuerer, G. (1985), "Turbulence Models for Near-Wall and Low Reynolds Number Flows: A Review," AIAA Journal, Vol. 23, pp. 1308-1319.

Rai, M.M. (1994), Private conversation.

Reshotko, E. (1994), "Boundary Layer Instability, Transition and Control," AIAA Paper 94-0001.

Reshotko, E. (1995), Private conversation.

Roach, P.E. (1986), "The Generation of Nearly Isotropic Turbulence by Means of Grids," International Journal of Heat & Fluid Flow, Vol. 8, No. 2, pp. 82-92.

Rodi, W. and Scheuerer, G. (1985), "Calculation of Heat Transfer to Convection-Cooled Gas Turbine Blades," ASME Journal of Engineering for Gas Turbines and Power, Vol. 107, pp. 620-627.

Rogallo, R.S. (1981), "Numerical Experiments in Homogeneous Turbulence," NASA Tech Mem. 81315.

Rohr, J.J., Itsweire, E.C., Helland, K.N. and Van Atta, C.W. (1988), "An Investigation of the Growth of Turbulence in a Uniform Mean Shear Flow," Journal of Fluid Mechanics, Vol.187, pp. 1-33.

Rued, K. (1985), "Transitionale Grezschichten unte dem Einfluss hoher Freistrom-turbulenze, intensiver Wandkuehlung und starken Druckgradienten in Heissgasstroemungen," Thesis sumitted at the University of Karsruhe.

Rued, K. and Witting, S. (1985), "Free-Stream Turbulence and Pressure Gradient Effects on Heat Transfer and Boundary Layer Development on Highly Cooled Surfaces," ASME Journal of Engineering for Gas Turbine and Power, Vol. 107, pp. 54-59.

Savill, A.M. (1990), "Synthesis of T3 Test Case Predictions," in *Numerical Simulation of Unsteady Flows and Transition to Turbulence*, Edited by Pironneau, O., Rodi, W., Ryhming, I.L., Savill, A.M. and Truong, T.V., Cambridge University Press.

Schiestel, R. (1974), "Sur un nouveau modele de turbulence applique aux transferts de quantite de mouvement et de chaleur," These Doct. es Sc. Phys, Universite de Nancy-I. (in French)

Schiestel, R. (1983a), "Multiple Scale Concept in Turbulence Modelling, Part I Multiple-Scale Model for Turbulence Kinetic Energy and Mean Square of Passive Scalar Fluctuations," Journal de Mecanique Theorique et Appliquee, Vol.2, No. 3, pp. 417-449. (in French)

Schiestel, R. (1983b), "Multiple Scale Concept in Turbulence Modelling, Part II Reynolds Stresses and Turbulence Fluxes of a Passive Scalar, Algebraic Modelling and Simplified Model Using Boussinesq Hypothesis," Journal de Mecanique Theorique et Appliquee, Vol.2, No. 4, pp. 601-628. (in French)

Schiestel, R. (1987), "Multiple-Time-Scale Modeling of Turbulent Flows in One Point Closures," Physics of Fluids, Vol. 30, pp. 722-731.

Schmidt, R.C. and Patankar, S.V. (1988), "Two-Equation Low-Reynolds-Number Turbulence Modeling of Transitional Boundary Layer Flows Characteristic of Gas Turbine Blades," NASA CR 4145.

Schubauer, G.B. and Klebanoff, P.S. (1955), "Contributions on the Mechanics of Boundary-Layer Transition," NACA TN 3489.

Sharma, O.P., Wells, R.A., Schlinker, R.H. and Bailey, D.A. (1982), "Boundary Layer Development on Turbine Airfoil Suction Surfaces," ASME Journal of Engineering for Power, Vol. 104, pp. 698-706.

Simon, F.F. and Stephens, C.A. (1991), "Modeling of the Heat Transfer in Bypass Transitional Boundary-Layer Flows," NASA TP 3170.

Sohn, K. and Reshotko, E. (1991), "Experimental Study of Boundary Layer Transition With Elevated Freestream Turbulence on a Heated Flat Plate," NASA CR 187068.

Spalding, D.B. (1977), *GENMIX: A General Computer Program for Two-Dimensional Parabolic Phenomena*, Pergamon Press, New York.

Speziale, C.G. (1987), "On Nonlinear K-l and K-ε Models of Turbulence," Journal of Fluid Mechanics, Vol. 178, pp. 459-475.

Speziale, C.G. and Mac Giolla Mhuiris, N. (1989), "On the Prediction of Equilibrium States in Homogeneous Turbulence," Journal of Fluid Mechanics, Vol. 209, pp. 591-615.

Stephens, C.A. and Crawford, M.E. (1990), "An Investigation into the Numerical Prediction of Boundary Layer Transition Using the K. Y. Chien Turbulence Model," NASA CR 185252.

Suder, K.L., O' Brien, J.E. and Reshotko, E (1988), "Experimental Study of Bypass Transition in a Boundary Layer," NASA TM 100913.

Sullivan, T.J. (1988), "Simulating Transitional Flow and Heat Transfer Over Flat Plates and Circular Cylinders Using a k-ε Turbulence Model," M.S. Thesis, Cleveland State University, Cleveland, Ohio.

Tavoularis, S. (1985), Asymptotic Laws for Transversely Homogeneous Turbulent Shear Flows," Physics of Fluids, Vol. 28, pp. 999-1004.

Tavoularis, S. and Corrsin, S. (1981), "Experiments in Nearly Homogeneous Turbulent Shear Flows with a Uniform Mean Temperature Gradient," Par 1., Journal of Fluid Mechanics, Vol. 104, pp. 311-347.

Thole, K.A. (1992), "High Freestream Turbulence Effects on the Transport of Heat and Momentum," Ph.D. Dissertation, the University of Texas at Austin, Austin, Texas.

Vancoillie, G. and Dick, E. (1988), "A Turbulence Model for the Numerical simulation of the Transition Zone in a Boundary Layer," International Journal of Engineering Fluid Mechanics, Vol. 1, No. 1, pp. 28-49.

Van Driest, E.R. and Blumber, C.B. (1963), "Boundary Layer Transition: Freestream Turbulence and Pressure Gradient Effects," AIAA Journal, Vol. 1, pp. 1303-1306.

Volino, R.J. and Simon, T.W. (1991), "Bypass Transition in Boundary Layers Including Curvature and Favorable Pressure Gradient Effects," NASA CR 187187.

Walker, G.J. (1993), "The Role of Laminar-Turbulent Transition in Gas Turbine Engines: A Discussion," ASME Journal of Turbomachinery, Vol. 115, pp. 207-217.

Walker, G.J. and Gostelow, J.P. (1990), "Effects of Adverse Pressure Gradients on the Nature and Length of Boundary Layer," ASME Journal of Turbomachinery, Vol. 112, pp. 196-205.

Wang, J.H., Jen, H.F. and Hartel, E.O. (1985), "Airfoil Heat Transfer Calculation Using a Low Reynolds Number Version of a Two-Equation Turbulence Model," ASME Journal of Engineering for Gas Turbines and Power, Vol. 107, pp. 60-67.

Wang, T. (1984), "An Experimental Investigation of Curvature and Freestream Turbulence Effects on Heat Transfer and Fluid Mechanics in Transitional Boundary Layer Flows," Ph.D. Thesis, Department of Mechanical Engineering, University of Minnesota.

Wang, T. and Simon, T.W. (1987), "Heat Transfer and Fluid Mechanics Measurements in a Boundary Layer Undergoing Transition on a Convex-Curved Wall," ASME Journal of Turbomachinery, Vol. 109, No. 3, pp. 443-452.

Wilcox, D.C. (1975), "Turbulence-Model Transition Predictions," AIAA Journal, Vol. 13, pp. 241-243.

Wilcox, D.C. (1977), "A Model for Transitional Flows," AIAA Paper 77-126.

Wilcox, D.C. and Rubesin, W.M. (1980), "Progress in Turbulence Modeling for Complex Flow Fields Including Effects of Compressibility," NASA TP 1517.

Wygnanski, I. J. and Champagne, F. H. (1973), "On Transition in a Pipe, Part 1. The Origin of Puffs and Slugs and the Flow in a Turbulent Slug," Journal of Fluid Mechanics, Vol. 59, pp. 281-335.

Wygnanski, I. J., Sokolov, M. and Friedman, D. (1975), "On Transition in a Pipe, Part 2. The Equilibrium Puff," Journal of Fluid Mechanics, Vol. 69, pp. 785-819.

Yang, Z. and Shih, T.H. (1992), "A k-ε Calculation of Transitional Boundary Layers," NASA TM 105604.

Young, T.W., Warren, E.S., Harris, J.E. and Hassan, H.A. (1993) "New Approach for the Calculation of Transitional Flows," AIAA Journal, Vol. 31, pp. 629-636.

APPENDIX A

DERIVATION OF THE MULTIPLE SCALE TURBULENCE MODEL

This appendix presents the derivation of the proposed turbulence model by the multiple scale concept. The conventional k-ε model can be obtained by considering only one splitting wavenumber. The double-scale model is the one shown in Chapter 2 and applied in this work. The equations are derived in tensor notation.

A.1. Partial Turbulent Kinetic Energy Equations

The dynamic equation of the incompressible, two-point velocity correlation for anisotropic inhomogeneous turbulence can be written as (Hinze, 1975)

$$\begin{aligned}
&\frac{\partial}{\partial t}Q_{i,j}+\frac{1}{2}\left[(U_k)_A+(U_k)_B\right]\left(\frac{\partial}{\partial x_k}\right)_{AB}Q_{i,j} \\
&\quad+Q_{k,j}\left(\frac{\partial U_i}{\partial x_k}\right)_A+Q_{i,k}\left(\frac{\partial U_j}{\partial x_k}\right)_B+\left[(U_k)_B-(U_k)_A\right]\frac{\partial}{\partial \xi_k}Q_{i,j} \\
&\quad=-\frac{1}{2}\left(\frac{\partial}{\partial x_k}\right)_{AB}\left(S_{i,kj}+S_{ik,j}\right)-\frac{\partial}{\partial \xi_k}\left(S_{i,kj}-S_{ik,j}\right) \\
&\quad-\frac{1}{2\rho}\left[\left(\frac{\partial}{\partial x_i}\right)_{AB}K_{p,j}+\left(\frac{\partial}{\partial x_j}\right)_{AB}K_{i,p}\right]+\frac{1}{\rho}\left(\frac{\partial}{\partial \xi_i}K_{p,j}-\frac{\partial}{\partial \xi_j}K_{i,p}\right) \\
&\quad+\frac{1}{2}\nu\left(\frac{\partial^2}{\partial x_k \partial x_k}\right)_{AB}Q_{i,j}+2\nu\frac{\partial^2}{\partial \xi_k \partial \xi_k}Q_{i,j}
\end{aligned} \tag{A-1}$$

where the subscripts A and B refer to points in the flow, and U_k is the mean velocity. The mean values of the various correlations of the turbulence quantities are functions of the mid-location of these two points $(x_k)_{AB}$ and the distance between them ξ_k, they are defined as

$$(x_k)_{AB} = \frac{1}{2}\left[(x_k)_A + (x_k)_B\right] \tag{A-2}$$

$$\xi_k = (x_k)_B - (x_k)_A \tag{A-3}$$

In this dynamic equation (A-1), the correlation, after carrying out an averaging procedure with respect to time, are

$$Q_{i,j} \equiv Q_{i,j}(x_1, x_2, x_3, \xi_1, \xi_2, \xi_3, t) = \overline{(u_i)_A (u_j)_B} \tag{A-4a}$$

$$S_{i,kj} \equiv S_{i,kj}(x_1, x_2, x_3, \xi_1, \xi_2, \xi_3, t) = \overline{(u_i)_A (u_k)_B (u_j)_B} \tag{A-4b}$$

$$S_{ik,j} \equiv S_{ik,j}(x_1, x_2, x_3, \xi_1, \xi_2, \xi_3, t) = \overline{(u_i)_A (u_k)_A (u_j)_B} \tag{A-4c}$$

$$K_{p,j} \equiv K_{p,j}(x_1, x_2, x_3, \xi_1, \xi_2, \xi_3, t) = \overline{(p)_A (u_j)_B} \tag{A-4d}$$

$$K_{i,p} \equiv K_{i,p}(x_1, x_2, x_3, \xi_1, \xi_2, \xi_3, t) = \overline{(u_i)_A (p)_B} \tag{A-4e}$$

where u and p are instantaneous fluctuation velocity and pressure. If the turbulence is homogeneous, all the derivatives with respect to $(x_k)_{AB}$ will vanish. First, we make

an approximation of small ξ_k which gives the direct connection to the one-point Reynolds stress equation for Q_{ij} $(\xi_k = 0)$.

$$
\begin{aligned}
&\frac{\partial}{\partial t}Q_{i,j} + (U_k)_{AB}\left(\frac{\partial}{\partial x_k}\right)_{AB} Q_{i,j} \\
&\quad + Q_{k,j}\left(\frac{\partial U_i}{\partial x_k}\right)_{AB} + Q_{i,k}\left(\frac{\partial U_j}{\partial x_k}\right)_{AB} + \left(\frac{\partial U_k}{\partial x_l}\right)\xi_l \frac{\partial}{\partial \xi_k} Q_{i,j} \\
&\quad = -\frac{1}{2}\left(\frac{\partial}{\partial x_k}\right)_{AB}\left(S_{i,kj} + S_{ik,j}\right) - \frac{\partial}{\partial \xi_k}\left(S_{i,kj} - S_{ik,j}\right) \\
&\quad - \frac{1}{2\rho}\left[\left(\frac{\partial}{\partial x_i}\right)_{AB} K_{p,j} + \left(\frac{\partial}{\partial x_j}\right)_{AB} K_{i,p}\right] + \frac{1}{\rho}\left(\frac{\partial}{\partial \xi_i} K_{p,j} - \frac{\partial}{\partial \xi_j} K_{i,p}\right) \\
&\quad + \frac{1}{2}\nu\left(\frac{\partial^2}{\partial x_k \partial x_k}\right)_{AB} Q_{i,j} + 2\nu \frac{\partial^2}{\partial \xi_k \partial \xi_k} Q_{i,j} \\
&\quad + \frac{\xi_l}{2}\left[Q_{k,j}\left(\frac{\partial^2 U_i}{\partial x_k \partial x_l}\right)_{AB} - Q_{i,k}\left(\frac{\partial^2 U_j}{\partial x_k \partial x_l}\right)_{AB}\right] \\
&\quad - \frac{\xi_l \xi_m}{8}\left(\frac{\partial^2 U_k}{\partial x_l \partial x_m}\right)_{AB}\left(\frac{\partial}{\partial x_k}\right)_{AB} Q_{i,j}
\end{aligned}
\qquad \text{(A-5)}
$$

The inhomogeneous terms are analogous to the corresponding terms in one-point equation. The terms involving ξ_k derivatives can be treated as in the homogeneous anisotropic turbulence and the last two terms are approximated from Taylor series expansions. The last term can be neglected because it is second order in ξ_k. Now, the Fourier transforms $E_{i,j}$, $F_{i,kj}$ and $H_{i,p}$ of the correlation tensors $Q_{i,j}$, $S_{i,kj}$ and $K_{i,p}$ are introduced:

$$
Q_{i,j} = \iiint E_{i,j}(\kappa_1, \kappa_2, \kappa_3, t) e^{\imath \kappa_l \xi_l} d\kappa_1 d\kappa_2 d\kappa_3 \qquad \text{(A-6a)}
$$

$$S_{i,kj} = \iiint F_{i,kj}(\kappa_1, \kappa_2, \kappa_3, t) e^{\iota \kappa_l \xi_l} d\kappa_1 d\kappa_2 d\kappa_3 \tag{A-6b}$$

$$K_{i,p} = \iiint H_{i,p}(\kappa_1, \kappa_2, \kappa_3, t) e^{\iota \kappa_l \xi_l} d\kappa_1 d\kappa_2 d\kappa_3 \tag{A-6c}$$

and similarly for $S_{ik,j}$ and $K_{p,j}$. In these transforms, κ_i is the wave number and ι is the complex number $\sqrt{-1}$. The integrations are performed for the whole wave number range, i.e. from $-\infty$ to $+\infty$, in each direction. Thus, we have the dynamic equation for the energy spectrum function $E_{i,j}$

$$\frac{D}{Dt} E_{i,j} = \phi_{i,j} + \varphi_{i,j} - \theta_{i,j} - \vartheta_{i,j} + \pi_{i,j} + \chi_{i,j} + \sigma_{i,j} - \omega_{i,j} + \psi_{i,j} \tag{A-7}$$

where $$\frac{D}{Dt} E_{i,j} = \left(\frac{\partial}{\partial t} + U_l \frac{\partial}{\partial x_l} \right) E_{i,j} \tag{A-8a}$$

$$\phi_{i,j} = \left(\frac{\partial U_l}{\partial x_n} \right) \kappa_l \frac{\partial}{\partial \kappa_n} E_{i,j} \tag{A-8b}$$

$$\varphi_{i,j} = -E_{l,j} \left(\frac{\partial U_i}{\partial x_l} \right) - E_{i,l} \left(\frac{\partial U_j}{\partial x_l} \right) \tag{A-8c}$$

$$\theta_{i,j} = \iota \kappa_l \left(F_{i,lj} + F_{il,j} \right) \tag{A-8d}$$

$$\vartheta_{i,j} = \frac{1}{2} \frac{\partial}{\partial x_l} \left(F_{i,lj} + F_{il,j} \right) \tag{A-8e}$$

$$\pi_{i,j} = \frac{\iota}{\rho} \left(\kappa_i H_{p,j} - \kappa_j H_{i,p} \right) \tag{A-8f}$$

$$\chi_{i,j} = -\frac{1}{2\rho}\left(\frac{\partial}{\partial x_i}H_{p,j} + \frac{\partial}{\partial x_j}H_{i,p}\right) \tag{A-8g}$$

$$\sigma_{i,j} = \frac{\nu}{2}\frac{\partial^2}{\partial x_l \partial x_l}E_{i,j} \tag{A-8h}$$

$$\omega_{i,j} = 2\nu\kappa_l\kappa_l E_{i,j} \tag{A-8i}$$

$$\psi_{i,j} = \frac{1}{2}\left[\frac{\partial E_{n,j}}{\partial \kappa_l}\left(\frac{\partial^2 U_i}{\partial x_n \partial x_l}\right) - \frac{\partial E_{i,n}}{\partial \kappa_l}\left(\frac{\partial^2 U_j}{\partial x_n \partial x_l}\right)\right] \tag{A-8j}$$

Equations (A-7) and (A-8) are obtained after integration by parts with respect to κ_l and assuming

$$\lim_{\kappa_l \to \pm\infty} E_{i,j} = 0 \tag{A-9}$$

Define the partial Reynolds stress $R_{i,j}^{(m)}$ as the partial integration over the m-th slice of the energy spectrum (see figure A-1),

$$R_{i,j}^{(m)} = \int_{\kappa_{m-1}}^{\kappa_m} E_{i,j}\, d\kappa \tag{A-10}$$

where κ is the three-dimensional spectrum wave number. The transport equation of the partial Reynolds stress can be obtained by partial integration of equation (A-7). The integration yields

$$\frac{D}{Dt}R_{i,j}^{(m)} = D_{i,j}^{(m)} + P_{i,j}^{(m)} + F_{i,j}^{(m-1)} - F_{i,j}^{(m)} + \Pi_{i,j}^{(m)} - \varepsilon_{i,j}^{(m)} \tag{A-11}$$

where $$D_{i,j}^{(m)} = -\frac{1}{2}\int_{\kappa_{m-1}}^{\kappa_m} \frac{\partial}{\partial x_l}\left(F_{i,lj} + F_{il,j}\right)d\kappa$$
$$-\frac{1}{2\rho}\left(\int_{\kappa_{m-1}}^{\kappa_m} \frac{\partial}{\partial x_i}H_{p,j}d\kappa + \int_{\kappa_{m-1}}^{\kappa_m} \frac{\partial}{\partial x_j}H_{i,p}d\kappa\right)$$
$$+\frac{\nu}{2}\frac{\partial^2}{\partial x_l \partial x_l}R_{i,j}^{(m)} + \frac{\nu}{2}\left(\frac{\partial E_{i,j}^{(m-1)}}{\partial x_l}\frac{\partial \kappa_{m-1}}{\partial x_l} - \frac{\partial E_{i,j}^{(m)}}{\partial x_l}\frac{\partial \kappa_m}{\partial x_l}\right)$$
$$+\frac{\nu}{2}\frac{\partial}{\partial x_l}\left(E_{i,j}^{(m-1)}\frac{\partial \kappa_{m-1}}{\partial x_l} - E_{i,j}^{(m)}\frac{\partial \kappa_m}{\partial x_l}\right) \tag{A-12a}$$

$$P_{i,j}^{(m)} = -R_{l,j}^{(m)}\frac{\partial U_i}{\partial x_l} - R_{i,l}^{(m)}\frac{\partial U_j}{\partial x_l} \tag{A-12b}$$

$$F_{i,j}^{(m-1)} = \int_0^{\kappa_{m-1}}\left[\theta_{i,j} - \left(\psi_{i,j} + \phi_{i,j}\right)\right]d\kappa - E_{i,j}\Big|_{\kappa_{m-1}}\frac{D\kappa_{m-1}}{Dt} \tag{A-12c}$$

$$F_{i,j}^{(m)} = \int_0^{\kappa_m}\left[\theta_{i,j} - \left(\psi_{i,j} + \phi_{i,j}\right)\right]d\kappa - E_{i,j}\Big|_{\kappa_m}\frac{D\kappa_m}{Dt} \tag{A-12d}$$

$$\Pi_{i,j}^{(m)} = \int_{\kappa_{m-1}}^{\kappa_m}\pi_{i,j}d\kappa \tag{A-12e}$$

$$\varepsilon_{i,j}^{(m)} = \int_{\kappa_{m-1}}^{\kappa_m}\omega_{i,j}d\kappa \tag{A-12f}$$

Each term in equation (A-11) can be interpreted as follows:

$D_{i,j}^{(m)}$ is the diffusion term composed of the triple velocity correlation, the pressure-velocity correlation and the molecular diffusion.

$P_{i,j}^{(m)}$ is the turbulence production from the mean shear within the m-th region.

$F_{i,j}^{(m-1)} - F_{i,j}^{(m)}$ is the net partial turbulent energy flux in spectral space. There are three different transferring processes, they are transferred by inertial cascade, by distortion of mean shear and by influence of the variation of wave number.

$\Pi_{i,j}^{(m)}$ is the redistribution of partial turbulent kinetic energy by pressure deformation correlation. This pressure term will vanish in the contracted equation, and

$\varepsilon_{i,j}^{(m)}$ is the viscous dissipation in the m-th region.

Contracting the partial Reynolds stress equation (A-11), yields the partial turbulent energy equation for the m-th region of the spectrum

$$\frac{De^{(m)}}{Dt} = D^{(m)} + P^{(m)} + F^{(m-1)} - F^{(m)} - \varepsilon^{(m)} \qquad \text{(A-13)}$$

where $e^{(m)} = \frac{1}{2} R_{i,i}^{(m)}$ $\qquad D^{(m)} = \frac{1}{2} D_{i,i}^{(m)}$ $\qquad$ (A-14a,b)

$$P^{(m)} = \frac{1}{2} P_{i,i}^{(m)} \qquad \varepsilon^{(m)} = \frac{1}{2} \varepsilon_{i,i}^{(m)} \qquad \text{(A-14c,d)}$$

$$F^{(m)} = \frac{1}{2} F_{i,i}^{(m)} \qquad F^{(m-1)} = \frac{1}{2} F_{i,i}^{(m-1)} \qquad \text{(A-14e,f)}$$

The turbulence energy flux across the energy spectrum $F^{(m)}$, which is continuously transferred to even higher wave region, can be written explicitly as

$$F^{(m)} = F^{(m)} - E^{(m)}\Big|_{\kappa_m} \frac{D\kappa_m}{Dt} \tag{A-15}$$

where $F^{(m)} = \int_0^{\kappa_m} \theta_{i,i} d\kappa - \left(\frac{\partial U_l}{\partial x_n}\right) \int_0^{\kappa_m} \kappa_l \frac{\partial E_{i,i}}{\partial \kappa_n} d\kappa$ (A-16a)

$$E^{(m)} = \frac{1}{2} E_{i,i}^{(m)} \tag{A-16b}$$

and $$\frac{D\kappa_m}{Dt} = \frac{\partial \kappa_m}{\partial t} + U_l \frac{\partial \kappa_m}{\partial x_l} \tag{A-16c}$$

In each slice of the spectrum, the turbulent energy generated by mean shear in the production terms, is then transferred into the higher wave number region accompanied with the diffusion and dissipation. In the lowest wave number region, $m = 1$ and $F^{(0)} = 0$. As for the highest wave number region where the wave number ranges from κ_m to infinity, we may assume that the dissipation equals the energy transferred from the lower wave number region, $\varepsilon^{(m)} = F^{(m-1)}$.

In the single-scale equation, such as the k-ε model, which does not consider the energy cascade in the energy spectrum, the turbulent energy $e^{(1)}$ is approximated as the total turbulent kinetic energy k, and the turbulent fluxes are $F^{(1)} = \varepsilon^{(2)} = \varepsilon$ and $F^{(0)} = \varepsilon^{(1)} = 0$. Equation (A-13) becomes the total turbulent kinetic energy equation.

$$\frac{Dk}{Dt} = D_k + P_k - \varepsilon \tag{A-17}$$

where D_k and P_k are diffusion and production of k respectively.

A.2. Energy Flux Equations

It is assumed that the averaged energy spectrum function of the m-th region is approximated by the partial turbulent kinetic energy per spectrum interval

$$\frac{1}{2}\left(E^{(m)} + E^{(m-1)}\right) = \beta_m \frac{e^{(m)}}{\kappa_m - \kappa_{m-1}} \tag{A-18}$$

with $E^{(0)} = 0$ and $\kappa_0 = 0$. It is also assumed that the wavelength interval of the m-th region of the energy spectrum is inversely proportional to the characteristic length scale,

$$\kappa_m - \kappa_{m-1} = \frac{\alpha_m}{\ell_t^{(m)}} \tag{A-19}$$

where α_m and β_m are constants. The length scale can be represented by

$$\ell_t^{(m)} = \frac{\left[e^{(m)}\right]^{3/2}}{F^{(m)} - F^{(m-1)}} \tag{A-20}$$

where the denominator is the net change of energy transfer function across the m-th slice of spectrum. This is different from Schiestel's (1987) assumption which uses $F^{(m)}$ instead of $F^{(m)} - F^{(m-1)}$ to represent the length scale. It is further assumed that the spectral transfer of turbulent energy $F^{(m)}$ is represented as

$$F^{(m)} = \gamma_m \left[E^{(m)}\right]^{3/2} \kappa_m^{5/2} \tag{A-21}$$

where γ_m is a constant. It is based on the dimensional analysis and is similar to the Kovasznay hypothesis (see Monin and Yaglom 1971). The direct derivative of equation (A-19), with the substitution of equations (A-13), (A-15), and (A-18) to (A-21), yields

$$\begin{aligned}\frac{DF^{(m)}}{Dt} = \frac{DF^{(m-1)}}{Dt} + \frac{3}{2}\frac{F^{(m)} - F^{(m-1)}}{e^{(m)}}\left[D^{(m)} + P^{(m)} - \varepsilon^{(m)}\right] \\ + \frac{\left[e^{(m)}\right]^{3/2}}{\alpha_m}\left[\frac{D\kappa_m}{Dt} - \frac{D\kappa_{m-1}}{Dt}\right] - \frac{3}{2}\frac{\left(F^{(m)} - F^{(m-1)}\right)^2}{e^{(m)}}\end{aligned} \tag{A-22}$$

$$\text{where } E^{(m)} = 2\sum_{n=1}^{m}(-1)^{n+1}\frac{\beta_n}{\alpha_n}\frac{\left[e^{(n)}\right]^{5/2}}{F^{(n)} - F^{(n-1)}} \tag{A-23}$$

$$G^{(m)} = \begin{cases} 1 & m = 0 \\ \sum_{n=1}^{m}\alpha_m \dfrac{F^{(n)} - F^{(n-1)}}{\left[e^{(m)}\right]^{3/2}} & m \geq 1 \end{cases} \tag{A-24}$$

$$\text{and} \quad \frac{D\kappa_m}{Dt} = \begin{cases} 0 & m = 0 \text{ and } m = M \\ \gamma_m\left[E^{(m)}\right]^{1/2}\left[G^{(m)}\right]^{5/2} - F^{(m)}/E^{(m)} & 0 < m < M \end{cases} \tag{A-25}$$

Equation (A-25) implies that the first wave number is zero and beyond the cut-off wave number ($m = M$) $D\kappa_m/Dt$ is negligible. Thus, equation (A-22) is the energy flux equation. In single-scale turbulence, such as the k-ε model, κ is located at very high wave number and inversely proportional to the characteristic length

$$\kappa = \alpha \frac{F^{(1)}}{\left[e^{(1)}\right]^{3/2}} = \alpha \frac{\varepsilon}{k^{3/2}} \tag{A-26}$$

The energy flux equation becomes the turbulent dissipation rate equation

$$\frac{D\varepsilon}{Dt} = \frac{3}{2}\frac{\varepsilon}{k} D_k + C_1 P_k \frac{\varepsilon}{k} - C_2 \frac{\varepsilon^2}{k} \tag{A-27}$$

where from (A-22) $C_1 = 3/2$ which is close to the standard k-ε model constant $C_{\varepsilon 1} = 1.44$, and $C_2 = \frac{3}{2} + \frac{1}{2\beta} - \gamma\alpha\sqrt{2\beta}$.

A.3. Two-scales Turbulence Model

If we split the energy spectrum into three regions, the lowest region is the turbulent energy production region which has no dissipation, the middle region is the transfer region which transfers the energy into the higher wave number region without any energy production, and the last one is the viscous dissipation dominant region (as shown in Figure A-2). We write

$$k_p = e^{(1)} \qquad k_t = e^{(2)} \tag{A-28a,b}$$

$$\varepsilon_p = F^{(1)} \quad \text{and} \quad \varepsilon_t = F^{(2)} - F^{(1)} \tag{A-28c,d}$$

Here, subscript p and t denote the production region and transfer region respectively. In the last spectrum section, the equilibrium is supposed to prevail, then real energy dissipation rate ε is the sum of ε_p and ε_t. From equation (A-13) and (A-22), the two-scale turbulent model equations are

$$\frac{Dk_p}{Dt} = D_{kp} + P_k - \varepsilon_p \tag{A-29}$$

$$\frac{Dk_t}{Dt} = D_{kt} - \varepsilon_t \tag{A-30}$$

$$\frac{D\varepsilon_p}{Dt} = D_{\varepsilon p} + C_{p1}\frac{P_k \varepsilon_p}{k_p} - C_{p2}\frac{\varepsilon_p^2}{k_p} \tag{A-31}$$

$$\frac{D\varepsilon_t}{Dt} = D_{\varepsilon t} + C_{t1}\left(\frac{k_t}{k_p}\right)^{3/2}\frac{\varepsilon_p^2}{k_p} - C_{t2}\frac{\varepsilon_t^2}{k_t} \tag{A-32}$$

where $D_{\varepsilon p} = \frac{3}{2}\frac{\varepsilon_p}{k_p}D_{kp}$ and $D_{\varepsilon t} = \frac{3}{2}\frac{\varepsilon_t}{k_t}D_{kt}$. Here, all C's are constants, D_{kp} ($D_{\varepsilon p}$) and D_{kt} ($D_{\varepsilon t}$) are turbulent energy diffusion (energy transfer function) in production and transfer regions respectively; and P_k is the generation of turbulent energy in production region.

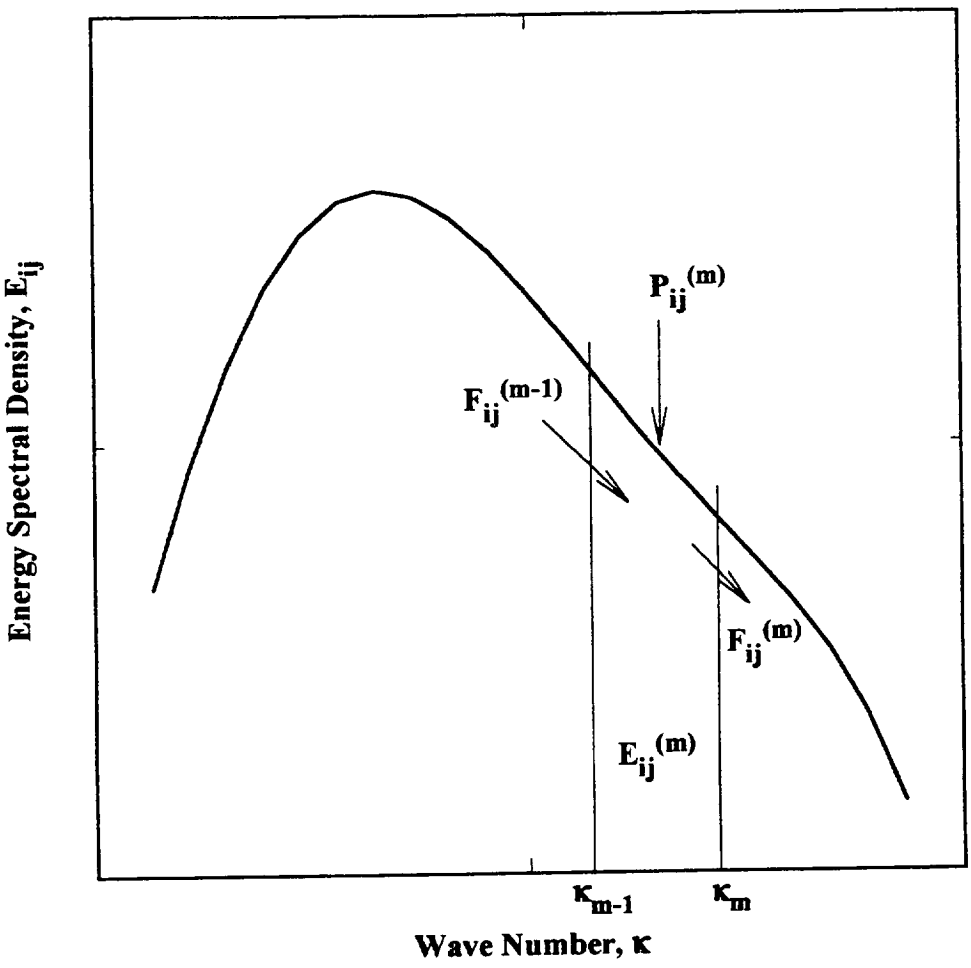

Figure A-1 Sketch of spectral partitioning for *m*-th shell in three-dimensional wave number space

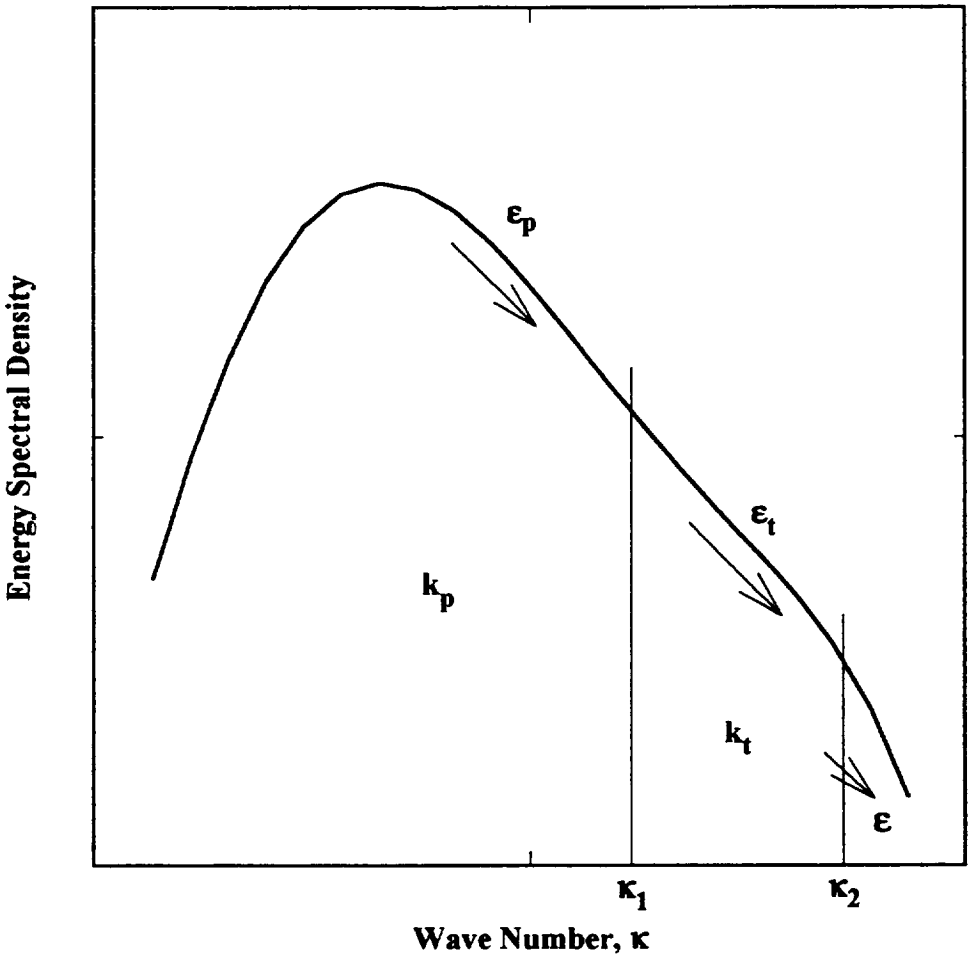

Figure A-2 Spectral division of turbulent energy and energy transfer function for two-scale turbulence model.

APPENDIX B

CALIBRATION OF MODEL CONSTANTS

It has been observed that there are certain flows for which the double-scale turbulence model constants can be determined. The flows used here are the grid turbulence, the homogeneous shear flow and the near-wall equilibrium turbulent flow. The application of the model to each flow provides different relationships between the model constants. These constants are then determined by the experimental data and the energy spectrum of grid turbulence for transitional boundary layer calculation.

B.1 Grid Turbulence

Grid turbulence is generated by the flow through a grid or mesh composed of single or double rows of round and/or square bars. After the build-up period, the flow is almost homogeneous and isotropic, then the turbulence decays monotonically. There is no turbulent production in the flow and the diffusion is negligible. The turbulence model can be simplified into one-dimensional equations as follows:

$$U\frac{dk_p}{dx} = -\varepsilon_p \tag{B-1}$$

$$U\frac{dk_t}{dx} = -\varepsilon_t \tag{B-2}$$

$$U\frac{d\varepsilon_p}{dx} = -C_{p2}\frac{\varepsilon_p^2}{k_p} \tag{B-3}$$

$$U\frac{d\varepsilon_t}{dx} = C_{t1}\left(\frac{k_t}{k_p}\right)^{3/2}\frac{\varepsilon_p^2}{k_p} - C_{t2}\frac{\varepsilon_t^2}{k_t} \tag{B-4}$$

Equations (B-1) and (B-3) are independent of the other two equations and can be solved analytically. The exact solutions, subject to the initial conditions $k_p = k_{p0}$ and $\varepsilon_p = \varepsilon_{p0}$ at $x = x_0$, are

$$\frac{k_p}{k_{p0}} = \left(1 + \frac{\varepsilon_{p0}}{k_{p0}}\frac{t}{n}\right)^{-n} \tag{B-5}$$

$$\frac{\varepsilon_p}{\varepsilon_{p0}} = \left(1 + \frac{\varepsilon_{p0}}{k_{p0}}\frac{t}{n}\right)^{-(n+1)} \tag{B-6}$$

where $t = \dfrac{x - x_0}{U}$ and $n = \dfrac{1}{C_{p2} - 1}$ (B-7a,b)

Since the flow is homogeneous the ratio k_t/k_p is a constant r_g which characterizes the shape of the spectrum, then equation (B-1) and (B-2) give $\varepsilon_t/\varepsilon_p$ be the same constant. From the homogeneous assumption and equation (B-5), we know that the *total* turbulent kinetic energy k $(= k_p + k_t)$ will follow the same decay law. Thus, equations (B-3) and (B-4) give

$$\sqrt{r_g}C_{t1} + C_{p2} = C_{t2} \tag{B-8}$$

This equation is valid as long as the turbulence is homogeneous and follows the power law decay. As is well known (Batchelor and Townsend, 1948a, 1948b; Comte-Bellot and Corrsin, 1966, 1971) the exponent of decay is from *1.11* to *10/7* during the initial period and up to *2.5* in the final period. To simulate both conditions, Nagano and Tagawa (1990) suggested that equation (B-3) should be modified as

$$U\frac{d\varepsilon_p}{dx} = -C_{p2}f_{p2}\frac{\varepsilon_p^2}{k_p} \tag{B-9}$$

$$f_{p2} = 1 - A_p \exp\left(-R_t^2/B_p^2\right) \tag{B-10}$$

where $R_t = k^2/\nu\varepsilon$ is the turbulent Reynolds number; $\varepsilon = \varepsilon_p + \varepsilon_t$ is the turbulent energy dissipation rate which is just the energy transferred from the transfer region to the dissipation region; and A_p and B_p are constants. Substituting equations (B-5) and (B-6) into (B-9), we obtain

$$C_{p2}f_{p2} = (n+1)/n \tag{B-11}$$

If we take $n = 1.1$ for the initial period (R_t is large, $f_{p2} = 1$), the model constant C_{p2} is *1.9*. In the final period, we obtain $A_p = 0.3$ by substituting $n = 2.5$ and $C_{p2} = 1.9$ into equation (B-11). The other constant $B_p = 6$ is determined by numerical optimization. Comparing with the experimental data of Batchelor and Townsend (1948), as shown in Figure B-1, the modified equation (B-9) predicts both initial and final periods well.

B.2 Homogeneous Shear Flow

The concept of homogeneous turbulence with a uniform mean shear has long been used in verification of turbulence modeling. The flow is subjected to the turbulence by uniform shear only; there is no solid wall in the flow and diffusion is small. In this flow, the turbulent Reynolds number is large and all the damping functions are unity. From equations (A-29) to (A-32), the turbulence model can be written as

$$U\frac{dk_p}{dx} = C_\mu S^2\left(k_p + k_t\right)^{1/2}\frac{k_p^{3/2}}{\varepsilon_p} - \varepsilon_p \tag{B-12}$$

$$U\frac{dk_t}{dx} = -\varepsilon_t \tag{B-13}$$

$$U\frac{d\varepsilon_p}{dx} = C_{p1}C_\mu S^2\left(k_p + k_t\right)^{1/2}k_p^{1/2} - C_{p2}\frac{\varepsilon_p^2}{k_p} \tag{B-14}$$

$$U\frac{d\varepsilon_t}{dx} = C_{t1}\left(\frac{k_t}{k_p}\right)^{3/2}\frac{\varepsilon_p^2}{k_p} - C_{t2}\frac{\varepsilon_t^2}{k_t} \tag{B-15}$$

where $S = dU/dy$ is a constant by definition and the eddy viscosity is characterized in the production zone by the length scale $\left(k_p^{3/2}/\varepsilon_p\right)$ and the velocity scale $\left(k_p + k_t\right)^{1/2}$. It is reasonable to assume that the ratio of partial turbulent kinetic energy $k_t/k_p = r_s$ is a constant. With this assumption, equations (B-12) and (B-14) can be combined as

$$\frac{d\phi}{d\tau} = C_\mu (1+r_s)^{1/2}(C_{p1}-1) - (C_{p2}-1)\phi^2 \tag{B-16}$$

where $\phi = \varepsilon_p/(k_p S)$ is the time scale ratio between mean shear and turbulence; and $\tau = S(x-x_0)/U$ is the nondimensional convection time. Here x_0 is the virtual origin location and hereafter the subscript 0 denotes the initial conditions. There is an equilibrium point (long-time solution) to equation (B-16), which is

$$\phi_\infty = (1+r_s)^{1/4}\sqrt{\frac{C_\mu}{\gamma}} \quad \text{where} \quad \gamma = \frac{C_{p2}-1}{C_{p1}-1} \tag{B-17a,b}$$

Therefore, at the equilibrium point, the ratio between production P_k and the energy transfer function ε_p becomes a constant

$$\left(\frac{P_k}{\varepsilon_p}\right)_\infty = \left[\frac{C_\mu (1+r_s)^{1/2}}{\phi^2}\right]_\infty = \gamma \tag{B-18}$$

Now, consider that the mean velocity U is the characteristic mean velocity which is function of y only and is typically taken to be the centerline mean velocity of the uniform mean shear. If we assume that the initial conditions are $k_p = k_{p0}$ and $\varepsilon_p = \varepsilon_{p0}$ at $x = x_0$, then equation (B-16) can be integrated directly. The transient solution of ϕ is

$$\phi = \begin{cases} \phi_\infty \coth(a\tau + b) & \text{for } \phi_0 > \phi_\infty \\ \phi_\infty \tanh(a\tau + b) & \text{for } \phi_0 < \phi_\infty \end{cases} \tag{B-19}$$

where $a = \phi_\infty (C_{p2} - 1)$, $b = \frac{1}{2} \ln \left| \frac{\phi_0 + \phi_\infty}{\phi_0 - \phi_\infty} \right|$ and $\phi_0 = \frac{\varepsilon_{p0}}{k_{p0} S}$ (B-20a,b,c)

Hence, the k_p equation becomes

$$\frac{dk_p}{d\tau} = \begin{cases} \phi_\infty \left[\gamma \tanh(a\tau + b) - \coth(a\tau + b) \right] k_p & \text{for } \phi_0 > \phi_\infty \\ \phi_\infty \left[\gamma \coth(a\tau + b) - \tanh(a\tau + b) \right] k_p & \text{for } \phi_0 < \phi_\infty \end{cases} \tag{B-21}$$

The integration of equation (B-21) yields

$$\frac{k_p}{k_{p0}} = \begin{cases} \left[\frac{\sinh(a\tau + b)}{\sinh b} \right]^{-\alpha} \left[\frac{\cosh(a\tau + b)}{\cosh b} \right]^{\beta} & \text{for } \phi_0 > \phi_\infty \\ \left[\frac{\sinh(a\tau + b)}{\sinh b} \right]^{\beta} \left[\frac{\cosh(a\tau + b)}{\cosh b} \right]^{-\alpha} & \text{for } \phi_0 < \phi_\infty \end{cases} \tag{B-22}$$

where $\alpha = 1/(C_{p2} - 1)$ and $\beta = 1/(C_{p1} - 1)$. Consequently, the solution for ε_p is

$$\frac{\varepsilon_p}{\varepsilon_{p0}} = \begin{cases} \left(\frac{k_p}{k_{p0}} \right) \left(\frac{\phi_\infty}{\phi_0} \right) \coth(a\tau + b) & \text{for } \phi_0 > \phi_\infty \\ \left(\frac{k_p}{k_{p0}} \right) \left(\frac{\phi_\infty}{\phi_0} \right) \tanh(a\tau + b) & \text{for } \phi_0 < \phi_\infty \end{cases} \tag{B-23}$$

From these equations, the long-time solutions of k_p and ε_p will grow exponentially at the same rate

$$\frac{k_p}{k_{p0}} \sim e^{\lambda \tau} \quad \text{and} \quad \frac{\varepsilon_p}{\varepsilon_{p0}} \sim e^{\lambda \tau} \tag{B-24a,b}$$

where $\lambda = (\gamma - 1)(1 + r_s)^{1/4}\sqrt{C_\mu/\gamma}$. From equations (B-12) and (B-13), we have

$$\frac{d}{d\tau}\left(\frac{k_t}{k_p}\right) = -\phi\left[\frac{\varepsilon_t}{\varepsilon_p} + C_\mu\left(\frac{k_t}{k_p}\right)\left(1 + \frac{k_t}{k_p}\right)^{1/2}\frac{1}{\phi^2} - \frac{k_t}{k_p}\right] = 0 \tag{B-25}$$

Thus, $\varepsilon_t/\varepsilon_p$ is generally not a constant but depends on time, (since $k_t/k_p = r_s$ was assumed constant)

$$\frac{\varepsilon_t}{\varepsilon_p} = r_s\left(1 - \gamma\frac{\phi_\infty^2}{\phi^2}\right) = \begin{cases} r_s\left(1 - \gamma\tanh^2(a\tau + b)\right) & \text{for } \phi_0 > \phi_\infty \\ r_s\left(1 - \gamma\coth^2(a\tau + b)\right) & \text{for } \phi_0 < \phi_\infty \end{cases} \tag{B-26}$$

but at the equilibrium point, $(\varepsilon_t/\varepsilon_p)_\infty$ reaches the constant $r_s(1-\gamma)$. From equations (B-14) and (B-15), we have

$$\frac{d}{d\tau}\left(\frac{\varepsilon_t}{\varepsilon_p}\right) = \phi\left\{C_{t1}r_s^{3/2} - \frac{C_{t2}}{r_s}\left(\frac{\varepsilon_t}{\varepsilon_p}\right)^2 - C_{p1}\gamma\frac{\phi_\infty^2}{\phi^2}\left(\frac{\varepsilon_t}{\varepsilon_p}\right) + C_{p2}\left(\frac{\varepsilon_t}{\varepsilon_p}\right)\right\} \tag{B-27}$$

At the equilibrium point, C_{t1} and C_{t2} are related to other model constants such as:

$$\sqrt{r_s}C_{t1} - (\gamma - 1)^2 C_{t2} = (1 - \gamma)(C_{p1}\gamma - C_{p2}) \tag{B-28}$$

Physical experiment and direct numerical simulation, such as by Rose (1960), Champagne et al. (1970), Harris et al. (1977), Tavoularis et al. (1981), and Rohr et al. (1988), indicate that the ratio of production over dissipation, P_k/ε, remains a constant between *1.8* to *2.0*. Also from the experiment (Rogallo, 1981) and theoretical analysis

(Tavoularis, 1985), the turbulent kinetic energy and dissipation rate grow exponentially for long times. Now, write equation (B-18) as

$$\gamma = \frac{1 + r_s}{(\varepsilon / P_k)_\infty + r_s} \tag{B-29}$$

where $\varepsilon = \varepsilon_p + \varepsilon_t$. If we define the partition of the energy spectrum (i.e. define r_s), then the constant γ is fixed. It follows that the model constants C_{p1} can be calculated by equation (B-17b); and C_{t1}, C_{t2} can be obtained by solving equations (B-8) and (B-28).

$$C_{t1} = \frac{(\gamma - 1)^2 (C_{p2} - 1)}{\sqrt{r_s} - \sqrt{r_g}(\gamma - 1)^2} \tag{B-30}$$

$$C_{t2} = \sqrt{r_g} C_{t1} + C_{p2} \tag{B-31}$$

From these results, we know that the model constant C_{p2} depends on the decay law of the grid turbulence only, however, C_{p1}, C_{t1} and C_{t2} depend on both the characteristics of homogeneous shear flow and grid turbulence. Figure B-2 shows that C_{t1} and C_{t2} vary with r_g, in other words, they depend on the energy spectrum considered. When $r_g = 0$ and $r_s = 0$, the model becomes the single-scale k-ε model and the model constants are $C_{p1} = 1.45$ and $C_{p2} = 1.90$ which are very close to the standard k-ε model constants $C_{\varepsilon 1} = 1.44$ and $C_{\varepsilon 2} = 1.92$.

In physical experiments, the total turbulent kinetic energy k $(= k_p + k_t)$ is the only measured quantity. The turbulent dissipation rate ε $(= \varepsilon_p + \varepsilon_t)$ is computed from

the turbulent kinetic energy equation. In order to compare with experimental data, the initial condition ϕ_0 should be written in terms of $(\varepsilon/kS)_0$. From the definition of ϕ and equation (B-26), we have

$$\phi_0 = \frac{1}{2}\left[\left(\frac{\varepsilon}{kS}\right)_0 + \sqrt{\left(\frac{\varepsilon}{kS}\right)_0^2 + 4\frac{C_\mu r_s}{\sqrt{1+r_s}}}\right] \tag{B-32}$$

Consequently, the ratios k/k_0 and $\varepsilon/\varepsilon_0$ are computed from the following

$$\frac{k}{k_0} = \frac{k_p}{k_{p0}} \quad \text{and} \quad \frac{\varepsilon}{\varepsilon_0} = \frac{\varepsilon_p}{\varepsilon_{p0}}\left[\frac{1+r_s\left(1-\gamma\phi_\infty^2/\phi^2\right)}{1+r_s\left(1-\gamma\phi_\infty^2/\phi_0^2\right)}\right] \tag{B-33a,b}$$

Direct comparisons with the experiments of Champagne et al. (1970, hereafter called CHC) and Harris et al. (1977, hereafter called HGC) are shown in Figures B-3. The initial dissipation has some uncertainty in the CHC case. Here, the initial condition of $(\varepsilon/kS)_0$ is set at *1.3* as suggested by Speziale et al. (1989). The experimental data of HGC has higher shear rate ($S = 44\ s^{-1}$) than that for CHC ($S = 12.9\ s^{-1}$) and represents a more stringent test. For proposed model the data suggest that $r_s = 0.3$ mimics both cases well, which the single scale model ($r_s = 0$) shows much higher energy levels. In Figure B-4, the time evolution of kinetic energy is compared with the experiment of Tavoularis and Corrsin (1981, hereafter called TC) which also has high shear rate ($S = 46.8\ s^{-1}$). By comparison with the experimental data, the double-scale model yields a much improved solution for the turbulent kinetic energy. It should be noted that $\tau = 0$ in the Figure B-4 corresponds to $\tau = 6.67$ in the experiment of TC.

In Figures B-5 and B-6, the time evolution of turbulent kinetic energy and dissipation rate are compared with the large eddy simulation (LES) by Bardina et al. (1983). When r_s is within *0.2* to *0.3*, the prediction of kinetic energy is in good agreement with the large-eddy simulation results, however, dissipation rate is generally lower. This trend is very similar to the results by the Reynolds stress model as shown in Speziale et al. (1989).

In this work, we define $n = 1.1$, $r_s = 0.3$, and $P_k/\varepsilon = 2.0$, therefore, C_{p1} and C_{p2} are *1.55* and *1.90* respectively. The constants C_{t1} and C_{t2} will depend on the energy spectrum in the external flow of the transitional boundary layer.

B.3 Near-Wall Equilibrium Turbulent Flow

In the near-wall region, the convection effects are small compared with the diffusion effects and can be neglected. We assumed that the flow is in equilibrium, i.e. the production of turbulent kinetic energy is approximately equal to the dissipation rate. It is written as

$$P_k = C_\mu (k_p + k_t)\frac{k_p}{\varepsilon_p}\left(\frac{\partial U}{\partial y}\right)^2 = \varepsilon_p + \varepsilon_t \qquad \text{(B-34)}$$

Because the turbulent kinetic energy is contributed to largely from the large size eddies (low wavenumber production region), we assume that the net energy transfer rate of

the transfer region is almost zero, i.e. $\varepsilon_t \approx 0$. In this flow, the molecular diffusion is much less than the turbulent diffusion ($\nu << \nu_t$) and can be neglected. Then the turbulence model equations are approximated as

$$\frac{\partial}{\partial y}\left(\frac{\nu_t}{\sigma_{kp}}\frac{\partial k_p}{\partial y}\right)=0 \tag{B-35}$$

$$\frac{\partial}{\partial y}\left(\frac{\nu_t}{\sigma_{kt}}\frac{\partial k_t}{\partial y}\right)=0 \tag{B-36}$$

$$\frac{\partial}{\partial y}\left(\frac{\nu_t}{\sigma_{\varepsilon p}}\frac{\partial \varepsilon_p}{\partial y}\right)+\left(C_{p1}-C_{p2}\right)\frac{\varepsilon_p^2}{k_p}=0 \tag{B-37}$$

$$\frac{\partial}{\partial y}\left(\frac{\nu_t}{\sigma_{\varepsilon t}}\frac{\partial \varepsilon_t}{\partial y}\right)+C_{t1}\left(\frac{k_t}{k_p}\right)^{3/2}\frac{\varepsilon_p^2}{k_p}-C_{t2}\frac{\varepsilon_t^2}{k_t}=0 \tag{B-38}$$

Since $\varepsilon_t \approx 0$ in the flow, equation (B-38) tells that

$$\frac{k_t}{k_p}=\left(\frac{C_{t2}}{C_{t1}}\right)^{2/5}\left(\frac{\varepsilon_t}{\varepsilon_p}\right)^{4/5} \tag{B-39}$$

the ratio of kinetic energy k_t/k_p is also small and can be neglected. Now, consider the logarithmic region of turbulent boundary layer in which the mean velocity profile follows

$$\frac{U}{U_\tau}=\frac{1}{\kappa}\ln\left(\frac{yU_\tau}{\nu}\right)+E \tag{B-40}$$

where κ and E are constants and $U_\tau = \sqrt{\tau_w/\rho}$ is the friction velocity. Since the shear stress in the logarithmic layer is assumed constant, the solution of equation (B-35) and (B-37) are similar to the single-scale k-ε model results,

$$k_p = \frac{U_\tau^2}{\sqrt{C_\mu}}, \qquad \varepsilon_p = \frac{U_\tau^3}{\kappa y} \tag{B-41a,b}$$

and $$\kappa^2 = \sigma_{\varepsilon p}\sqrt{C_\mu}\left(C_{p2} - C_{p1}\right) \tag{B-42}$$

If we take $C_\mu = 0.09$ and $\kappa = 0.4$ in the double-scale model, the model constant $\sigma_{\varepsilon p}$ becomes 1.5. In the single-scale model ($r_s = 0$), we have $\sigma_{\varepsilon p} = 1.2$ which is lower than the standard k-ε model constant $\sigma_\varepsilon = 1.3$. Therefore, in order to minimize the modification of model constants, it is adjusted to retain the typical values. In this work, we propose that $\sigma_{kp} = \sigma_{kt} = \sigma_k = 1.0$, and $\sigma_{\varepsilon p} = \sigma_{\varepsilon t} = \sigma_\varepsilon = 1.3$ as in the standard k-ε model.

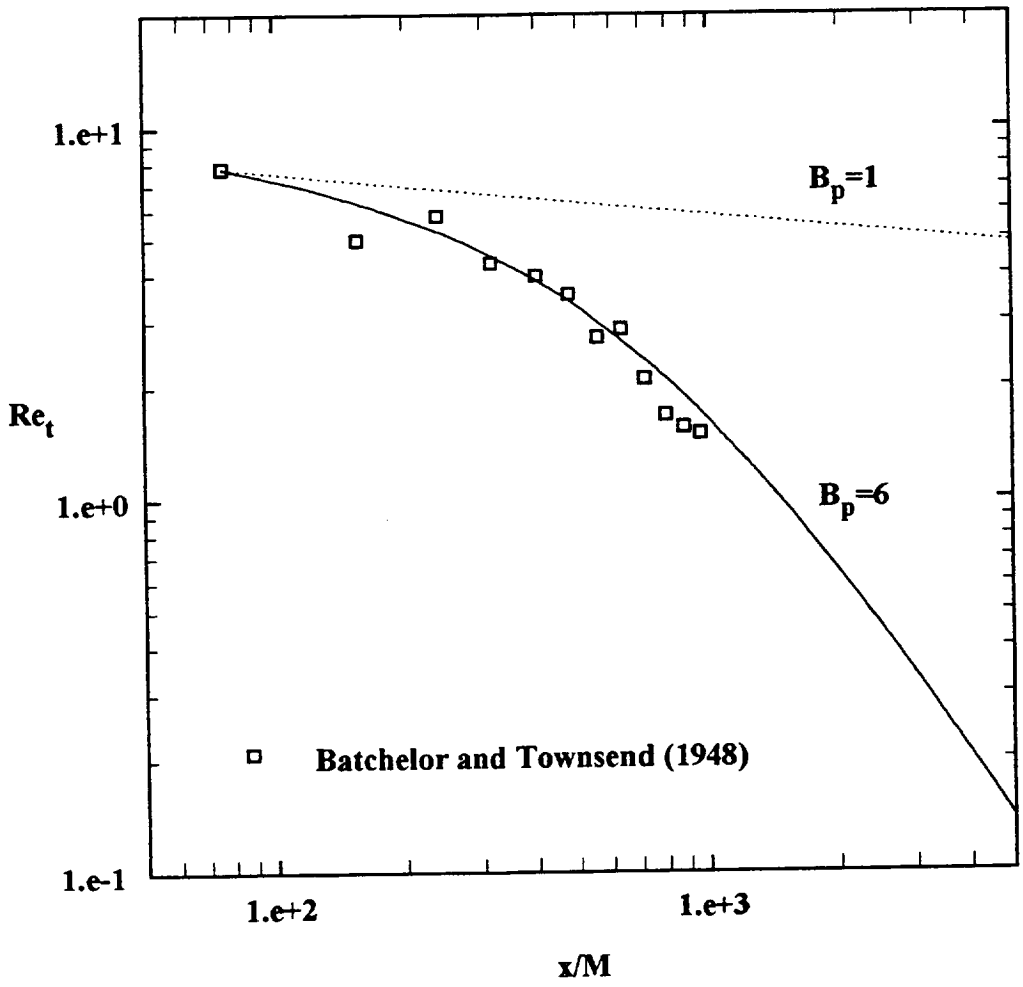

Figure B-1 Decay law of homogeneous turbulence: comparison with the experiment of Batchelor and Townsend (1948).

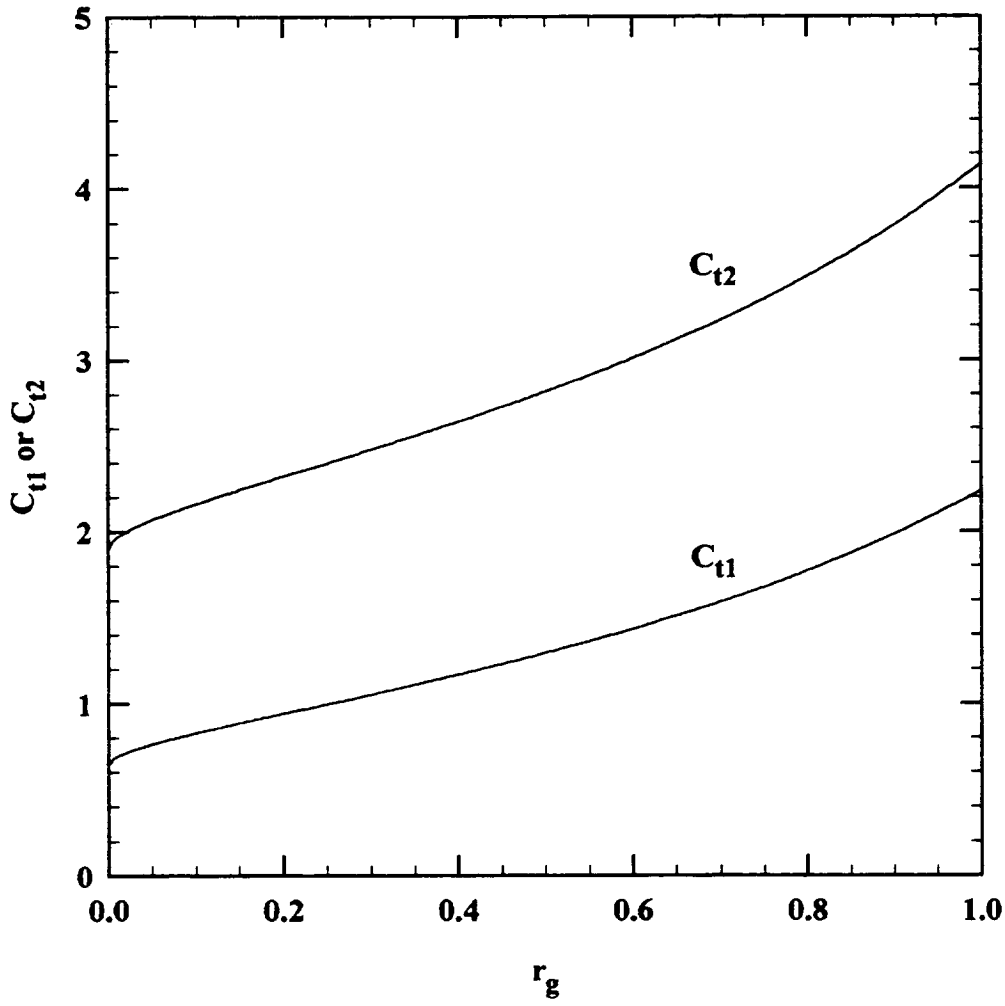

Figure B-2 The model constants C_{t1} and C_{t2} vary with grid turbulence spectrum parameter r_g. $(r_s = 0.5)$

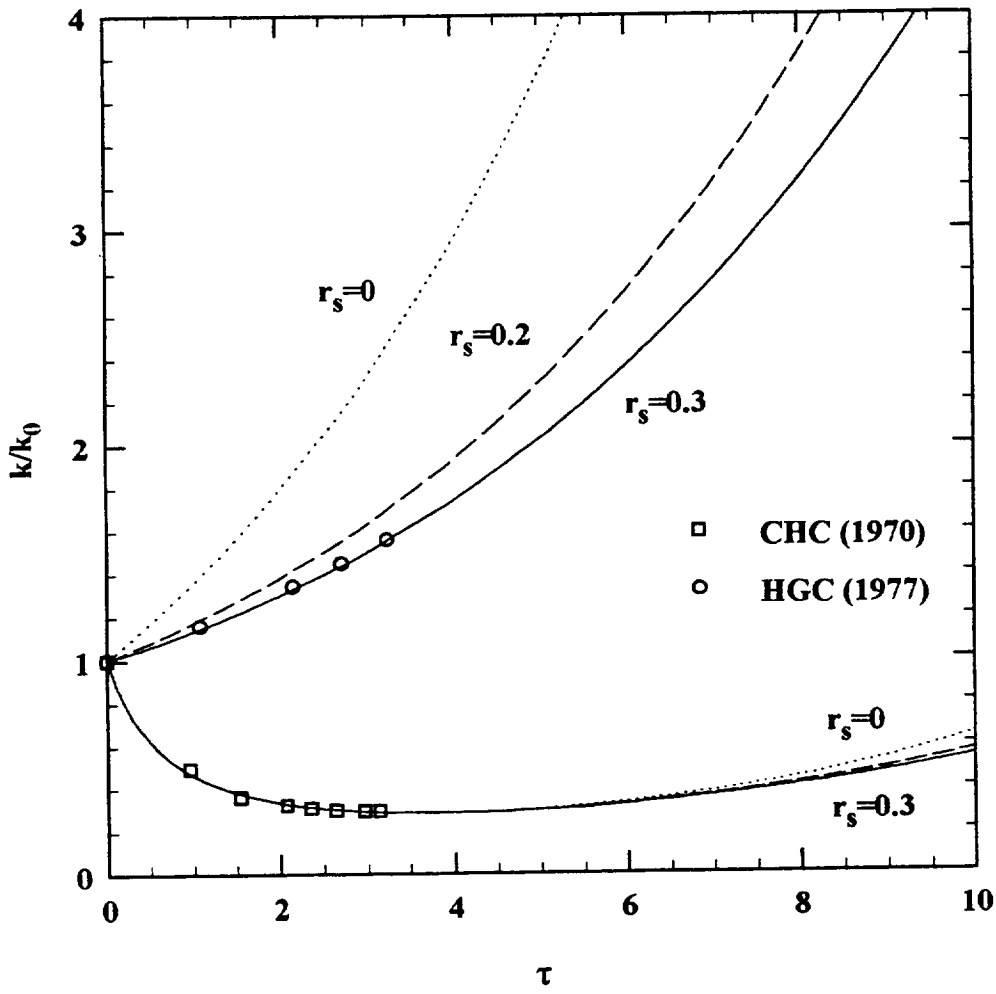

Figure B-3 Time evolution of the turbulent kinetic energy for homogeneous shear flow: comparison of the model with the experiment of Champagne et al (CHC, 1970) and the experiment of Harris et al (HGC, 1977).

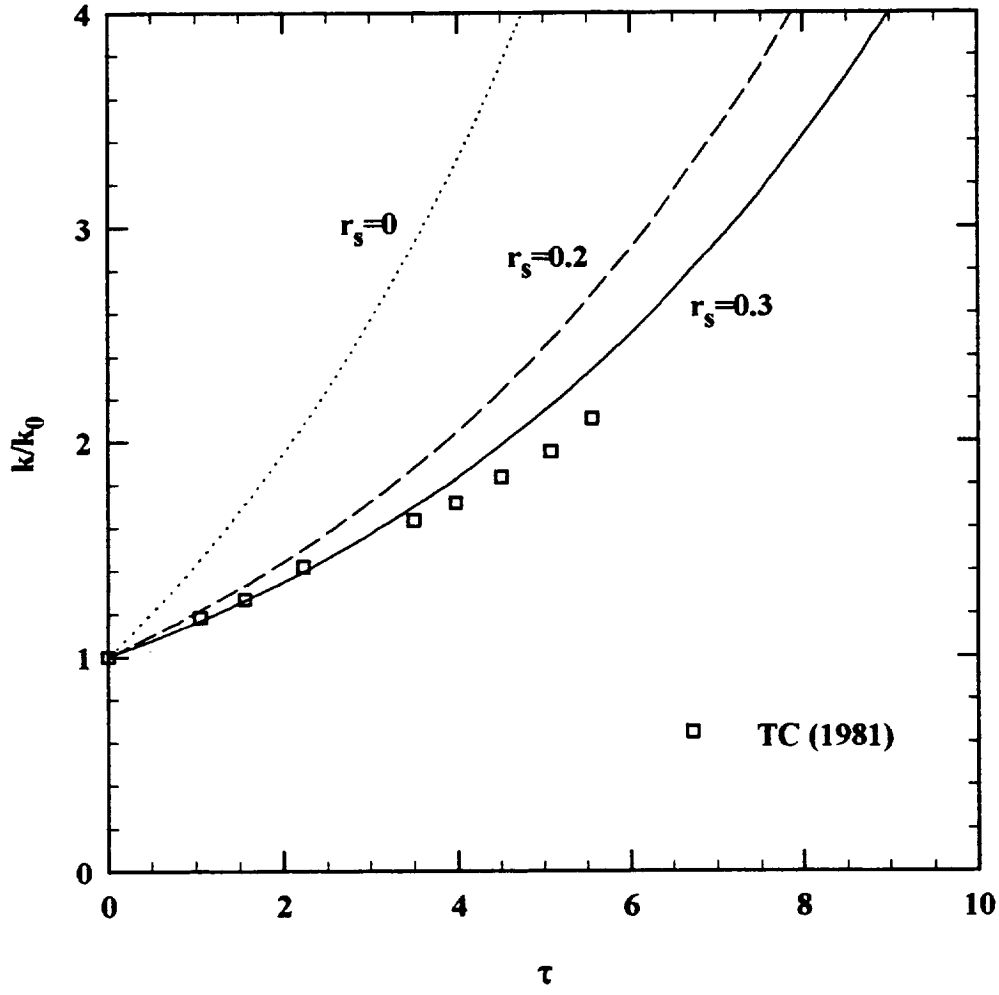

Figure B-4 Time evolution of the turbulent kinetic energy for homogeneous shear flow: comparison of the model with the experiment of Tavoularis and Corrsin (TC, 1981).

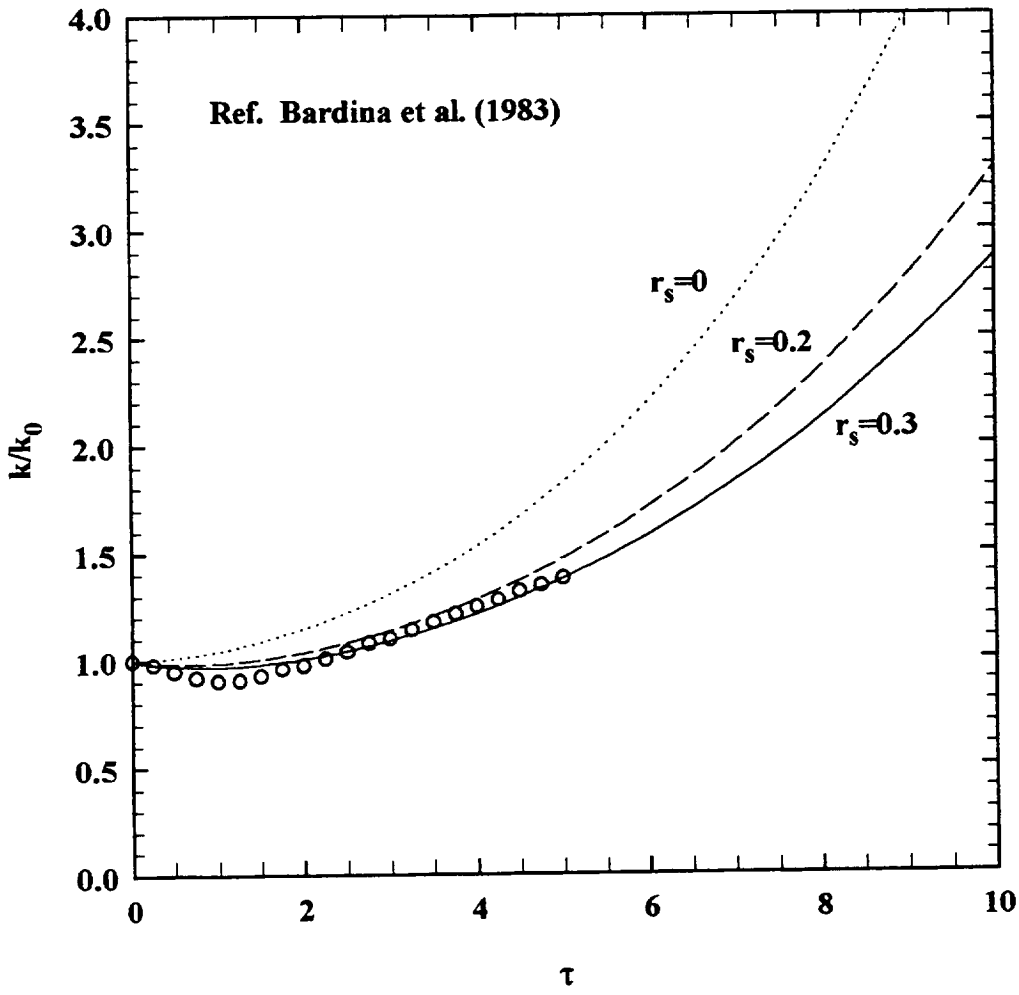

Figure B-5 Time evolution of the turbulent kinetic energy for homogeneous shear flow: comparison of the model with the large-eddy simulation of Bardina et al. (1983).

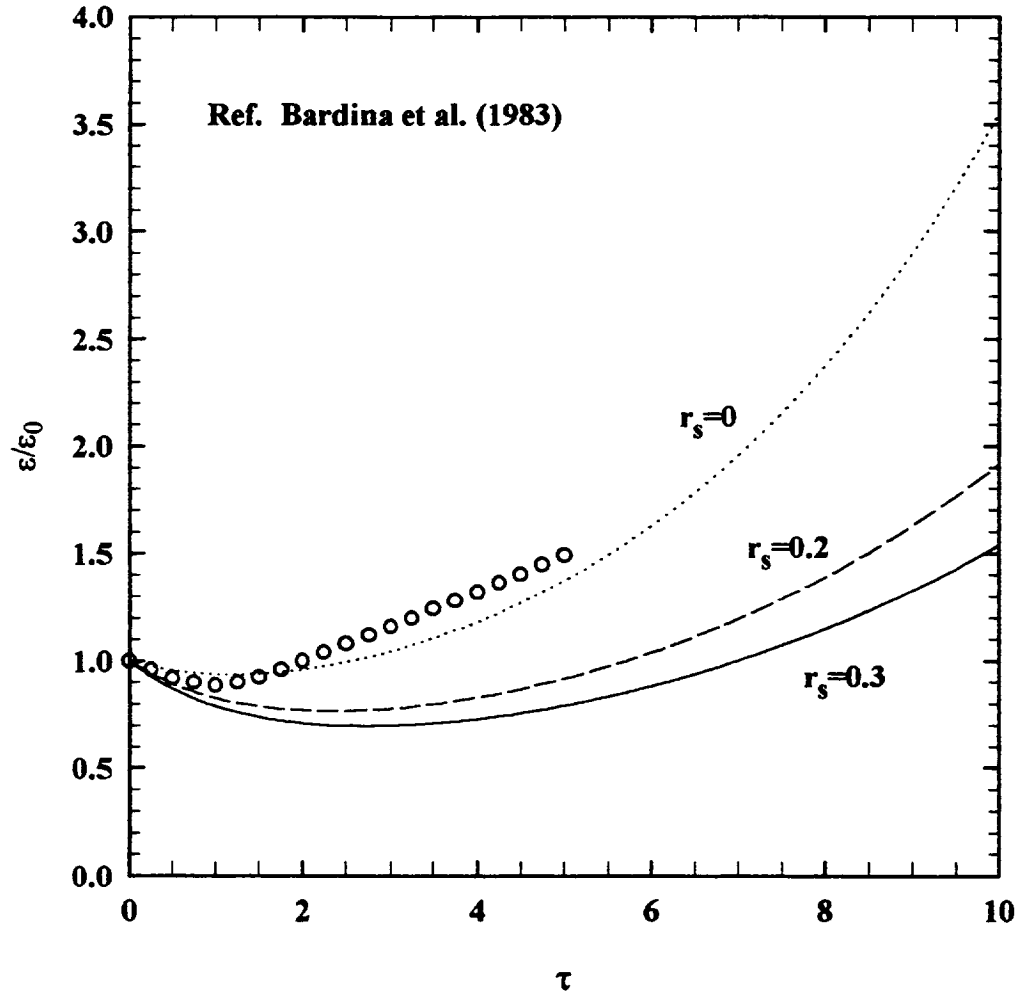

Figure B-6 Time evolution of the turbulent dissipation rate for homogeneous shear flow: comparison of the model with the large-eddy simulation of Bardina et al. (1983).

APPENDIX C

DERIVATION OF RESHOTKO PROFILE IN DESCRIBING INITIAL TURBULENT KINETIC ENERGY

This appendix presents the derivation of Reshotko's solution in describing the initial profiles of turbulent kinetic energy. To develop the formulation, it is assumed that the velocities satisfy the Blasius equation $2f''' + f''f = 0$ with the similarity variable $\eta = y\sqrt{U_e/\nu x}$ and boundary conditions $f(0) = f'(0) = 0$, $f'(\infty) = 1$. The velocity can be written as

$$U = U_e f' \tag{C-1}$$

The differential of equation (C-1) yields

$$dU = dU_e\left(f' + \frac{1}{2}\eta f''\right) - \frac{U_e}{2x}\eta f'' dx \tag{C-2}$$

At a fixed x location ($dx = 0$), equation (C-2) implies that the velocity fluctuation dU is proportional to the free-stream velocity fluctuation dU_e. Since the turbulent kinetic energy is proportional to $(dU)^2$, Reshotko's profile is defined as

$$\frac{k}{k_e} = \left(f' + \frac{1}{2}\eta f''\right)^2 \tag{C-3}$$

REPORT DOCUMENTATION PAGE

Form Approved
OMB No. 0704-0188

1. AGENCY USE ONLY (*Leave blank*)	2. REPORT DATE	3. REPORT TYPE AND DATES COVERED
	May 1996	Final Contractor Report

4. TITLE AND SUBTITLE

Multiple Scale k-ε Turbulence Modeling of the Transitional Boundary Layer for Elevated Freestream Turbulence Levels

5. FUNDING NUMBERS

WU–505–62–52
NCC3–124

6. AUTHOR(S)

Sheng-Yi Wu and Eli Reshotko

7. PERFORMING ORGANIZATION NAME(S) AND ADDRESS(ES)

Case Western Reserve University
Department of Mechanical and Aerospace Engineering
Glennam Bldg.
Cleveland, Ohio 44106

8. PERFORMING ORGANIZATION REPORT NUMBER

E–10260

9. SPONSORING/MONITORING AGENCY NAME(S) AND ADDRESS(ES)

National Aeronautics and Space Administration
Lewis Research Center
Cleveland, Ohio 44135–3191

10. SPONSORING/MONITORING AGENCY REPORT NUMBER

NASA CR–198487

11. SUPPLEMENTARY NOTES

Project Manager, Frederick F. Simon, Internal Fluid Mechanics Division, NASA Lewis Research Center, organization code 2630, (216) 433–5894.

12a. DISTRIBUTION/AVAILABILITY STATEMENT

Unclassified - Unlimited
Subject Category 34

This publication is available from the NASA Center for AeroSpace Information, (301) 621–0390.

12b. DISTRIBUTION CODE

13. ABSTRACT (*Maximum 200 words*)

A multiple-scale k-ε turbulence model is developed to calculate the development of the transitional flat-plate boundary layer under elevated freestream turbulent conditions. The model uses the split-spectrum concept which divides the energy spectrum into low and high wavenumber regions, each of which have their own modeling equations. Damping functions are used to accommodate the near-wall and transitional behaviors. The model constants are determined from the exact solutions of the simplified model equations for the cases of grid turbulence flow, homogeneous shear flow, and the near-wall equilibrium turbulent flow. By this calibration, the model constants are automatically tuned to the characteristics of the freestream energy spectrum. The results show that the partition of the energy spectrum in the freestream also affects the transition location. A spectrum partitioning parameter S_g is identified whose optimal value correlates with freestream turbulence level. Comparison with five different sets of experimental data shows that the multiple-scale model with the optimal values of S_g emulates many features of the transitional boundary layer. The start of transition can be predicted reasonably well, however the length of the transition zone is consistently shorter than in the experiments. The present model is insensitive to the shape of the initial turbulence energy and dissipation profiles.

14. SUBJECT TERMS

Transition; Turbulence model; Turbines; Multiple scale

15. NUMBER OF PAGES

168

16. PRICE CODE

A08

17. SECURITY CLASSIFICATION OF REPORT	18. SECURITY CLASSIFICATION OF THIS PAGE	19. SECURITY CLASSIFICATION OF ABSTRACT	20. LIMITATION OF ABSTRACT
Unclassified	Unclassified	Unclassified	

National Aeronautics and
Space Administration

Lewis Research Center
21000 Brookpark Rd.
Cleveland, OH 44135-3191